

Dissertation zur Erlangung des Doktorgrades
der Fakultät für Chemie und Pharmazie
der Ludwig-Maximilians-Universität München

Nanostructured labels for enhanced paper based immunoassays



Elisângela Moura Linares

aus

Campinas (São Paulo), Brasilien

2013

Erklärung

Diese Dissertation wurde im Sinne von § 7 der Promotionsordnung vom 28. November 2011 von Herrn PD. Dr. Stefan Thalhammer betreut, und von Herrn Prof. Jens Michaelis von der Fakultät für Chemie und Pharmazie vertreten.

Eidesstattliche Versicherung

Diese Dissertation wurde eigenständig und ohne unerlaubte Hilfe erarbeitet.

München, 10 Dezember 2012.

Elisângela Moura Linares

Dissertation eingereicht am 10.12.2012

1. Gutachter: Prof. Dr. Jens Michaelis
2. Gutachter: PD Dr. Stefan Thalhammer

Mündliche Prüfung am 25.02.2013

„And yet the true creator is necessity, who is the mother of our invention.”
(The Republic, Plato)

Summary

In the developing world, there is a lack of convenient and accurate tools to diagnose pathogens. As a consequence, numerous diseases remain untreated or receive inappropriate treatment. The World Health Organization recommends that an ideal point-of-care assay has to be ASSURED: it must be affordable, sensitive, specific, user-friendly, rapid and robust, equipment-free, and delivered to those who need it. In line with the strategy of simplicity, lateral flow immunoassays (LFIA) based on nanoparticle (NP) labels are very promising nanodiagnostic tools, fulfilling most of the specified requirements. LFIA have already been successfully applied to the detection of various acute and chronic diseases. However, they show limitations in terms of sensitivity, a shortcoming that can prevent early stage disease detection. Dengue fever (DF) is a tropical viral mosquito-transmitted disease that affects 50-100 million people every year. About 400 000 people develop hemorrhagic fever and 5% of them die annually. In this case, the death rate may be reduced from 5 to less than 1% when early detection is provided. Commercially available LFIA for DF based on non-structural protein 1 (NS1) detection show low sensitivity for the first days of the infection. This low sensitivity is due to the inefficiency of the detection label consisted of gold nanoparticles.

This thesis aims to enhance the performance of paper based immunoassays by selecting and comparing the performance of already used labels for LFIA and developing nanostructures to replace the conventional gold nanoparticles. A screening of possible labels using the biotin-streptavidin system was performed among the four most used detection labels: gold and silver coated gold NPs, polystyrene beads and carbon black. The results from an immunospot assay showed that carbon black provides the lowest detection limit (DL) of all labels. Therefore, it was used as detection system for DF in LFIA, achieving a DL 50 times lower (10ng/L) than the commercially used standard gold NPs (500 ng/L). Due to the high sensitivity of tools based on fluorescence, fluorescent NPs were used to produce immunospot assays (ISA) combining the principles of LFIA, fluorophore linked immunosorbent assay and enzyme linked immunospotting. This assay is an alternative for the time-consuming enzyme linked immunosorbent assay (ELISA). The procedure needs 10 times less serum sample (4 μ L) and requires 2-4h less than ELISA (45-60 min). The DL for NS1 protein, 5.2 ng/mL, is comparable to ELISA. The evaluation of 83 serum samples compared to a commercial ELISA showed sensitivity of 81% and specificity of 88%. The method allowed faster, cheaper and convenient detection using common laboratory equipment. Another problem affecting the paper based assay performance is the particle agglomeration. To overcome this problem, poly[styrene-co-(2-hydroxyethyl methacrylate)] core-shell particles containing [Ru(4,4'-dicarboxylate-2,2'-bpy)₃] luminescent complexes were synthesized and used as alternative labels for ISA. These particles showed promising uses in diagnostics, besides cell tracking and imaging, due to their low aggregation, monodispersity, biocompatibility and easy functionalization. The best performance for LFIA and ISA was obtained by combining colorimetry and fluorescence detection using clusters of gold and fluorescent NPs. The cluster concentrates gold NPs reducing the NS1 DL (10 ng/mL) by 50 times in comparison to gold labels. The use of fluorescent portable lamps additionally decreases the NS1 DL (2.5 ng/mL), resulting in a 200 times overall DL reduction. The sensitivity improvements observed by using carbon black and NP cluster anticipate the Dengue fever diagnosis to the first day of the infection in comparison to the third day detected by commercial kits. Faster, cheaper and reliable methods were also possible by using fluorescence detection. The scientific progress described in this work is an important step forward towards to produce more reliable and sensitive diagnostic tools for developing countries, maintaining the necessary assay simplicity. The improvements are not only relevant for DF detection, but apply to every analytes that make use of LFIA to provide point-of-care assistance.

Zusammenfassung

Abseits der großen Industriestaaten existiert auch heute ein Mangel an einfachen und genauen Verfahren zur Diagnose von Pathogenen. Aus diesem Grund wird eine Vielzahl verschiedener Erkrankungen nicht oder nur unzureichend behandelt. Ideale "Point-Of-Care Assays" (POC) entsprechen laut Empfehlung der Weltgesundheitsorganisation dem Merkmal ASSURED: "affordable, sensitive, specific, user-friendly, rapid and robust, equipment-free, and delivered to those who need it". Um diese Analysetools einfach zu halten, sind "Lateral Flow Immunoassays (LFIAs)", welche auf Nanopartikeln (NP) basieren, sehr vielversprechend, da sie die meisten der genannten Anforderungen erfüllen. LFIAs wurden bereits erfolgreich zur Detektion verschiedener akuter und chronischer Krankheiten eingesetzt. Trotzdem weisen sie durch ihre eingeschränkte Empfindlichkeit einen Nachteil auf, der sich im Besonderen auf die Erkennung von Erkrankungen im Frühstadium auswirkt. Denguefieber (DF) ist eine von Moskitos übertragene Viruserkrankung, welche jährlich 50-100 Millionen Menschen befällt. Etwa 400.000 von ihnen entwickeln hämorrhagisches Fieber, die Letalitätsrate beträgt 5%. Die Letalitätsrate könnte jedoch auf weniger als 1% gesenkt werden, wenn eine Diagnose im Frühstadium der Erkrankung möglich wäre. Kommerziell verfügbare LFIAs, welche auf der Detektion des "Non-Structural Protein 1" (NS1) basieren, sind jedoch nicht empfindlich genug um eine Diagnose an den ersten Tagen der Erkrankung zu ermöglichen, weil das Detektionssystem, welches auf antikörperbeschichtete Goldnanopartikel aufbaut, nicht ausreichend effizient ist.

Diese Arbeit beschreibt, wie sich die Leistungsfähigkeit von papierbasierten Immunoassays durch die Wahl und den Vergleich bereits vorhandener LFIA Labels sowie der Entwicklung neuer Nanostrukturen zum Ersatz der konventionellen goldbasierten Strukturen verbessern lässt. Eine Untersuchung möglicher Labels unter Verwendung eines Biotin-Streptavidin Systems wurde für die vier gebräuchlichsten Detektionslabels durchgeführt: gold- und silberbeschichtete Goldnanopartikel, Polystyrenpartikel und carbon black (CB). Die mit einem Immunospotassay (ISA) erzielten Ergebnisse zeigen, dass der Einsatz von CB die niedrigsten Detektionsschwellen (DL) aller Labels ermöglicht. Aus diesem Grund wurde es im Folgenden als Detektionssystem für DF in LFIA eingesetzt und erzielte eine DL, welche 50-mal geringer (10ng/L) ist als das kommerzielle Verfahren mit normalen Goldnanopartikeln (500ng/L). Wegen der hohen Empfindlichkeit fluoreszenzbasierter Verfahren wurden darauf basierende Labels genutzt, um Immunospotassays, welche die Prinzipien von LFIA, FLISA (fluorophore linked immunosorbent assay) und ELISPOT (enzyme linked immunospotting) verbinden, als Alternative zu den zeitaufwändigen ELISA (enzyme linked immunosorbent assay) zu produzieren. Das dadurch entstandene System benötigt nur ein Zehntel der ursprünglichen Serummenge (4µL) und lässt sich um 2-4h schneller durchführen als ELISA (45-60min). Dabei bleibt das Detektionslimit für NS1 mit 5,2ng/mL vergleichbar zu ELISA. Die Überprüfung und der Vergleich des Verfahrens mit einem kommerziellen ELISA Test, durchgeführt mit 83 Serumproben, zeigte eine Empfindlichkeit von 81% und eine Spezifität von 88%. Die Methode erlaubt eine schnellere, billigere und einfachere Erkennung auch bei Einsatz normaler Laborausstattung. Um das Problem der Agglomeration der lumineszierenden Polymerpartikel während des Flusses zu umgehen, wurden Poly[styren-co-(2-hydroxyethyl methacrylat)] Kern/Hülle- Partikel, die lumineszierende [Ru(4,4'-dicarboxylate-2,2'-bpy)3]-Komplexe enthielten, synthetisiert und als alternative Labels für ISA verwendet. Diese Partikel zeigen durch ihre geringe Aggregation, Monodispersität, Biokompatibilität und leichte Funktionalisierung vielversprechende Eigenschaften für mögliche Diagnosen, welche über Zell-Tracking und Bildgebung hinausgehen. Die besten Ergebnisse für LFIA und ISA wurden durch Kombination von Kolorimetrie und Fluoreszenzdetektion unter Verwendung von Clustern von Gold- und fluoreszierenden NPs erzielt. Die Cluster konzentrieren Gold-NPs,

dies reduziert das NS1 DL (10ng/L) auf 1/50 im Vergleich zu Goldlabels. Die Verwendung von tragbaren Fluoreszenzlampen ermöglicht eine weitere Reduktion des NS1 DL auf 2,5ng/L, womit sich in Summe eine Verbesserung um den Faktor 200 ergibt. Die Empfindlichkeitsverbesserungen, welche bei Verwendung von CB und Nanopartikelclustern beobachtet wurden, werden die DF Diagnose am ersten Tag der Erkrankung ermöglichen. Dies war bisher erst am dritten Tag möglich. Billige, schnelle und zuverlässige Methoden wurden auch mit Einsatz von Fluoreszenzdetektion gezeigt. Der in dieser Arbeit erzielte wissenschaftliche Erkenntnisgewinn ist ein wichtiger Schritt zur Entwicklung zuverlässigerer und empfindlicherer Diagnoseverfahren zum Einsatz abseits der führenden Industrienationen, da die nötige Einfachheit der Assays beibehalten wird. Die Verbesserungen sind dabei nicht nur für die DF-Diagnostik relevant, sondern lassen sich auch auf alle vernachlässigten Krankheiten übertragen und andere Analyten, welche LFIA einsetzen, übertragen um point-of-care Unterstützung zu gewährleisten.

Acknowledgements

First and above all, I praise God for providing me this opportunity and granting me the capability to proceed successfully. Thank for the wisdom and perseverance that has been bestowed upon me during this research project, and indeed, throughout my life. The more I delve into science, the more I realize His existence and presence.

This thesis appears in its current form due to the assistance and guidance of several people. I would like to extend my sincere appreciation to all of them. In particular, I want to thank...

- ... Prof. Jens Michaelis for accepting the invitation to be the first supervisor and for the careful corrections and important comments to improve my thesis.
- ... PD. Dr. Stefan Thalhammer for giving me the opportunity to develop my thesis at his lab and encouraging me to perform my own ideas. Thank for all support with DAAD-Capes project and for the precious advices to develop and improve writing and presentation skills. No words can say my immense gratitude to his help.
- ... Prof. Lauro Kubota for allowing me to be part of his group and all support during my experiments in Brazil.
- ... Prof. Claudio Pannuti for opening the doors of his laboratories and providing me Dengue serum samples.
- ... Staff from Biophysics group at Helmholtz Zentrum Munich for the nice dairy moments and especially to our group meetings and retreats. Thank you for the friendly and helpful environment. In particular, I would like to thank Bárbara Miranda, Anahí Philippart and Cátia Correa who worked direct with me for all valuable discussions. This showed me science develops faster when minds work together.
- ... Norbert Menzel for being always ready to help in the lab. I greatly appreciate his assistance that made some of my experiments possible.
- ... Prof. Walch for allowing me to use the transmission electron microscope, which provided me important information for my thesis.
- ... Marilena Pinto for the support in Munich even before arriving in Germany. I would like to thank for her efforts to organize the IDK program so brilliantly.
- ... All my friends (near or far) for listening to me and giving me support. In particular, I would like to thank Anahí Philippart, Bárbara Miranda, Luciana Afonso, Martin Schmid and Willian Portes for the support and encouragements.
- ... My special friends, Heloísa and Paulo Schumacher, for the friendship. One only knows who is a real friend when difficult moments appear and these two friends showed me the real meaning of a friendship, even with the distance.

- ... Elite Network of Bavaria for the fellowship and the International Doctorate Program NanoBioTechnology (IDK-NBT) for the interdisciplinary lectures and environment.
- ... Stefan Fikar for the support, patience and encouragement during the last and hardest moments of my doctorate work. I am thankful for having you in my life.
- ... Last but not least, my family for believing me. I thank my parents, Alceu and Enedir, and my brother, Alceu Júnior, for all unconditional support and help during these three years far away from them. Even with the distance, they shared the happiest moments and supported me in the difficult situations. This achievement was only possible because you stand by my side and made me see further.

Preface

This thesis was prepared as a cumulative thesis and it was divided in 5 chapters:

- Chapter 1: Introduction and summary of the most relevant results described in the next chapters.

- Chapter 2: it is a publication in Journal of Immunological Methods, volume 375, 264 – 270, 2012. The article is named “Enhancement of the detection limit for lateral flow immunoassays: Evaluation and comparison of bioconjugates”.

- Chapter 3: it is a publication in Biosensors and Bioelectronics, in press, under the DOI number: 10.1016/j.bios.2012.08.005, named “Immunospot assay based on fluorescent nanoparticles for Dengue fever detection”.

- Chapter 4: it is a publication in Journal of Materials Chemistry B, under DOI: 10.1039/c3tb00316g, titled “One step synthesis of polymer core-shell particles with carboxylated Ruthenium complex: potential tool for biomedical applications”. The article was published after the thesis submission and therefore it is presented in the same format as the submission template from the journal.

- Chapter 5: it is a manuscript prepared for submission to a journal, but the results are described in a patent requisition and they could not be published up to the time of the thesis submission. A letter from the technology transfer office of the Helmholtz Zentrum München is attached to this thesis in Appendix A1.

TABLE OF CONTENTS

CHAPTER 1	1
1. Introduction	1
1.1 Nanoparticles in diagnostics	1
1.2 Nanoparticle-bioconjugates and antibodies	2
1.2.1 <i>Antibodies</i>	2
1.2.2 <i>Gold nanoparticles</i>	6
1.2.3 <i>Carbon black particles</i>	6
1.2.4 <i>Polymer particles</i>	7
1.3 Point-of-care testing: assays on paper	7
1.4 Lateral flow immunoassay	9
1.5 Immunospot assay	12
1.6 Components of lateral flow immunoassay	13
1.6.1 <i>Sample pad: blood filter matrices</i>	13
1.6.2 <i>Antibodies and conjugate pad</i>	14
1.6.3 <i>Reaction membrane</i>	15
1.6.4 <i>Capillary flow rate</i>	16
1.6.5 <i>Absorbent Pad</i>	18
1.6.6 <i>Backing material</i>	18
1.6.7 <i>Particles used as detection labels</i>	19
1.7 Detection techniques	19
1.7.1 <i>Colorimetric detection</i>	20
1.7.2 <i>Fluorescence detection</i>	21
1.7.3 <i>Charge-transfer absorption and phosphorescence</i>	23
1.8 Dengue fever	25
1.8.1 <i>Disease stages</i>	27
1.8.2 <i>Serology</i>	28
1.8.3 <i>Lateral flow immunoassay based on viral NS1 protein</i>	29
1.9 Aim and structure	30
2. Results and Discussion	31
2.1 Optical based detection systems	31

2.1.1 <i>Enhancement of the detection limit for lateral flow immunoassays: evaluation and comparison of bioconjugates</i>	31
2.1.2 <i>Lateral flow immunoassay based on carbon black particles</i>	34
2.2 Fluorescence based detection system	36
2.2.1 <i>Immunospot</i>	36
2.3 Phosphorescence based detection system	41
2.3.1 <i>Polymer core-shell particles of poly(styrene-co-hydroxyethylmethacrylate), PHEMA, containing luminescent ruthenium complex</i>	41
2.4 Colorimetry and fluorescence based detection system	45
2.4.1 <i>Gold and fluorescent nanoparticle clusters</i>	45
2.5 Detection limit comparison	47
3. References	50
CHAPTER 2	58
<i>Enhancement of the detection limit for lateral flow immunoassays: evaluation and comparison of bioconjugates</i>	58
CHAPTER 3	73
<i>Immunospot assay based on fluorescent nanoparticles for dengue fever detection</i>	73
Supplementary Information	73
CHAPTER 4	77
<i>One step synthesis polymer core-shell particles with carboxylated ruthenium complex: potential tool for biomedical applications</i>	77
Electronic Supporting Information	98
CHAPTER 5	105
<i>Enhanced lateral flow immunoassay based on gold and fluorescent particle clusters for dengue detection: comparison with gold and carbon black label</i>	105
supplementary information	123
Conclusion and Outlook	126
Curriculum Vitae	133
Appendix	135

CHAPTER 1

1. Introduction

1.1 Nanoparticles in diagnostics

The use of nanotechnologies for diagnostic applications shows great promise to meet the rigorous demands of the clinical laboratories for sensitivity and cost-effectiveness (Azzazy et al., 2006). Nanodiagnostics, defined as the use of nanotechnology for clinical diagnostic purposes (Jain, 2005), are promising to provide higher sensitivity, lower sample volume and faster analysis than conventional diagnostic tools (Azzazy et al., 2006).

Numerous nanostructures have been investigated to determine their properties and possible applications in diagnostics (Jianrong et al., 2004). Nanoparticles (NPs), defined as structures with lengths in two or three dimensions between 1 nm and 100 nm (Web ref. 1 ASTM 2456, 2006), are successfully used as probes in biosensing applications. A variety of NPs has been described for this purpose, including metal NPs (Parolo et al., 2012), silica NPs (Xie et al., 2009), polymer NPs (Juntunen et al., 2012) and quantum dots (Yang et al., 2011).

While NPs have their own intrinsic properties, it is generally necessary in diagnostic applications to impart additional properties or functions through physical or chemical coupling between a NP and one or more molecules. Nanostructures can be conjugated to biological molecules, including enzymes, antibodies, affinity proteins, cell receptor ligands and drugs, producing a measurable signal characteristic of the target biomolecules (Fortina et al., 2007). The association of one or more biologically relevant molecules at the interface of a NP defines a NP-bioconjugate and combines the unique optoelectronic or physicochemical properties of NP with biological activity such as selective binding (Algar et al., 2011).

Among the diagnostic tools that use NP-bioconjugates, the immunoassays are especially interesting due to the combination of high specificity of antibodies with the variety of NP properties. In these assays, an analyte is determined by an immune reaction with an antibody that binds specifically to the analyte. This type of reaction involves the binding of one type of molecule, the antigen, with a second type, the antibody. The immune reaction is signaled by a detectable label. Herein a label is defined as every molecule/structure responsible by developing a signal (light absorption, luminescence, magnetism etc), which indicates the interaction between the antigen and the antibody. Thus, a large variety of labels have been used, including enzymes, fluorophores, chemiluminescent dyes, radioactive elements and

recently nanoparticles.

1.2 Nanoparticle-bioconjugates and antibodies

NP-bioconjugates can be prepared via the formation of new chemical bonds between functional groups associated with a NP and a biomolecule or a small molecule of interest. NPs may also offer the potential for association through coordinate bonding, electrostatic interactions, and van der Waals interactions (Algar et al., 2011). The choice of the binding mechanism of a biomolecule to the NPs depends on the biomolecule and the nature of the NPs. Main characteristics of antibodies and bioconjugation with particles are detailed in the next sections (1.2.1-1.2.4).

1.2.1 Antibodies

An antibody, also known as an immunoglobulin (Ig), is a globular plasma protein produced by B-cells that is used by the immune system to identify and neutralize foreign bodies, such as bacteria and viruses. The antibody recognizes a unique part of the foreign target, called *antigen*. The antibodies have a specific part, *paratope*, which binds specifically to a defined structure, *epitope*, of the antigen, allowing these two structures to bind together with precision. Using this binding mechanism, an antibody can interact with a microorganism or an infected cell to activate other parts of the immune system, or can neutralize its target directly (Cole et al., 1984). For example, an antibody can bind to a specific part (or to some parts) of a microorganism, which is essential for its invasion and survival, and inactivate it.

Antibodies exist in different varieties known as isotypes. In mammals, there are five antibody isotypes (Figure 1a) known as IgA, IgD, IgE, IgG and IgM. They differ in their structure, biological properties, functional locations and ability to deal with different antigens. The antibody monomer is composed of two different parts: *heavy* and *light chain* (Figure 1b). In mammals, there are five types of mammalian Ig heavy chain denoted by α , δ , ϵ , γ , and μ . These chains are found in IgA, IgD, IgE, IgG, and IgM antibodies, respectively. Distinct heavy chains differ in size and composition. Each heavy chain has two regions, the *constant region* and the *variable region*. The constant region is identical in all antibodies of the same isotype, but differs in antibodies of different isotypes. The variable region of each heavy chain

is approximately 110 amino acids long and is composed of a single Ig domain (Cole et al., 1984). Recently, small fragments of naturally occurring heavy-chain antibody, named nanobody, have been successfully used in biomedical applications. Nanobodies are strictly monomeric, very stable, and highly soluble entities, produced in camelids and sharks (Cortez-Retamozo et al., 2004). Although they show promising characteristics, their production has been done by a restricted number of companies, and therefore they are only available for a few antigens.

The light chain contains one constant domain and one variable domain. The approximate length of a light chain is 211 to 217 amino acids. Each antibody contains two light chains that are always identical; only one type of light chain, κ or λ , is present per antibody in mammals.

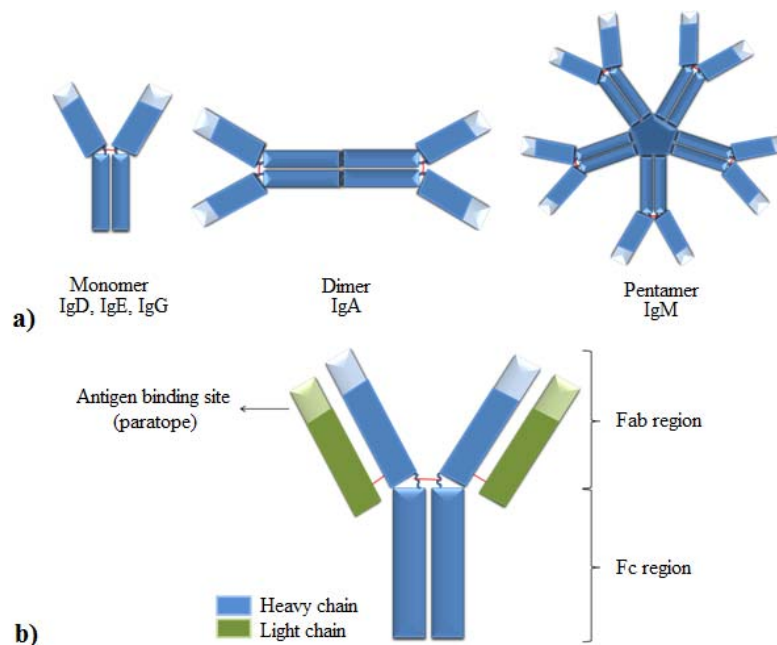


Figure 1. Scheme of mammal antibody isotypes and monomer structure. There are five different isotypes of antibodies in mammals (a): monomer (IgD, IgE, IgG), dimer (IgA) and pentamer (IgM). A monomer (b) is formed by a heavy (blue) and a light (green) chain and two different regions: antigen-binding fragment (Fab) and crystallisable fragment (Fc). Adapted from Cole et al. (1984).

The region on an antibody that binds to the antigen is called antigen-binding fragment, *Fab region*. It is composed of one constant and one variable domain of each of the heavy and the light chain. These domains shape the paratope. The two variable domains bind the epitope on the specific antigen (Cole et al., 1984).

The crystallisable fragment region, *Fc region*, is the tail region of the antibody that interacts with cell surface receptors, called Fc receptors, and some proteins of the complement

system. This property allows the antibodies to activate the immune system. The Fc region is composed of two heavy chains that contribute two or three constant domains depending on the class of the antibody. Thus, the Fc region ensures that each antibody generates an appropriate immune response for a given antigen, by binding to a specific class of Fc receptors, and other immune molecules, such as complement proteins. By doing this, it mediates different physiological effects including lysis of cells, and degranulation of mast cells, basophils and eosinophils (Cole et al., 1984).

The antibodies can cross react with similar epitopes on other antigens, usually with less affinity, due to the relatively small component recognized by them on the antigen. The specificity of an antibody refers to its ability to recognize a specific epitope in the presence of other epitopes. An antibody with high specificity would result in less cross-reactivity. The binding affinity of most antibodies is influenced by conformational determinants, and antibodies may not bind to the same protein in a denatured state. Conformation may be altered by many factors, including association with other proteins, temperature, pH, salt concentration, and fixation. The measure of the binding strength of an antibody for a monovalent epitope is defined as affinity. The interaction follows the thermodynamic principles of any reversible bimolecular interaction and is described by the affinity constant K_A . The affinity constant describes the amount of antigen-antibody complex forming at equilibrium:

$$K_A = \frac{[Ab - Ag]}{[Ab][Ag]} \quad (1)$$

where K_A is the affinity constant, Ab and Ag are the molar concentrations of unoccupied binding sites on the antibody or antigen respectively, and Ab–Ag is the molar concentration of the antibody-antigen complex (Lipman et al., 2005).

The time taken to reach equilibrium is dependent on the rate of diffusion and the affinity of the antibody for the antigen, and can vary widely. The affinity constant for antibody-antigen binding can span a wide range, extending from below 10^5 L/mol to above 10^{12} L/mol. The specific association of antigens and antibodies is dependent on hydrogen bonds, hydrophobic interactions, electrostatic forces, and van der Waals forces. Although these bonds are non-covalent, some of the associations between antigen and antibody can be very strong. Affinity constants can be affected by temperature, pH and solvent. (Lipman et al., 2005; Web ref. 2, Millipore tutorial, 2012).

Most antigens are highly complex and present numerous epitopes that are recognized by a large number of lymphocytes. Each lymphocyte is activated to proliferate and differentiate into plasma cells, producing antibodies that bind to different epitopes of the antigen, called polyclonal antibodies. In contrast, monoclonal antibodies (mAbs) are produced by a single B lymphocyte clone. The main differences between monoclonal and polyclonal antibodies are described in the Table 1. The mAbs were first recognized in sera of patients with multiple myeloma in which clonal expansion of malignant plasma cells produce high levels of an identical antibody resulting in a monoclonal gammopathy. In the mid-1970s, Köhler and Milstein devised the technique for generating monoclonal antibodies of a desired specificity, for which they were awarded the Nobel prize (Köhler and Milstein, 1975). They fused splenic B cells with myeloma cells with the resulting immortal hybridomas, each producing a unique mAb (Lipman et al., 2005)

Table 1. Comparison between the main characteristics of monoclonal and polyclonal antibodies (Liddell E. et al., 1995; Web ref. 3, Abcam tutorial, 2012)

Monoclonal antibodies	Polyclonal antibodies
<ul style="list-style-type: none">• Expensive to produce;• High technology required;• Training is required for the technology use;• Time scale is long for hybridomas;• Can produce large amounts of specific antibodies;• Recognizes only one epitope on an antigen;• Once a hybridoma is made it is a constant and renewable source and all batches will be identical.	<ul style="list-style-type: none">• Inexpensive to produce;• Technology required is low;• Skills required are low;• Time scale is short;• Produces large amounts of non-specific antibodies;• Recognizes multiple epitopes on any one antigen;• Can show batch to batch variability.

The use of antibodies produced in animals (mouse, rabbit, goat) and immobilized on NPs allows the development of assays, which are specific to the analyte. For analytical purposes, monoclonal antibodies are the preference in order to avoid cross-reaction with other analytes. The procedure adopted to immobilize an antibody on a particle depends on the nature of each

particle. As a protein, an antibody has side groups from the aminoacid sequence (-SH, -NH₂, -COO⁻) that provides the anchors for the bioconjugation. The following sections describe the bioconjugation with biomolecules for gold, carbon black and polymer particles, which are of interest to this thesis.

1.2.2 Gold nanoparticles

Gold NPs, ranging from 1-100 nm, are characterized by their strong optical absorption and light scattering. In imaging applications, gold NPs are potentially a very sensitive probe that can provide elastically scattered light intensities that are orders of magnitude larger than the fluorescence emission of dyes. Nanoparticles composed of gold offer good biocompatibility, facile synthesis, and conjugation to a variety of biomolecular ligands, antibodies, and other targeting moieties. The predominant chemistry for modifying gold NPs is the interaction with thiol groups. Small molecules, polymers, and a variety of biomolecules can be anchored to gold NPs through thiol-terminated linkers. Bifunctional thiol ligands that display, for example, carboxyl or amine groups also enable further modifications using standard techniques to prepare gold NP bioconjugates (Jain et al., 2008, 2011; Algar et al., 2011). In this thesis, gold NPs were conjugated to proteins by chemisorption on the particle surface.

1.2.3 Carbon black particles

Carbon black NPs labeled with reporter molecules can serve as signaling labels in rapid diagnostic assays as an alternative to gold, colored latex, silica, quantum dots, or up-converting phosphor NPs. Carbon black can be obtained from soot, commercially available from different sources, and shows variable sizes ranging from tens of nanometers to a few micrometers. These preparations are intended for other uses, such as in toner or ink for printers or in automobile tires. The number of functional groups on these NPs is very small, precluding the possibility of the covalent attachment of proteins or DNA. Bioconjugation mainly occurs by physical adsorption. Covalent attachment between biomolecules on carbon black particles can be achieved by the adsorption of the biomolecules on the particle surface followed by glutaraldehyde coupling (Rayev et al., 2008). This procedure produces very stable bioconjugates and it was the procedure adopted in this thesis.

1.2.4 Polymer particles

Polymer and amphiphile-based NPs are currently the most prominent materials being utilized in biomedical applications. These include polymer NPs, dendrimers, liposomes, polymersomes, and micelles (Guo et al., 2003; Torchilin, 2006; Discher et al., 2006; Peer et al., 2007). The interest in these materials arises from the combination of nanoscale or microscale size with the nearly infinite diversity of physical properties and chemical functionality that can be obtained through organic chemistry. Different properties are tailored through the selection of the polymer chemical composition. Bioconjugates of polymer NPs are typically prepared to assist targeting-antibody conjugates. While there is no characteristic surface chemistry due to the diversity of materials, the introduction of carboxyl or amine groups into the polymer composition for purposes of bioconjugation is standard procedure. Overall, the bioconjugation chemistry of these NPs is generally dictated by the functional groups associated with the material (Algar et al., 2011).

The most common method to bind a polymer NP to an antibody is the cross-linking reaction between amines and carboxylic acids using carbodiimide activation with 1-ethyl-3-(3-dimethylaminopropyl)carbodiimide, EDC. The polymer NPs are commonly prepared with carboxylic acid groups. Then, the target biomolecule of interest has one or more primary amines that allow binding to the carboxylated NP. During the reaction, a reactive *o*-acylisourea intermediate is produced through the activation of carboxylic acids, followed by the peptide bond formation with the biomolecule. In some cases, it is necessary to increase the reaction efficiency by producing a more stable reactive intermediate with *N*-hydroxysuccinimide (NHS) or a sulfonated derivative. Although the succinimidyl ester intermediate is not resistant toward hydrolysis, it hydrolyzes more slowly than the *o*-acylisourea intermediate, increasing the reaction efficiency (Algar et al., 2011). The carbodiimide procedure was adopted in this thesis to bind antibodies and spacers to polymer particles. It produced stable and functional bioconjugates for an efficient performance in immunoassays, especially in point-of-care assays.

1.3 Point-of-care testing: assays on paper

Point-of-care is defined as a medical testing at or near the site of patient care. Accurate point-of-care diagnosis required for effective medical treatments often calls for

qualitative/quantitative measurements of metabolites, enzymes, and other biomarkers. For urban and rural populations in developing countries, the need for such assessments is as pressing as in the developed world. However, practical methods for detecting and quantifying analytes in the developing world must be robust, lightweight, simple to operate, and above all, low-cost (Ellerbee et al., 2009). As suggested by the World Health Organization, WHO, an ideal test for impoverished environments has to be *ASSURED*: *A*ffordable, *S*ensitive, *S*pecific, *U*ser-friendly, *R*apid and *R*obust, *E*quipment-free and *D*elivered to those who need it (Web ref. 4, WHO, 2008).

Due to the lack of convenient accurate point-of-care assessment tools in the developing world, many health risks and illnesses remain poorly defined and receive inappropriate treatment. In addition, little information about the burden of disease is available to guide population health decisions. There is an increase necessity for point-of-care tools that provide (Ellerbee et al., 2009):

- unequivocal identification of pathogen type and subtype and drug sensitivity profile;
- rapid assessment of susceptibility and immunity to health threats;
- rapid diagnosis of exposure and disease;
- rapid detection of emerging pathogens;
- rapid parallel diagnosis of multiple infectious agents;
- accurate assessment of disease stage and prognosis;
- reliable detection and management of outbreaks, emerging acute and chronic health threats.

To overcome the problems related to costs, necessity of equipment and laboratory exhausting routines, paper-based analytical devices have been widely used since the 60's for many applications (Carrilho et al., 2009; Cheng et al., 2010; Haeberle et al., 2007; Mark et al., 2010; Martinez et al., 2010), mostly for biological assays and diagnosis as point-of-care devices (Gubala et al., 2012). Many advantages can be listed by using paper as a supporting substrate for diagnostic tools (Leung, 2011):

- paper is widely manufactured from renewable resources and it is inexpensive;
- it is combustible and biodegradable;
- the porous structure of paper enables wicking of liquid which is important for lateral flow assays and chromatography applications;
- paper is also suitable for biological applications since cellulose (and derivatives) is compatible with biological samples;

- paper surface can be easily manipulated through printing, coating and impregnation and can be fabricated in large scale;
- it can be easily stored, transported and disposed;
- paper properties can be easily altered to fulfill the requirements of different applications

Recently, many works have focused on the development of low-cost paper based medical diagnostic devices, especially lateral flow immunoassays (LFIAs). These test strips have been well-established diagnostic tool in laboratory by combining the mentioned advantages of paper based tests with the specificity of antibodies. This technology offers additional advantages when compared to the conventional detection methods: it is rapid, simple and cost-effective.

1.4 Lateral flow immunoassay

The technological basis for the development of lateral flow immunoassays, also called strip tests, was created in 1980, when Leuvering and col. (1980a) reported the use of colloidal particles as labels for immunoassays (Schubert-Ullrich et al., 2009). The first and most popular application to this test format was the use of human chorionic gonadotropin for the detection of pregnancy (Leuvering et al., 1980b, 1983).

LFIA follows the same principles of an enzyme linked immunosorbent assay (ELISA). Therefore, it is important to understand this technique before a complete description of LFIA. Different approaches can be used for ELISA: sandwich, competitive and indirect. The most used approach for pathogen detection is based on sandwich ELISA (Figure 2).

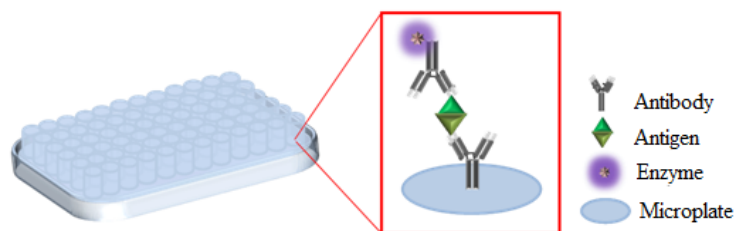


Figure 2. Scheme of a sandwich enzyme linked immunosorbent assay. Antibodies are immobilized on the microplate and the antigens from the sample are captured by the antibodies on the surface. The detection proceeds with antibodies that bind to the antigen (sandwich) and contain enzymes that catalyze a reaction with a colored product.

A capture antibody specific to the protein of interest is immobilized on a solid phase of an

ELISA microplate (e.g. microtiter plate or multiple well strips). The analytes in the sample are captured by the immobilized antibody and detected by a second analyte-specific antibody, which is enzyme-labeled and binds to the protein of interest by forming a “sandwich”. The light absorption of the product formed after adding the substrate is directly proportional to the analyte concentration. For sandwich ELISA, the antigen has to show more than one epitope, therefore this format is only applicable to large molecules such as proteins. Thus, the sandwich assay is the most common format for pathogen detection (Schubert-Ullrich et al., 2009).

Similar to sandwich ELISA, LFIA has antibodies that capture and detect the analyte (Figure 3a), but it has as principle the movement of a liquid sample along a strip made of different membranes. The LFIA is assembled by different components, including:

- Sample pad
- Conjugate pad
- Reaction membrane
- Absorbent pad
- Backing material

The membranes are assembled as shown in the Figure 3b.

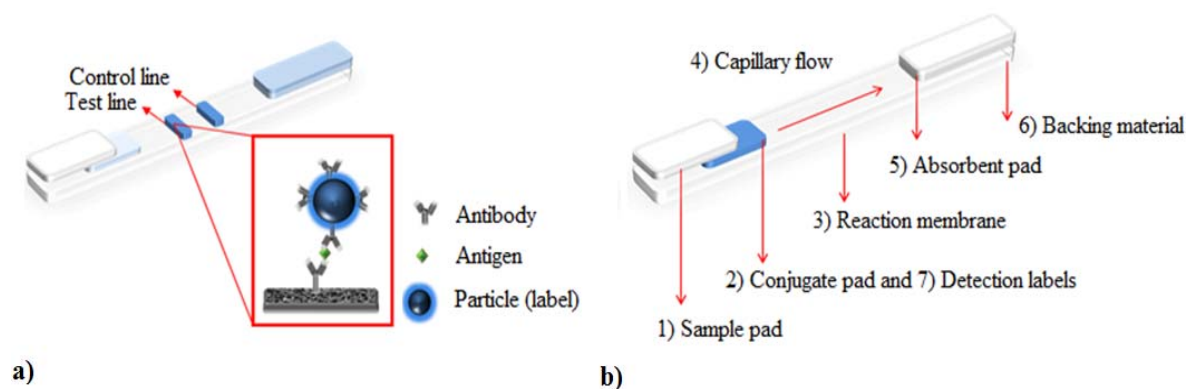


Figure 3. Scheme with the components of a lateral flow immunoassay. (a) The assay has two lines (test and control) that appear when a positive sample is added to the sample pad and it indicates that an antibody coated label bound to the antigen captured by the antibody immobilized on the nitrocellulose membrane. (b) The strip test is composed by 5 membranes: sample (1) and conjugate (2) pads, reaction membrane (3), absorbent pad (5) and backing material (6). The visible detection is based on detection labels (7) and the flow of liquid is assured by capillary forces (4).

In order to run the test, a liquid sample (whole blood, serum, urine, food extract) is added on the sample pad to remove solid materials and possible contaminants (Figure 4a). The volume used to run a LFIA usually ranges from 50 to 500 μL . Then, the liquid containing the analyte flows into the conjugate pad, where antibodies coupled to particles were previously deposited. The gold nanoparticles are the “gold standard” for LFIA. When the analytes interact with the particle coupled antibodies, they produce complexes consisting of analyte-antibody-particles (Figure 4b). These complexes move to the reaction membrane, where antibodies that bind specifically to the analyte (test line) and to the particle coupled antibodies (control line) are immobilized in the line geometry (Figure 4c). The analyte-antibody-particle complexes are trapped at the test line due to the analyte-antibody interactions. Thus, the final complex consists of antibody (immobilized)-antigen-antibody-particle. The positive result is indicated by the signal provided by the particles. In the case of gold nanoparticles, it is produced a red line and its color intensity is proportional to the analyte concentration.

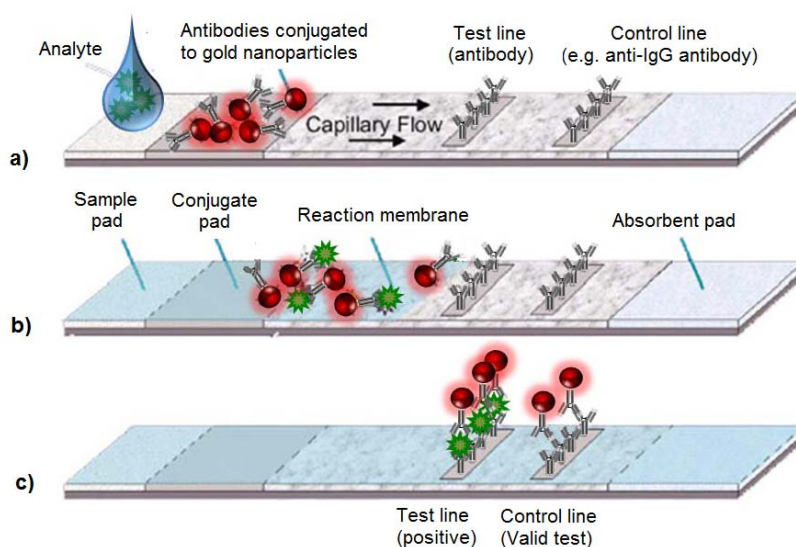


Figure 4. Operation of the lateral flow immunoassay. First, the sample is added to the sample pad (a) and starts to flow through the membrane due to capillary forces. The analyte molecules move to the second membrane, conjugate pad, where particles containing antibodies specific for the analyte are deposited. The analyte interacts with the antibody coated particle, producing the complex: analyte-antibody-particle. The complexes flow into the reaction membrane (b), where antibodies specific to the analyte (test line) and to the antibody from the particles (control line) are immobilized in line format. In the first line, the analyte-antibody-particle complexes are trapped by antigen-antibody interactions and develop a signal, which is characteristic of the particles (c). Most of the commercial tests are based on gold nanoparticles, developing red line as a positive result. The antibody coated particles that do not bind to the analyte are trapped in the control line by antibody-antibody interactions. The excess of liquid is absorbed in the absorbent pad.

This sandwich format is also only applicable for analytes with more than one epitope (high-molecular mass analytes) (Schubert-Ullrich et al., 2009). The antibodies coupled to a particle that did not bind to the antigens pass through the test line and achieve the control line, where they are trapped by antibody-antibody interactions. The signal response at the control line confirms the proper flow of the liquid through the strip and it works as the positive control (Posthuma-Trumpie et al., 2009). More test lines can be applied, allowing multianalyte testing (Snowden et al., 1991; Zhang et al., 2006) or for semi quantitative evaluation of the response (Laitinen et al., 1996a; Cho et al., 2001). The various elements will be discussed in more detail in the section 1.6.

When the analyte has low molecular weight and only one epitope, the format is restricted to the competitive design. In this layout, antibody is sprayed at the test line, and then a mixture of sample analyte and labeled analyte is applied at the conjugate pad. The sample analyte and labeled analyte compete for binding sites on the antibody at the test line (Laitinen et al., 1996b). In the competitive LFIA format the response is negatively correlated to the analyte concentration (i.e. more analyte present, less signal; no analyte gives the highest signal). For analytes with more than one epitope, the sandwich format is applicable. The response is directly proportional to the amount of analyte in the sample (O’Keeffe et al., 2003). The preferred layout is dependent on the particular application (Posthuma-Trumpie et al., 2009).

LFIA technology is currently widely applied in different fields, including diagnostics, detection of specific pathogens such as biowarfare agents, presence of toxic compounds in food, feed or environment and abuse of (illicit) drugs. They are especially designed for single use at point of care/need, i.e. outside the laboratory. Applications are often designed where an on/off signal is sufficient and the results are usually provided within 10–30 min (Posthuma-Trumpie et al., 2009).

1.5 Immunospot assay

The principle of an immunospot assay is similar to the LFIA, but without a mobile phase moving up the test strip. The term immunospot has been used to refer to a method, where capture antibody is immobilized on the membrane. After the incubation with the liquid sample, the membrane is immersed in the solution containing the detection antibodies. The detection antibodies are usually labeled with an enzyme which subsequently reacts with a

substrate to form a colored product (Bathoorn et al., 2011; Franci et al., 1986). NPs can be also used as detection labels. In such “sandwich” assays, the absorbance of the product is directly proportional to the concentration of the analyte present in the sample.

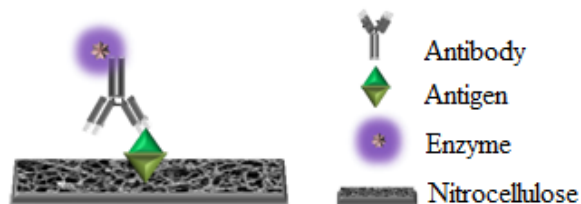


Figure 5. Scheme of an immunospot assay. The antigen from the sample is spotted on the nitrocellulose surface and interacts with the fibers. The detection proceeds with antibodies that bind to the antigen and contain enzymes that catalyze a reaction with a colored product.

An immunospot assay can also be performed by depositing the sample directly at the membrane (Figure 5). The use of paper, such as nitrocellulose membranes, has provided a useful and simple base for fast and low cost tests (Liu et al., 2011; Martinez et al., 2010). This format is similar to indirect ELISA and it is used when the analyte has high molecular weight like proteins. The analysis time for such immunospot assay ranges from 10 min up to 3 h and depends on the number of incubation cycles involved and the time needed for all incubations.

Similar to LFIA, immunospot assays provide qualitative or semi quantitative results (Schubert-Ullrich et al., 2009) and do not include flow steps. In the next section, a detailed explanation of LFIA components is described. Many characteristics required for LFIA are also necessary for ISA, although flow requirements are dispensable.

1.6 Components of lateral flow immunoassay

The function and characteristics of each component is described in the next sections with numeric references from the Figure 3.

1.6.1 Sample pad: blood filter matrices

The sample pad is a membrane that stores chemicals to increase the wettability and it also filtrates solids and contaminants from the sample. For analytes found in serum, a highly desirable performance assigned to a LFIA would be its ability to accommodate whole blood

as a sample. The sample pad should be capable of separating cells from serum or plasma so that enough volume of sample is generated to run the test. Efficient separation of blood cells from serum is extremely difficult. Blood contains 35% to 45% solids, mostly as red blood cells, meaning that a 200 μL aliquot of blood would be expected to yield at most 130 μL if the separation was 100% efficient. The filter material must be capable to work over the full range of blood variability, yielding enough serum to fill the bed volume of the entire test strip reproducibly and with the same flow kinetics. Nowadays, the most efficient sample pad consists of glass fiber (Ponti et al., 2009; Web ref. 5, Millipore protocol, 2008).

1.6.2 Antibodies and conjugate pad

Antibodies used in LFIA must have sufficient sensitivity, specificity, purity, and stability to accomplish the performance requirements of the test. Depending on the assay design, antibodies may be used as the capture reagent at the test line, as the conjugate on the detector particle, or both. Minimally, the antibody must remain reactive after being adsorbed to a solid surface, retain its structural integrity when completely dried, and then be instantly reactive when rehydrated by the sample. While the formation of an immunocomplex at the test line is most commonly used as the result indicator, it is theoretically possible to achieve a result using any ligand recognition system where a detector particle becomes bridged to a capture reagent on the membrane. In such systems the reagents employed, whether purified from a natural source or prepared as a synthetic construct, are subject to the same requirements for sensitivity and stability as antibodies (Ponti et al., 2009; Web ref. 5, Millipore protocol, 2008).

The membrane and buffer used for dilution of the capture reagents have to be optimized to allow high protein immobilization, maintenance of reagent reactivity, and no alteration of the membrane flow properties. The most common membrane is constituted of glass fiber, but also polyester pad can be chosen with good results. Some capture reagent may show many possibilities in the buffer formulation, but certain antibodies and synthetic constructs may require a specific formulation to maintain structural stability and reactivity. Problems can arise from chemical interactions that occur during evaporation, when the concentration of the salts from the buffer becomes transiently very high. For example, if the reagent solution is buffered with a primary amine such as tris(hydroxymethyl)aminomethane (TRIS) or glycine, salt bridging can occur between acidic amino acid residues (glutamic acid and aspartic acid) in the capture reagent and the $-\text{NH}_3^+$ group of the buffer molecule, reducing the capture

reagent ability to bind analyte. The ionic strength of the buffer should be reduced as much as possible. Ions in solution can interfere with electrostatic interactions between the membrane and the capture reagents. In addition, physiological concentrations of buffer salts and sodium chloride promote the solubility of most proteins and reduce the hydrophobic attraction of the nitrocellulose membrane (Ponti et al., 2009; Web ref. 5, Millipore protocol, 2008).

1.6.3 Reaction membrane

For lateral flow test strips, the membrane must irreversibly bind capture reagents at the test and control lines. The polymer from which the membrane is made determines most of its binding characteristics. If the membrane undergoes a secondary process that chemically alters the polymer or buries it under a second polymer, protein binding properties may be dramatically altered. Typical polymers are nitrocellulose, polyvinylidene fluoride, nylon and polyethersulfone. For the most part, the membrane protein binding capacity is determined by the amount of polymer surface area available for immobilization. The membrane surface area is determined by pore size, porosity (amount of air in the three dimensional structure), thickness, and, to a minor extent, structural characteristics unique to the polymer (Ponti et al., 2009; Web ref. 5, Millipore protocol, 2008).

Membranes made from nitrocellulose and nitrocellulose/cellulose acetate blends are hydrophobic. They easily wet in water because detergents or surfactants have been added to the membrane during production. A minimum concentration of surfactant or detergent is needed to make the membrane wettable. Once this concentration is reached, further increases have little impact on wettability. Surfactants and detergents can affect protein adsorption, whether derived from the membrane or included in the reagent buffer. If their concentration in the membrane is too high, they will prevent adsorption by masking the nitrocellulose. Tween 20, Triton X-100, glycerin, polyvinyl alcohol (PVA), polyvinylpyrrolidone (PVP), and polyethylene glycol (PEG) can reduce protein binding by adsorbing to the membrane preferentially or forming a complex with a protein molecule before it adsorbs. Their use should be minimized or avoided completely after the capture reagents have been immobilized and fixed. If they are applied to the membrane as part of a blocking process, their concentrations should be kept as low as possible to prevent displacement of the capture reagent (Ponti et al., 2009; Web ref. 5, Millipore protocol, 2008).

Membrane thickness has mainly three impact aspects on the LFIA performance:

- *Impact on the bed volume:* the bed volume is directly related to the thickness. As the thickness increases, the bed volume increases, since the three dimensional space equals the length of the strip times the width times the thickness. The bed volume can be increased by the use of an absorbent pad at the end of the membrane strip. Under these circumstances, the total volume of sample taken up by the strip is governed mainly by the bed volume of the absorbent pad (Ponti et al., 2009; Web ref. 5, Millipore protocol, 2008);

- *Impact on the width of the test and control lines:* since the bed volume increases with thickness, the width of the test and control lines can be influenced. In most instances, the capture reagents are applied to the membrane at a constant volume per unit distance. The liquid is absorbed into the membrane, displacing the air from a comparable volume within the pores. The liquid usually penetrates down into the membrane and then moves laterally. Spreading of the reagent on relatively thinner membranes will be greater than on relatively thicker membranes because there is less depth to allow downward penetration of the liquid. If the same mass of capture reagent is spread out over a wider area, the detector reagent will be similarly diffused, the net result being less color intensity and lower sensitivity (Ponti et al., 2009; Web ref. 5, Millipore protocol, 2008);

- *Impact on signal visibility:* thicker membranes absorb more sample, thereby increasing the mass of analyte that passes by the capture line. The signal should also be intrinsically stronger. Both of these potential advantages are negated by a physical limitation of the membrane. Due to the opacity of the nitrocellulose, detector reagent bound at the test and control lines is visible only if it is located near the surfaces of the membrane. In some cases, the antibody may be more concentrated on the side to which it is applied; but for the most part, no discernible gradient is observed. Consequently, detector reagent is captured evenly through the depth of the membrane. Relative to visualization, however, any detector reagent bound deeper than $\sim 10 \mu\text{m}$ from the surface becomes invisible to the user, as its color is masked by the membrane opacity. Since the visible depth is constant for a given membrane, the amount of visible signal is inversely proportional to membrane thickness (Ponti et al., 2009; Web ref. 3, Millipore protocol, 2008).

1.6.4 Capillary flow rate

In LFIA, the sample solution is absorbed by the membranes as a result of capillary action. The lateral flow in the membranes can be modeled by Darcy's law (Masoodi et al., 2010),

$$Q = \frac{KA' \Delta P}{\eta L} \quad (2)$$

where Q is the volumetric flow rate, K is the permeability of the paper, A' is the cross-sectional area perpendicular to flow, ΔP is the pressure gradient, η is the viscosity of the solution and L is the height of the liquid. Assuming that there are no applied pressures and neglecting gravitational terms, ΔP can be calculated using the Laplace equation,

$$\Delta P = \frac{2\gamma \cos \theta}{r} \quad (3)$$

where γ is the surface tension of the solution, θ is the contact angle and r is the effective pore radius of the filter paper. Capillary forces are responsible for the speed, or capillary flow rate, at which a sample front moves along a membrane strip when liquid is introduced at one end. This value is very difficult to measure accurately since the rate decays exponentially as the liquid moves further along the membrane. An easier parameter to measure is the capillary flow time, the time required for liquid to move along and fill completely a strip of defined length. The flow rate of a membrane depends on the aggregate properties of the porous structure. Ultimately, the capillary flow rate is determined by the overall distribution of pore sizes and not of the single largest pore. As the aggregate pore size increases, the flow rate of the membrane increases. All other parameters (pore size, pore size distribution, thickness) being equal, capillary flow rate increases linearly with increasing porosity. Capillary flow rate is the most critical performance parameter of the membrane due to the effective concentration of analyte in the sample being inversely proportional to the change in flow rate. In a lateral flow test strip, the antigen is unable to bind once it passes the immobilized antibody, because test strips are designed to flow in only one direction. As a consequence of this strip property, the effective antigen concentration decreases with the increase in flow rate because of the reduced length of time that the components of the reactive pair are close enough to bind to each other. The amount of complex formed is a relation among the rate constant related to the affinity of the antibody for the antigen and the concentrations of the reactants (Ponti et al., 2009; Web ref. 5, Millipore protocol, 2008):

$$R = k[\text{Ab}][\text{Ag}] \quad (4)$$

where R is the amount of formed complex, k is the rate constant related to the affinity of the antibody for the antigen, [Ab] and [Ag] are the concentration in mol/L of the antibody and the antigen.

The capillary flow rate decreases exponentially as the distance of the sample front from the origin increases. This means that the placement of the test line has a significant impact on achievable sensitivity. As the capture line is placed further from the origin, the flow rate at which the analyte passes the capture reagent line is slower; and the effective concentration of analyte in the sample is higher. For this reason, it is advantageous to locate the test line relatively far up the strip. Furthermore, a given volume of liquid spreads out further on the membrane when the capillary flow rate increases, maintaining other physical properties constant. Reagent lines applied to faster flowing membranes will be wider than the same lines applied to slower flowing membranes. This causes the signal to be spread out over a wider area, making it more difficult to visualize a weak signal (Ponti et al., 2009; Web ref. 5, Millipore protocol, 2008).

1.6.5 Absorbent Pad

Absorbent pads, when used, are placed at the distal end of the test strip. The primary function of the absorbent pad is to increase the total volume of sample that can be allowed to enter the test strip. This increased volume can be used to wash out unbound detector particles from the test and control lines, thereby lowering the background and enhancing assay sensitivity. Since the volume of sample that contributes to the signal is controlled by the volume required to solubilize the detector particles, the addition of the absorbent pad may not have a dramatic impact on overall assay sensitivity. If the strip design does not include an absorbent pad, the volume of sample analyzed in the strip is determined solely by the bed volume of the membrane.

1.6.6 Backing material

The reaction membrane is often thin and fragile, so it is attached to a plastic or nylon basic layer to allow cutting and handling, besides supporting the other membranes. The film

provides a high level of mechanical strength, making it nearly impossible to break the membrane during routine processing operations. Membranes without a backing card, in comparison, are extremely fragile and can be very difficult to manipulate during test strip assembly. Using backing card, it is common to provide an additional treatment to the nitrocellulose membrane with a thin film that acts as a barrier to chemical contamination from adhesives that are used to mount the membrane on cards. Although adhesives typically do not penetrate into a microporous membrane more than a few microns, volatile organic solvents released from the adhesive during long term storage may adsorb to the nitrocellulose. This can alter the membrane wetting properties and adversely affect lateral flow properties (Web ref. 3, Millipore protocol, 2008).

1.6.7 Particles used as detection labels

Various types of detector reagents can be used for the visualization of the signal in LFIA. Particles ranging from 10 nm to 1 μ m are commonly used in commercially available tests. Gold nanoparticles are the most used detection particle due to their optical properties and they are considered “gold standard” in LFIA (Verheijen et al., 1998). Some other examples are latex (Gussenhoven et al., 1997), selenium (Lou et al., 1993), carbon (Lonnberg et al., 2001) and liposomes (Zaytseva et al., 2004). Latex particles and liposomes incorporate dyes or fluorophores, which allow visualization and, when applicable, quantitation of the response. The newest labels contain or are composed of quantum dots (Goldman et al., 2004). Other possibilities include enzyme conjugates, other colloidal metals, dye sacs, fluorescent particles, and magnetic particles (Posthuma-Trumpie et al., 2009).

1.7 Detection techniques

The detection limit in LFIA is related to the detection particles, which must be inexpensive and provide a high signal (absorption, fluorescence, phosphorescence, magnetic field). Particles that provide a colorimetric signal are preferable due to the ease of visualization and no need for equipment, according to ASSURED criteria. The coupling of colored nanoparticles to the detection molecule is one of the most powerful techniques for an immediate readability of the tests. The production of a stable and sensitive immunosensor based on real color appearance requires a criterious screening of possible colored labels.

Fluorescent particles are also a promising option for LFIA owing to the high sensitivity. In addition, inexpensive apparatus can be used to excite the fluorophores, such as fluorescent lamps or LED, and visually read the emission in the visible spectral range. In the next section, the basic theories of light absorption and luminescence are described.

1.7.1 Colorimetric detection

Absorption of electromagnetic radiation is the way in which the energy of a photon is taken up by matter, typically the electrons of an atom. The absorption of light during wave propagation attenuates the beam in accordance to the absorption law, Beer-Lambert law. This law quantitatively describes how the attenuation depends on the concentration of the absorbing bodies and the path length over which the absorption occurs. Due to the interaction between the photons and absorbing particles, the radiant power of the beam decreases (Skoog et al., 2004). The transmittance of the solution is the fraction of incident radiation transmitted by the solution and it is expressed as:

$$T = \frac{P}{P_0} \quad (6)$$

where T is the transmittance, P is the beam after passing through the absorbing solution and P_0 is the initial beam.

The absorbance of a solution is related to the transmittance in a logarithmic manner:

$$A = \log \frac{P_0}{P} = \epsilon bc \quad (7)$$

where A is the absorbance, ϵ is a proportionally constant named molar absorptivity, b is the path length and c is the molar concentration of the absorbing structure (Skoog et al., 2004).

Gold nanoparticles at 40 nm are the standard labels for LFIA and show high optical absorption at 528 nm. This optical property arises from the phenomenon of surface plasmon resonance (SPR), wherein the conduction band electrons of a gold NP oscillate collectively and in resonance with certain wavelengths of incident light (Jain et al., 2008) The wavelength-dependent intensity of the SPR is very sensitive to changes in the dielectric environment surrounding the gold NP, as well as plasmonic coupling between NPs (Algar et al., 2011).

Carbon black is a refractory and most strongly light-absorbing component of soot, a nearly omnipresent by-product of inefficient combustion (Schwarz, et al., 2008). Carbon black is highly extended fused benzene rings terminated with quinone groups and phenol groups. This structure allows the π electrons to delocalize over large areas absorbing all light at the visible region.

1.7.2 Fluorescence detection

Fluorescence is an emission process in which atoms or molecules are excited by the absorption of an electromagnetic radiation beam. The excited species then relax to the ground state, giving up their excess of energy as photons. Fluorescence occurs rapidly and it is generally complete in about 10^{-5} s from the time of excitation. The lifetime of an excited specie is brief due to several mechanisms that an excited molecule gives up its excess of energy and relaxes to its ground state. Two of the most important mechanisms are nonradioative relaxation and fluorescence emission (Figure 6).

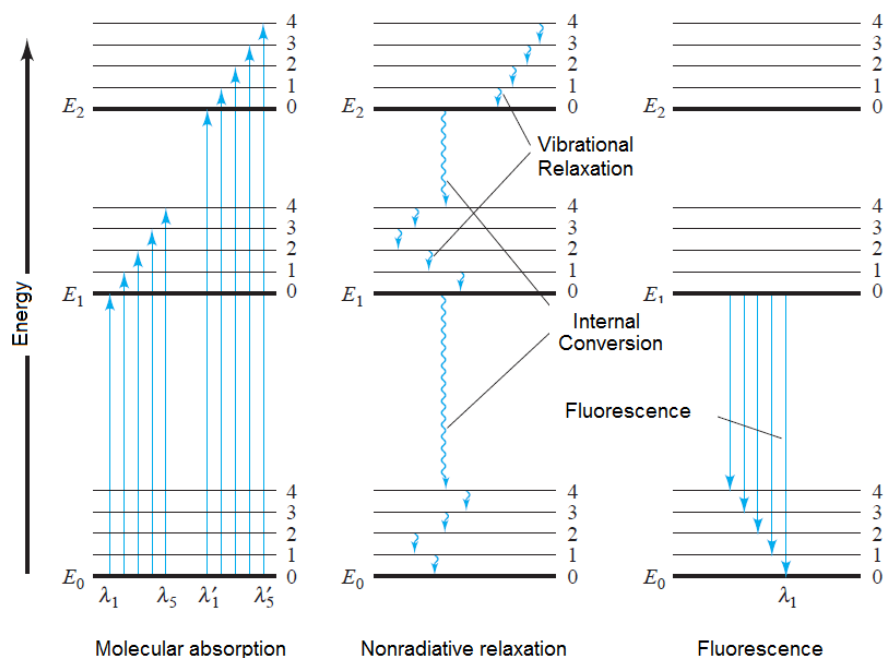


Figure 6. Partial energy diagram for a hypothetical molecular species. Three electronic energy states are shown, E_0 , E_1 , E_2 . E_0 is the ground state, and E_1 and E_2 are excited states. Each state is shown as having four excited vibrational levels. The diagram also indicates the nonradiative relaxation and fluorescence phenomena.

Vibration relaxation, depicted by the short wavy arrows between vibrational energy levels, occurs during collisions between excited molecules and molecules of the solvent. During the

collisions, the excess of vibrational energy is transferred to solvent molecules in a series of steps. The average lifetime of an excited vibrational state is only about 10^{-15} s. Nonradiative relaxation between the lowest vibrational level of an excited electronic state and the upper vibrational level of another electronic state can also occur. This type of relaxation is called internal conversion, depicted by the two longer wavy arrows, and it is less efficient than vibrational relaxation with a life time between 10^{-9} and 10^{-6} s. The effect of both nonradiative relaxations is a rise in the temperature of the medium (Skoog et al., 2004).

Irradiation of a fluorophore between the wavelengths λ_1 to λ_5 , as shown in the Figure 6, results in the momentary population of the vibrational levels of the first excited state E_1 . When higher energy is used (λ'_1 to λ'_5), the vibrational levels of the higher energy electronic state E_2 become populated. Bands of radiation are produced when molecules relax from the lowest vibrational state of an excited state E_1 to the many vibrational levels of the ground state E_0 . Like molecular absorption bands, molecular fluorescence bands are formed by a large number of closely spaced lines that are usually difficult to resolve. The transition from E_1 to the lowest vibrational state of the ground state (λ_1) has the highest energy of all the transitions in the band. As a result, all the other lines that terminate in higher vibrational levels of the ground state are lower in energy and produce fluorescence emission at longer wavelength than λ_1 . Thus, molecular fluorescence bands consist of longer wavelengths than the band of absorbed radiation responsible for their excitation, the Stokes shift (Skoog et al., 2004).

The power of fluorescence radiation (F) is proportional to the radiant power of the excitation beam absorbed by the system:

$$F = K'(P_0 - P) \quad (8)$$

where P_0 is the power of the beam incident on the solution and P is its power after it passes through the medium. The constant K' depends on the quantum efficiency of the fluorescence. To relate F to the concentration c of the fluorescent structure, equations (7) and (8) are combined:

$$F = K' P_0 (1 - 10^{-\epsilon bc}) \quad (9)$$

In fluorescence, the radiation power emitted is directly proportional to the source intensity, but absorbance is essentially independent of source intensity, because it is related to the ratio of radiant powers. Fluorescence is recognized as one of the most sensitive detection methods

because the emission signal is measured above a low background level. It is inherently more sensitive (~1000 times) than absorption methods.

Therefore, fluorescence based detection systems are very promising for immunoassays in order to produce assays with lower detection limits than obtained with colorimetric detection based tests. The only concern of fluorophores is the easy decomposition in presence of oxygen molecule, a photobleaching phenomenon. Thus, the incorporation of fluorophores inside a particle decreases this effect due to the limited oxygen diffusion. In addition, the incorporation of fluorophores within a particle allows enhancing the sensitivity of assays. In this case, when an antibody coated fluorescent particle binds to the antigen, numerous fluorophore molecules contribute to the signal. On the other hand, in conventional assays using antibodies labeled with fluorophore molecules, only a few fluorophores per analyte contribute to the signal (Linares et al., 2012b).

1.7.3 Charge-transfer absorption and phosphorescence

For high sensitivity purposes, charge-transfer absorption is particularly interesting due to the usual high molar absorptivities ($> 10,000 \text{ L mol}^{-1} \text{ cm}^{-1}$). Many inorganic complexes exhibit this type of absorption and are named charge-transfer complexes. A charge-transfer complex consists of an electron-donor group bonded to an electron acceptor. When the light is absorbed, an electron from the donor is transferred to an orbital that is largely associated with the acceptor. The excited state is thus the product of a kind of internal oxidation/reduction process. Due to the high absorptivity, particles containing inorganic complexes have been successfully used for biomedical application (Lin et al., 2011).

In this thesis, $[\text{Ru}(4,4'\text{-dicarboxylate-2,2'-bipyridine})_3]^{2+}$ complex was incorporated in polymer particles and used in ISA as the detection label. The carboxylated bipyridine ligand contributes to the stability of the complex by having empty π orbitals that can bond with the metal d orbital subshell and by being a chelating ligand. Each derivative bipyridine bonds twice to the metal center through the donation of the single pair electrons on both nitrogen atoms. If one of the metal-nitrogen bonds is broken, the other metal-nitrogen bond will hold the ligand in place long enough for the broken bond to reform (Watts 1984; *Web ref. 6*).

Optical transitions result from the absorption of photons and transfer of electrons to higher energy molecular orbitals. The degree of allowedness depends on the symmetry and the multiplicity (or electron spin count) of the different states. Allowed transitions have no

change in electron spin ($\Delta S = 0$). Forbidden transitions have a difference in electron spin between the ground and excited states. This means that only transitions from the singlet ground state, i.e. all electrons paired, to singlet excited states are allowed. Transitions from the singlet ground state to triplet excited states with two unpaired electrons, are forbidden. The allowedness of a transition can be inferred from the magnitude of the extinction coefficient for a given band in the optical absorbance spectrum. Allowed transitions have values of molar extinction coefficient in the thousands ($\text{L mol}^{-1} \text{cm}^{-1}$), forbidden transitions have much smaller values (Watts 1984; *Web ref. 6*).

The lowest energy excited state of ruthenium(II) tris-bipyridine (Figure 7) is a metal-to-ligand charge transfer state, MLCT. This state is formed by the promotion of an electron from the filled metal highest occupied molecular orbital, HOMO, to an empty ligand π^* lowest unoccupied molecular orbital, LUMO. This transition is fully allowed by the laws of quantum mechanics (symmetry and spin selection rules) and the transition has a large extinction coefficient. The value of the extinction coefficient is in the thousands for MLCT transitions and much smaller for d-d or metal centered transitions. The MLCT excited state is not strongly anti-bonding with respect to the metal-ligand bond. The π^* character of the LUMO is primarily with respect to internal ligand pi bonds and not metal-ligand bonds. Creation of the MLCT excited state does not lead to the decomposition or photolysis of the complex to an appreciable degree (Watts 1984; *Web ref. 6*).

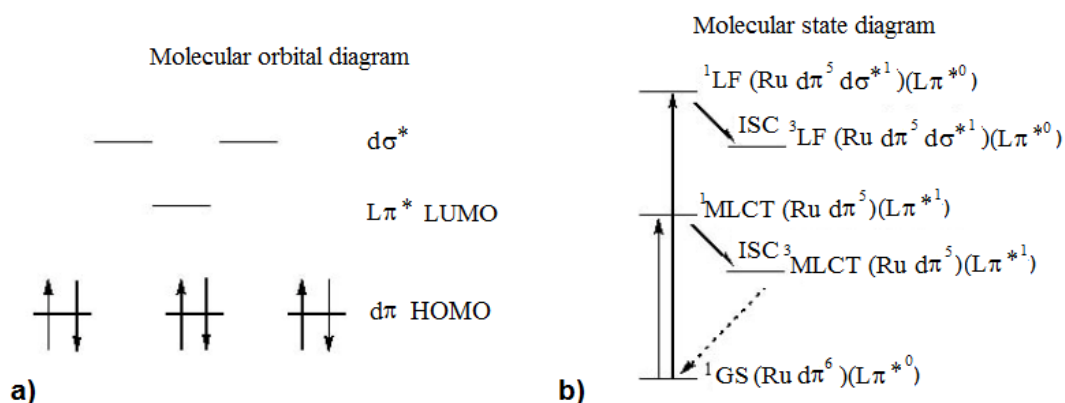


Figure 7. Molecular orbital diagram for ruthenium (II) polypyridine diagram. Scheme (a) of the molecular orbitals and electron distribution at the ground state (GS). After light absorption (b), allowed electron transitions occur (solid vertical arrows), but intersystem crossing (ISC) takes place in which singlet states convert to triplet states. A forbidden process (long lived emission) generates phosphorescence emission (dashed diagonal arrows). Adapted from *Web ref. 6*.

This state is formed by the promotion of an electron from the filled metal HOMO to the higher energy d^* orbital. This excited state is forbidden by the symmetry selection rules of quantum mechanics and a transition of this type will have a small extinction coefficient. In this case the anti-bonding character of the orbital is with respect to the metal-ligand bond. The probability of ligand loss (photolysis of the complex) increases with the formation of the ligand field (LF) excited state (Watts 1984; *Web ref. 4*).

After the allowed singlet ground state to singlet excited state transition, the excited molecule relaxes to lower energy states. One possible relaxation is called intersystem crossing and results in the relaxation of a singlet state to a lower energy triplet state. For quantum mechanical reasons, primarily due to exchange integrals, triplet states are at lower energy than the singlet states of the same orbital parentage. On the state diagram above this is clearly seen. The singlet and triplet MLCT excited states have the same occupied orbitals, they only differ in energy due to the differences in electron spin pairings (Watts, 1984; *Web ref 6*).

For ruthenium polybipyridine, the intersystem crossing efficiency is approximately 100%. This means that all singlet MLCT created upon absorption of a photon by the ground state become triplet MLCT states through intersystem crossing. The triplet MLCT is a long lived luminescent excited state, because relaxation to the singlet ground state is a slow process due to the difference in spin states. The relaxation process has a partially forbidden character. Ruthenium tris-bipyridine has a quantum yield of emission of about 8%. Only a small fraction of molecules go from the triplet excited state to the singlet ground state through the radiative mechanism. The majority of molecules relax to the ground state through non-radiative, vibrational relaxation processes. Release of a photon with an accompanying spin change is called phosphorescence (Watts 1984; *Web ref. 6*).

1.8 Dengue fever

Dengue fever (DF) is a tropical disease caused by a virus and transmitted mainly by *Aedes aegypti*, a species of mosquito with a global distribution. DF has emerged as a rapidly spreading vector-borne disease affecting mainly poor, urban populations and it is also the leading cause of hospital admissions in several countries (web ref. 7, WHO, 2010). The incidence of DF has dramatically grown over the world in recent decades. Over 2.5 billion people are now endangered from dengue. The World Health Organization (web ref. 8, WHO, 2012) currently estimates 100 million cases of DF. About 500,000 cases are dengue

hemorrhagic fever (DHF), resulting in 5% of annual mortality. The disease is now endemic in more than 100 countries in Africa, America, Eastern Mediterranean, South-east Asia and Western Pacific. The threat of a possible outbreak of DF now exists in Europe and local transmission of DF was reported for the first time in 2010. For DHF, early medical care can save lives, decreasing mortality rates to less than 1% (Allwinn, 2011).

The virus belongs to the family Flaviviridae and comprises four (DV-1–DV-4) distinct serotypes. The virus is composed of a nucleocapsid that is surrounded by a lipid membrane and covered by glycoproteins. Its genome consists of a single-stranded RNA that encodes a polyprotein precursor of viral proteins. This precursor is cleaved by host and viral proteases, which generates three structural proteins (C, capsid; prM, premembrane; and E, envelope) and seven nonstructural proteins (NS1, NS2a, NS2b, NS3, NS4A, NS4B and NS5). The structural proteins are incorporated into the mature infective virus, while the nonstructural proteins are involved in the replication and assembly of the virus.

Once the mosquito bites a person and the virus is carried into the body, it binds to Langerhans cells, which are in the skin and identify pathogens. The virus enters the cells through an interaction between the viral proteins and the membrane proteins on the Langerhans cell. The membrane proteins are specifically the C-type lectins, called dendritic cell-specific intercellular adhesion molecule-3-grabbing non-integrin (DC-SIGN) and mannose receptors. The DC-SIGN, as a non-specific receptor for foreign material on dendritic cells, seems to be the main point of entry. The dendritic cell moves to the nearest lymph node. Meanwhile, the virus genome is translated in membrane-bound vesicles on the endoplasmic reticulum of the cell, where the cell protein synthesis apparatus produces new viral proteins that replicate the viral RNA, forming viral particles. Immature virus particles are transported to the Golgi apparatus, the part of the cell where some of the proteins receive necessary sugar chains (glycoproteins). The new mature viruses bud on the surface of the infected cell and are released by exocytosis. They are then able to enter other white blood cells, such as monocytes and macrophages (Rodenhuis-Zybert et al., 2010).

The initial reaction of infected cells is to produce interferon, signaling molecule that raises a number of defenses against viral infection through the innate immune system by increasing the production of a large group of proteins. Interferon also activates the adaptive immune system, which leads to the generation of antibodies against the virus as well as T cells that directly attack any cell infected with the virus. Various antibodies are generated and most of them bind closely to the viral proteins and target them for phagocytosis (ingestion by

specialized cells and destruction) (Rodenhuis-Zybert et al., 2010).

1.8.1 Disease stages

After the incubation time of 4-9 days, the first symptoms appear, including abrupt onset fever, severe headache, muscle pain, joint pain and retro-orbital pain (Figure 8).

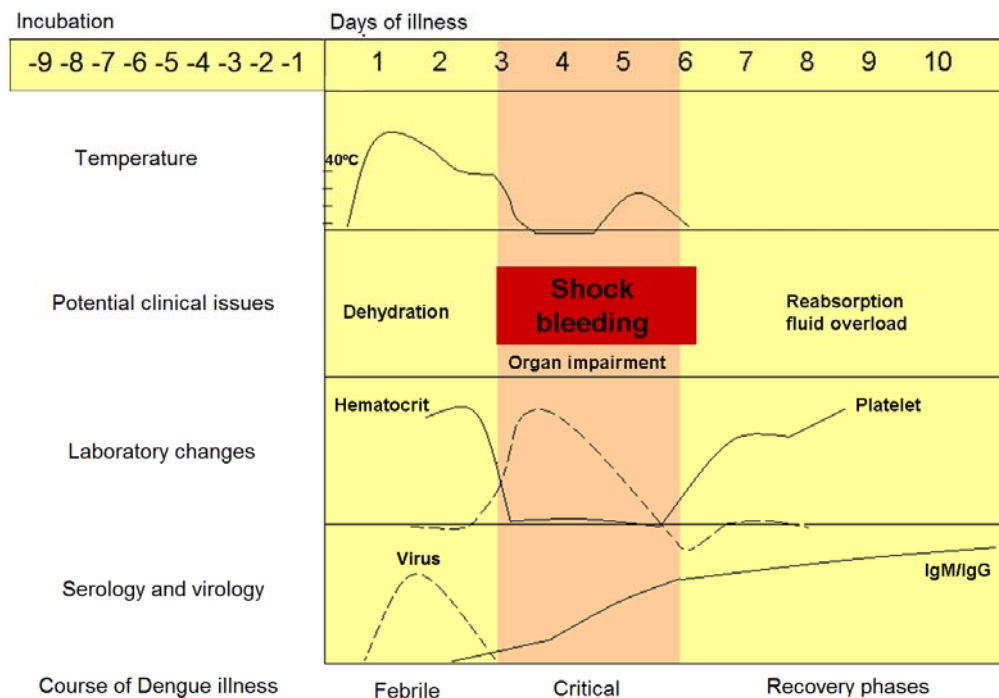


Figure 8. Characteristics of Dengue fever infection. Variation of temperature, potential clinical issues, laboratory changes and serology/virology with time dependence after the outbreak of the infection. The critical stage occurs from the third to the sixth day and it is marked by intense bleeding in case of hemorrhagic fever (Adapted from Web ref. 9).

Due to the severe musculoskeletal pain, DF is also referred as “breakbone fever”. The neutrophils (white cells related to inflammatory processes) count starts falling from day 1 and the thrombocyte (blood platelet responsible for blood coagulation) count starts falling from day 3. The thrombocyte count will keep on falling until patient temperature returns to normal. Those dengue patients who have DHF start to show bleeding in skin, nose and even gastrointestinal tract (Dengue, 2012). The critical phase starts on day 3 to 7 after onset of illness at the time of defervescence when temperature is returning to normal. There is an increase in capillary permeability associated with plasma leak from intravascular

compartment to interstitial compartment which marks the beginning of critical period and lasts for 24 to 48 hours after which plasma leak stops. Although, majority of dengue patients do not develop plasma leak, those who indeed develop worsens with fall in blood pressure and hypoproteinemia, low level of proteins in the blood. The hematocrit, volume percentage of red cells in the blood, starts rising as protein leak is accompanied by loss of water from blood making blood thicker with lower volume. Dengue shock syndrome is fatal, if it is not treated promptly. This plasma leakage is transient lasting for 24 to 48 hours and if circulatory blood volume can be maintained during these critical 48 hours, life can be saved. Then it starts the recovery phase. If the patient survives the 24 to 48 hours of critical phase, a gradual reabsorption of extravascular interstitial fluid takes place in 48 to 72 hours. Patient general condition improves and hemodynamic stabilizes (Web ref. 9).

1.8.2 Serology

Following the initial infection, the dengue virus replicates to high titers in the blood before patients present enough symptoms to go to a physician, with viremia peaking at the time or shortly after the onset of symptoms, as depicted in Figure 8. Virus remains detectable in the blood for up to 2 to 12 days after the onset of symptoms (Vaughn et al., 2000; Gubler et al.; 1981).

During the viremic phase where the virus has access to the bloodstream and starts the dengue infection, NS1 antigen is produced concomitantly during the virus replication process (Figure 9).

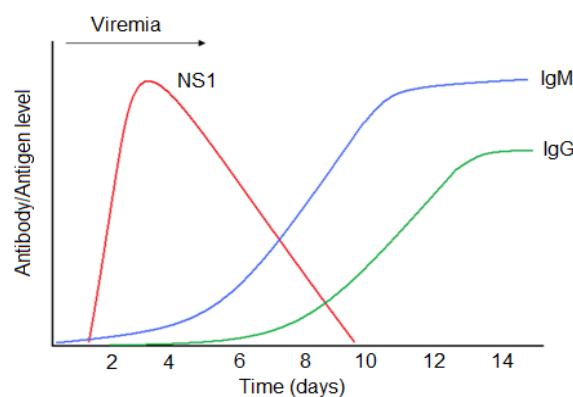


Figure 9. Target biomolecules for detection of Dengue fever infection. Antibody/Antigen level of NS1 protein and antibodies IgM and IgG in the blood stream after the outbreak of the symptoms (Adapted from Blacksell, 2012).

The NS1 antigen is a 46- to 50-kilodalton glycoprotein highly conserved for all dengue serotypes and is expressed in either membrane-associated or secreted forms (Flamand et al., 1999; Falconar et al., 1991). Soluble NS1 circulates in the serum of patients during the viremic phase of dengue virus infections and hence it is an excellent diagnostic target for acute dengue diagnosis. Difference in the persistence of soluble NS1 antigen in serum between primary (5-6 days post-onset of illness) and secondary dengue infections (6–12 days) has been noted. It is hypothesized that the presence of anti-NS1 antibodies, that are more frequently detected in dengue secondary infection (Koraka et al., 2003), modulates the formation of antibody-antigen complexes which impede the ability of the test to detect free NS1 antigen (Libraty et al., 2002; Young et al., 2000; Blacksell, 2012).

Dengue IgM antibodies are a reliable marker of recent infection but not necessarily acute infection. In primary dengue virus infections, IgM antibodies are detected following the decline of viremia between days 3–5 after the onset of infection using very sensitive detection methods, reaching peak levels approximately 2 weeks later. In dengue endemic settings, IgM antibodies may be detectable as soon as after 2-3 days of the infection and peak IgM antibody levels are usually lower than in primary infections. The IgG antibody response develops a few days after the onset of the IgM antibody response and is serotype specific. The IgG antibodies may persist for many years following a single infection. Secondary dengue virus infections generate IgG antibody response that is characterized by a rapid rise in IgG antibodies detectable at days 4-5 of illness. This production is much sooner than the normal IgG antibody response of a primary infection (Blacksell, 2012).

1.8.3 Lateral flow immunoassay based on viral NS1 protein

The most important development in dengue diagnostics in recent years is the advent of the dengue virus NS1 antigen detection. Dengue tests that detect NS1 antigen employ a number of serotype-specific anti-NS1 monoclonal antibodies to capture and detect soluble NS1 antigen in serum, plasma, or blood. ELISA is the most used method to detect NS1 protein, but LFIA is the most appropriate technology when point-of-care is necessary.

Although LFIA has been successfully used in numerous systems, its application is limited when high sensitivity is required, especially in early stage disease diagnostics. A current limitation for LFIA application related to detection limit has been reported for early stage detection of Dengue fever infection. Twelve studies evaluated a commercial strip test (Biorad)

for the diagnosis of acute dengue infection using admission samples, and the results demonstrated considerable variation in sensitivity (49.8%–98.7%) but the specificities reported were consistent for all (>90%). For 25% of the studies, the sensitivity was >89%. However, all of these studies used a skewed comparator of virus isolation, real-time polymerase chain reaction, RT-PCR, or NS1-ELISA and did not examine the possibility of false-negative results by testing paired serum samples to examine for dynamic rise in serological assays such as IgM or IgG capture ELISAs. Studies that used a more representative combination of virus or antigen detection and serology as reference comparators gave sensitivities for the Biorad strip test between 49.4% (Najioullah et al., 2011) and 78.9% (Pok et al., 2010).

The Standard Diagnostic Bioline Dengue Duo NS1 antigen detection strip was evaluated for acute dengue diagnosis in four studies with consistently high specificity estimates (96.7–100%) and sensitivities that ranged from 48.5% (Blacksell et al., 2011) to 65.4% (Wang et al., 2010) with the studies either using a combination of virus detection and serology (Wang et al., 2010; Osorio et al., 2010) as comparators or serology alone (Blacksell et al., 2011; Blacksell, 2012).

Similar limitations have been observed for other diseases, including HIV (Gray et al., 2007), influenza (Gavin et al., 2003), malaria (Murray et al., 2008), among other diseases.

1.9 Aim and structure

Based on the necessity of sensitivity improvement, this thesis aims to enhance the performance of paper based immunoassays by screening and developing nanostructures to replace the conventional gold nanoparticles in the detection system.

A brief summary of the results is presented in the next sections of this chapter:

- Section 2.1 (Chapter 2): Investigation of the most commonly used detection labels for LFIA based on colorimetry and comparison of their performance in terms of detection limit (section 2.1.1). The best label, carbon black, was used to develop an immunospot assay and a lateral flow immunoassay for Dengue fever detection. These last results are described in the Chapter 5, but it was placed in this section to facilitate the comprehension (section 2.1.2);
- Section 2.2 (Chapter 3): Development of an immunospot assay based on fluorescence for Dengue fever detection, addressing the challenge of fast and reliable tests for

low resources laboratories in epidemic periods;

- Section 2.3 (Chapter 4): Development of core-shell polymer particles as a detection label to overcome particle agglomeration for paper based tests;
- Section 2.4 (Chapter 5): Development of novel detection label for LFIA by combining colorimetry and fluorescence in order to produce test with high sensitivity.

A diagram summarizing the thesis structure is shown in the Figure 10.

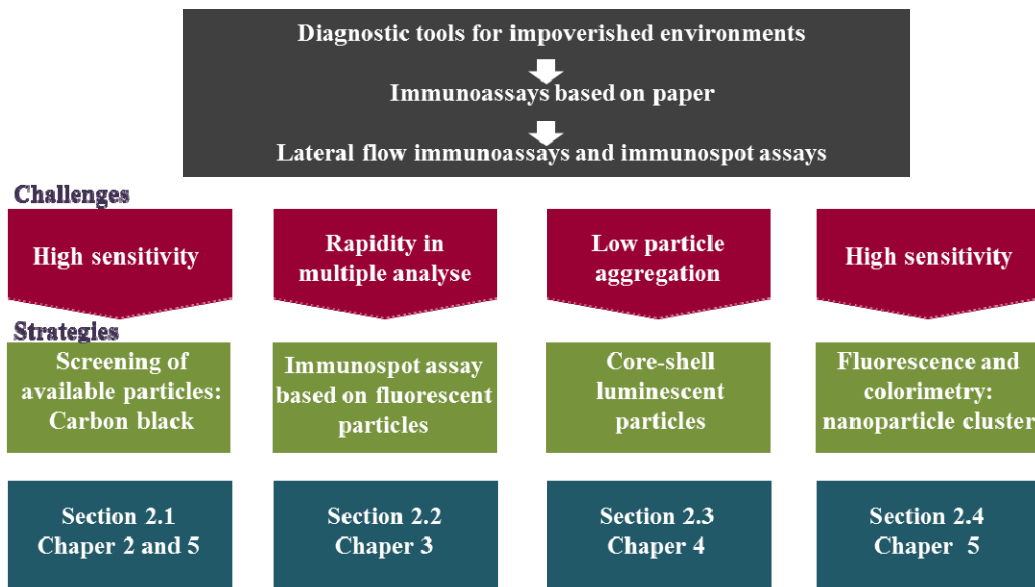


Figure 10. Diagram of the thesis organization. Description of the challenges and strategies of immunoassays based on paper for impoverished environments discussed in the thesis.

2. Results and Discussion

In the second part of this chapter, the main results are briefly described in four sections according to the detection method used (colorimetry, fluorescence, phosphorescence and colorimetry combined to fluorescence).

2.1 Optical based detection systems

2.1.1 Enhancement of the detection limit for lateral flow immunoassays: evaluation and comparison of bioconjugates

As described, LFIAs show limitations in applications that require high sensitivity, such as

early stage disease detection. In order to produce sensitive assays, a careful screening of detection labels has to be done during LFIA development. Although numerous particles have been already used as detection labels, there is a lack of studies to compare their sensitivities. Based on this necessity, this section compares the performance of the four commonly used labels in LFIA (more details are described in the Chapter 2):

- colloidal gold nanoparticles
- silver coated gold nanoparticles
- polystyrene beads
- carbon black

Each system was chosen according to the literature, using the most appropriate label characteristics for LFIA. For instance, gold nanoparticles with 40 nm diameter provides the most efficient flow through the membranes and high signal to noise ratio in comparison to bigger gold particles. On the other hand, due to low density, carbon black is used in bigger diameters without prevent dramatically its flow through the membranes in which pore size is 8-12 times the carbon black agglomerate diameter. The biomolecule immobilization was optimized for each particle and excess of labels was used in the experiments to ensure saturation in the nitrocellulose.

In order to compare the signal intensity for the four labels in comparable experimental conditions observed in LFIA, spot tests on nitrocellulose membrane were performed. Bioconjugates of those particles were prepared by functionalization with streptavidin and they were evaluated using the biotin-streptavidin system. Dilution series of biotinylated-bovine serum albumin (BSA) were spotted from 10 mg/mL to 0.01 $\mu\text{g/mL}$ onto the nitrocellulose membrane. Streptavidin coated particles flowed through the membranes and interacted with the biotinylated-BSA spots (more experimental details are described in the Chapter 2).

Curves comparing signal intensity for each label are presented in Figure 11. Carbon black presents the highest blackness percentage in comparison to the other labels and the difference becomes more pronounced at higher concentrations. The silver coated gold nanoparticle was the second label in signal intensity, followed by gold nanoparticle and blue-polystyrene bead. The expanded area in the graph of the Figure 12 shows the variation of gold, silver coated gold and blue polystyrene particle intensity with biotinylated-BSA concentration.

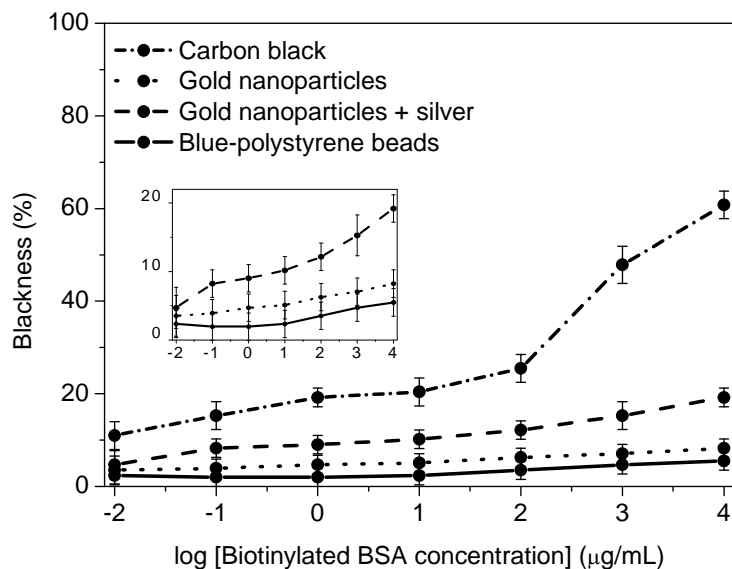


Figure 11. Comparison of blackness percentage for four different labels. Curves of blackness intensity for gold, silver coated gold, blue polystyrene beads and carbon black were acquired according biotinylated-BSA concentration after 20 minutes of label exposition. Expanded area within the graph shows blackness variation for all labels excluding carbon black.

Silver enhancement method provides an intensity superior to bare gold particles and detection limits of $1\mu\text{g/mL}$ and 100ng/mL for biotinylated-BSA, respectively. Carbon black has a visible signal until 10ng/mL of biotinylated BSA. On the other hand, blue polystyrene beads showed the lowest intensity, visually almost imperceptible when observed in low biotinylated BSA concentration (up to $100\mu\text{g/mL}$). The summary of label performance is shown in the table 2.

Table 2. Comparison of labels for LFIA based on biotin-streptavidin system.

Particles	Diameter (nm)	Detection limit for biotin ($\mu\text{g/mL}$)
carbon black	100-200 Agglomerates: 500-2000	0.01
silver coated gold nanoparticles	< 200	0.1
gold nanoparticles	39 ± 5	1
polystyrene beads	239 ± 9	100

Carbon black provides unmistakably the best signal to noise ratio and an incomparable

performance in relation to the other tested labels. In addition, it is readily available in several forms and particle sizes useful for different detection ranges (Lönnerberg et al., 2001). Based on these results, carbon black was chosen as label for Dengue fever detection, using Dengue virus NS1 glycoprotein as the biomarker. As previously described (section 1.8.2), early detection of Dengue fever can be performed by detecting NS1 protein. LFIA based on gold nanoparticles (section 1.8.3) as standard labels provide limited sensitivity for diagnosis in the first days of the disease and carbon black can overcome this limitation by lowering the detection limit of the assay.

The performance of gold and carbon black nanoparticles coated with anti-NS1 monoclonal antibodies were compared in terms of visual signal provided by each label and it is described in the next section 2.2. More details about label comparison are described in the Chapter 2.

2.1.2 Lateral flow immunoassay based on carbon black particles

In this section, the use of carbon black particles as detection labels is investigated with particular emphasis on viral NS1 protein in LFIA. Again gold NPs served as the reference for comparison in terms of sensitivity. The results described in this section are detailed in the Chapter 5, but they were summarized here to facilitate the work comprehension.

The employed assay follows the principles of lateral flow tests already described in the Section 1.4. However, owing to the fact that carbon black particles tend to agglomerate, some modifications were required. The conjugate pad was removed and the LFIA basically consisted of three parts: (i) the absorbent pad (glass fiber) to filter the serum, (ii) the nitrocellulose membrane and (iii) the absorbent pad. The test and control lines are composed of monoclonal anti-NS1 antibody and anti-streptavidin antibody, respectively.

In the actual experiment, the glass fiber pad was first immersed in the serum containing the NS1 proteins Figure 12. As the liquid flowed through the membrane, the anti-NS1 antibodies captured and immobilized the NS1 proteins from the serum. After five minutes, the pad was immersed in a dispersion containing a mixture of two differently coated carbon black detection labels, one with anti-NS1 antibodies, the other with streptavidin. On arrival at the test line, the anti-NS1 antibody coated particles were captured by interaction with the NS1 proteins. Accumulation of the captured carbon particles produced a visible black line, which provided evidence that the serum was infected with the Dengue virus. The detection limit was

determined by repeating the procedure with a series of differently diluted serum samples from an infected patient. The streptavidin coated carbon black particles were captured at the control line. The detection sensitivity could be improved by passing a washing buffer through the assay. The purpose was to transfer unbound carbon black particles from the membrane to the absorbent pad. The LFIA format with test immersion was preferred in relation to a conventional lateral flow test due to the formation of carbon black agglomerates during the drying step in the conjugate pad. This format avoids the formation of structures that block the membrane pores and consequently the flow.

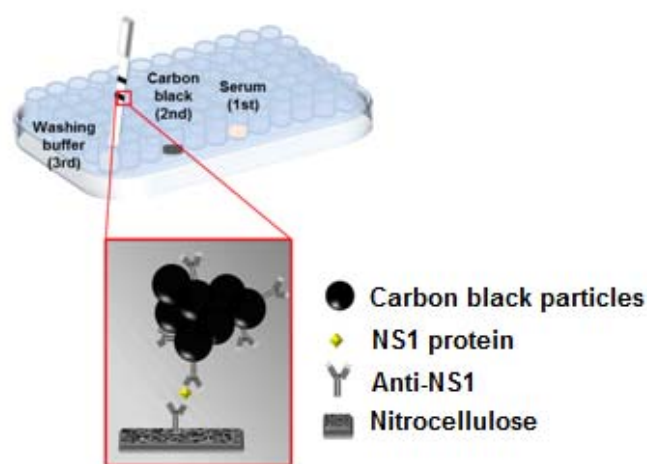


Figure 12. Scheme of lateral flow immunoassay based on carbon black. LFIA in a microplate after dipping one extremity in the serum, carbon black dispersion and washing buffer solution. The zoom of the test line shows the carbon black aggregate bound to the NS1 protein previously immobilized on the nitrocellulose membrane.

To compare the carbon black performance in LFIA, an assay based on standard gold NPs was developed for NS1 protein detection. The assay has the conventional set up of a LFIA with four membranes (see section 1.4). The test and control lines consist of anti-NS1 antibodies and biotinylated-albumin, respectively. Anti-NS1 protein capture antibody-gold NPs and streptavidin-gold NPs are the responsible labels for the color development.

For the LFIA based on gold NPs, the test line is visible until 500 ng/mL (Figure 13a), and below this concentration, the test lines are inconsistent. As observed in the last section (2.1.1) for the immunospot experiments, the carbon black particles show a lower detection limit, 10 ng/mL, than the gold nanoparticles (Figure 13b).

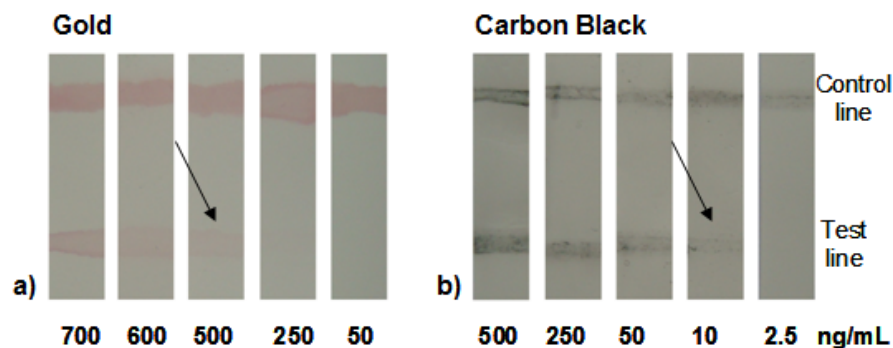


Figure 13. Pictures of the lateral flow immunoassay for Dengue virus NS1 protein. LFIA based on gold nanoparticles (a) and carbon black (b) for different concentrations of NS1 protein. The detection limits for gold nanoparticles and carbon black (indicated by the black arrows) are 500 ng/mL and 10 ng/mL, respectively.

The sensitivity enhancement indicated by 50 times lower detection limit is decisive for early Dengue fever detection based on NS1 protein. Libraty and colleagues (Libraty et al., 2002) showed that plasma levels of free Dengue-2 virus secreted NS1 protein by day of illness variate between 150-250ng/mL for the second day of the disease for patients infected with secondary infections and Dengue hemorrhagic fever. Differently than colloidal gold, carbon black particles are able to provide visual signal below the NS1 concentration existent in infected patients on the first days of the disease, which can be vital for the rapid assesment of patients developing more severe cases of the disease.

2.2 Fluorecence based detection system

2.2.1 Immunospot

The work described in this section was driven by the current limitations to combine speed of analysis, ease of use and sensitivity for Dengue fever detection in laboratories with low resources. Currently, ELISA is the method of choice to detect Dengue virus NS1 protein in laboratories. However, this is a time consuming method, requiring 3-5 hours, and it is the bottleneck for routine of clinical analysis laboratory in epidemic periods, when hundreds of samples should be tested. This section describes an easy method combining principles of fluorophore linked immunosorbent assay (FLISA) and enzyme linked immunospotting (ELISPOT). FLISA follows the same principles of ELISA, but replacing the enzyme by a flurophore, which provides faster results with comparable sensitivity. ELISPOT is a method,

where antibodies are immobilized on a membrane, compounds secreted by cells are captured and an enzyme conjugated antibody provides the colorimetric detection. The advantage of combining the fluorescence detection of FLISA with the sample deposition on a membrane of ELISPOT is the development of a sensitive and fast assay.

In the proposed test, a low volume of serum sample is applied onto a nitrocellulose membrane and mouse anti-NS1 IgG labeled with fluorescent nanoparticles are used for dengue detection. The test takes less time and the results can be qualitative/quantitative. The possibility of applying the sample directly to the nitrocellulose membrane with high protein affinity allows the use of low volume of samples and avoids the necessity of two antibodies for capture and detection. It reduces the costs, besides the time consuming incubation and washing steps. The use of fluorescent nanoparticles provides lower detection limit in comparison to conventional FLISA, additionally avoiding bleaching effects. As a general view, the immunospot test allows diagnosing DF in less than one hour with high specificity and sensitivity, less complexity and using conventional apparatus in clinical analysis laboratories. Detailed information about this section is described in the Chapter 3.

In order to select a suitable particle, three commercial fluorescent particles with 40 nm of diameter were evaluated. Fluorophores incorporated in polymer particles were chosen to overcome bleaching effects generally observed with fluorescent dyes. The particles consisted of polystyrene containing multiple carboxylic acids for covalent ligand attachment. The chosen particles showed highest fluorescence emission, peaking at 567 nm and mean diameter of 37 ± 5 nm.

Single and multiple tests were developed using commonly available materials and equipment in clinical laboratories. The single tests, or strip tests, were constructed combining cellulose and nitrocellulose membranes in a layer-by-layer structure, following LFIA principles (section 1.4). The test requires only 4 μ L of serum sample, in contrast with 50-100 μ L for ELISA. In case of multiple sample analysis, parallel tests can be performed by applying the samples directly on the same nitrocellulose membrane with sufficient 15 mm spacing between each spot to avoid contamination. The molecules in the spot are pulled out of solution by the membrane and stick to the paper avoiding cross contamination between neighboring spots. This also remains stable after several washing steps. After adding the sample and blocking unspecific sites with albumin, fluorescent NPs coated with anti-NS1 antibody is added and incubated during 15 min. The results of the test can be read after washing the membrane with washing buffer (more experimental details are explained in the

Chapter 3).

Experiments comparing the fluorescence intensity of the same samples analyzed in single and multiple tests revealed a variation lower than 16%. The presented direct sample application is analogous to indirect ELISA tests, with the advantage of a shorter incubation time and no further washing steps. By using nitrocellulose, the high membrane-protein affinity assures the retention of the analyte into the membrane.

Versatility was also achieved for the fluorescence measurement. Considering that laboratories around the world have varying amount of equipment availability and sometimes even lack of instruments altogether, three different instruments were used and evaluated: a simple fluorometer coupled to an optical fiber; an ELISA reader, which allows the measurement placing the membrane in a ELISA microplate; and a UV-lamp that can be used in unequipped laboratories providing qualitative results. Although, UV-lamp can only perform qualitative tests, it is a very cheap apparatus and can be easily obtained. The importance of such instrumentation is stressed by the fact that many tests only need a yes/no diagnostics. A lamp in the UVB range was chosen for the fact that they are mostly used in clinical laboratories and the emission is capable to excite the tail of the fluorophore excitation band.

To compare the performance and consequently the detection limits for measurements performed with these three apparatus, a NS1 protein dilution series starting from 1 until 500 ng/mL was analyzed by all of them (Figure 14).

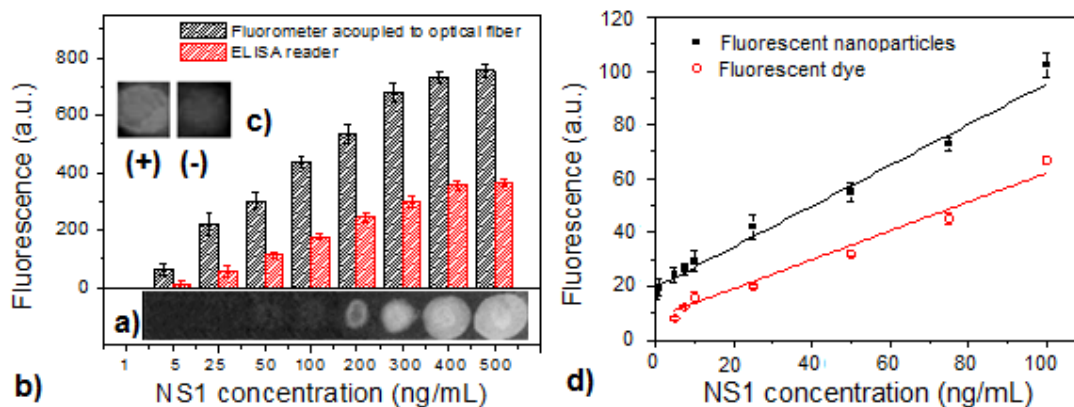


Figure 14. Comparison of detection instruments and conventional method. Fluorescent spots from serum dilution from an infected patient with anti-NS1 coated fluorescent particles measured under UV-lamp (a), by fluorometer coupled with optical fiber (black) and ELISA reader (red) (b). Positive (left) and negative (right) controls are shown in (c). Sandwich fluorescent immunosorbent assay (d) using fluorescent nanoparticles and fluorescent dye molecules.

The fluorescent spots under UV-lamp (Figure 14a) can be easily visualized from 200 ng/mL NS1 protein. Below this concentration, it is not possible to precisely confirm the positive NS1 protein serum signal. A positive and negative control is used to provide the limits for yes/no decision by comparison with the sample spot (Figure 14c). The negative control consists of a serum sample from a patient never infected with the virus. The positive control is a serum sample from a patient in the third day of the infection (highest NS1 concentration during the infection, Figure 9), which was confirmed by NS1-ELISA and RT-PCR.

The measurements performed by the fluorometer coupled to an optical fiber showed a lower detection limit compared to the ELISA reader (Figure 14b). The detection limits were calculated, showing 5.2 and 11.5 ng/mL for optical fiber coupled to fluorometer and ELISA reader measurements, respectively. The relative standard deviation of the proposed method was evaluated by performing ten successive determinations of two serum samples. The calculation was performed dividing the standard deviation by the mean of the measurements. The values, 17% and 12%, were low considering that the tests are performed on membranes, where the pore structure is not so homogeneous as ELISA substrate.

Although these two instruments showed different sensitivities for NS1 protein detection, both are adequate to be used for diagnosis. The immunospot is indeed capable of providing a reliable diagnostic below the NS1 concentration that exists in infected patients on the first-second day of the infection. The low detection limit is decisive for early Dengue fever detection based on the NS1 protein and it is important for the rapid assessment of patients. When an UV-lamp is the only available tool, Dengue fever can be detected on the third day of infection. Lateral flow immunoassay tests are faster than the presented immunospot assay, but they require 25 times more sample volume and two antibodies (capture and detection). Thus, immunospot assay may be more appropriate for laboratory analyses of numerous samples.

In order to evaluate the gain in performance of the proposed method in comparison to classical FLISA, analytical curves for NS1 antibody coated fluorescent particles and anti-mouse IgG-fluorescein isothiocyanate (IgG-FITC) antibodies were obtained on nitrocellulose. Figure 14 shows that higher signals were recorded when particles were used, resulting therefore in a more sensitive assay. Besides avoiding bleaching effects, the use of particles permits to concentrate the fluorophores and contribute to a higher fluorescence signal per antibody bound to the antigen, unlike FLISA. Precisely, considering the concentration range between 2 and 100 ng/mL, the particles used as enhancers resulted in a curve slope of 0.758

a.u. mL/ng, which is higher than the assay using only IgG-FITC (0.539 a.u. mL/ng). It means that the proposed assay is more sensitive to detect variations on the concentration axis.

In order to verify the potential of the proposed methodology in the biological analysis, 83 blood serum samples from infected patients were analyzed and compared to a commercial NS1 ELISA. ELISA reader and UV-lamp were chosen as detection, because they are more commonly available in laboratories. Analysis provided satisfactory results compared to the commercial test (Table 3). The fluorescence measurements performed in ELISA reader revealed sensitivity of 81% and specificity of 88%. However, the qualitative measurements using UV-lamp showed low sensitivity, 59%, and specificity of 83%. Although, they showed low sensitivity, it is still acceptable as a diagnostic tool due to its sensitivity be superior to 50%. The low sensitivity is justified by the difficulty to establish visual limits for considering a positive or a negative result. The limit was defined by the negative control, in which non-infected serum was analyzed and non-specific interaction provided background intensity. Thus, the diagnostic was obtained by comparing visually the sample spots with the established limit. After comparing the values obtained with commercial NS1 ELISA and fluorescent measurements in ELISA reader (paired t-test), no significant statistical differences were found.

Table 3. Dengue NS1 detection using the proposed method with reference to a commercial NS1 ELISA in 83 serum samples from infected patients.

NS1 status	Immunospot (ELISA reader)		Immunospot (UV-lamp)		Total
	Positive	Negative	Positive	Negative	
Positive	48	11	35	24	59
Negative	3	21	4	20	24
Total	51	32	39	44	83
Sensitivity	81%		59%		
Specificity	88%		83%		

The newly developed test has the advantage of being performed during 45 to 60 minutes in comparison to classical ELISA or FLISA, which usually take 3-5 hours. The use of fluorescent nanoparticles allowed high sensitivity and ease detection using different laboratory equipment. In addition, the application of reagents and samples on nitrocellulose

membrane provided easy manipulation, low volume samples and lower costs. The combination of principles of different assays can produce a fast and high sensitive test to be applied to Dengue fever detection, mainly in impoverished environments and epidemic areas, where sensitivity, speed and simplicity are essentials.

2.3 Phosphorescence based detection system

2.3.1 Polymer core-shell particles of poly(styrene-co-hydroxyethylmethacrylate), PSHEMA, containing luminescent ruthenium complex

Polymer particles are very promising as labels for diagnostic applications due to their property and functionality diversities. A current problem of polymer particles is the aggregation during synthesis or agglomeration after storage. For LFIA and ISA, the flow of particles through tortuous pathways inside the membranes is essential to assure reproducibility and reliability. The particle agglomeration can limit the label performance, and consequently the entire assay. Therefore, the work described in this section deals with the synthesis of polymer particles with low agglomeration, which can be used as labels in paper based immunoassays.

Polystyrene particles (PS) are predominantly applied to biomedical purposes, including LFIA. Unfortunately, PS particles show low colloidal stability resulting in agglomeration and instability during bioconjugation steps. Accordingly, poly[styrene-co-(2-hydroxyethyl methacrylate)] (PSHEMA) polymer particles may be a suitable material for bioapplications substituting PS particles. PSHEMA particles consist of a hydrophilic/hydrophobic heterogeneous surface with high colloidal stability, insensitive non-specific agglutinability, free-emulsifier polymerization and high monodispersity. The particles are characterized as core-shell structures, where the HEMA richer chains are more concentrated at the particle periphery, stabilizing the hydrophobic core. The colloidal stabilization is provided by strong electrostatic repulsion with contributions of steric stabilization (Cardoso et al., 1998; 1999; 2001; Okubo et al., 2003; Martin-Rodriguez et al., 1996).

Due to their numerous advantages, PSHEMA particles were synthesized and used as detection labels in immunospot assay for Dengue fever detection. Ru complexes with carboxylated ligands were incorporated into the particles during the synthesis in order to produce luminescent structures. The carboxylated groups enabled the conjugation with

biomolecules and consequently allowed biomedical application. More details about the synthesis and Ru complex are described in the Chapter 4.

The particle morphology was characterized using atomic force and transmission electron microscopies (Figure 15).

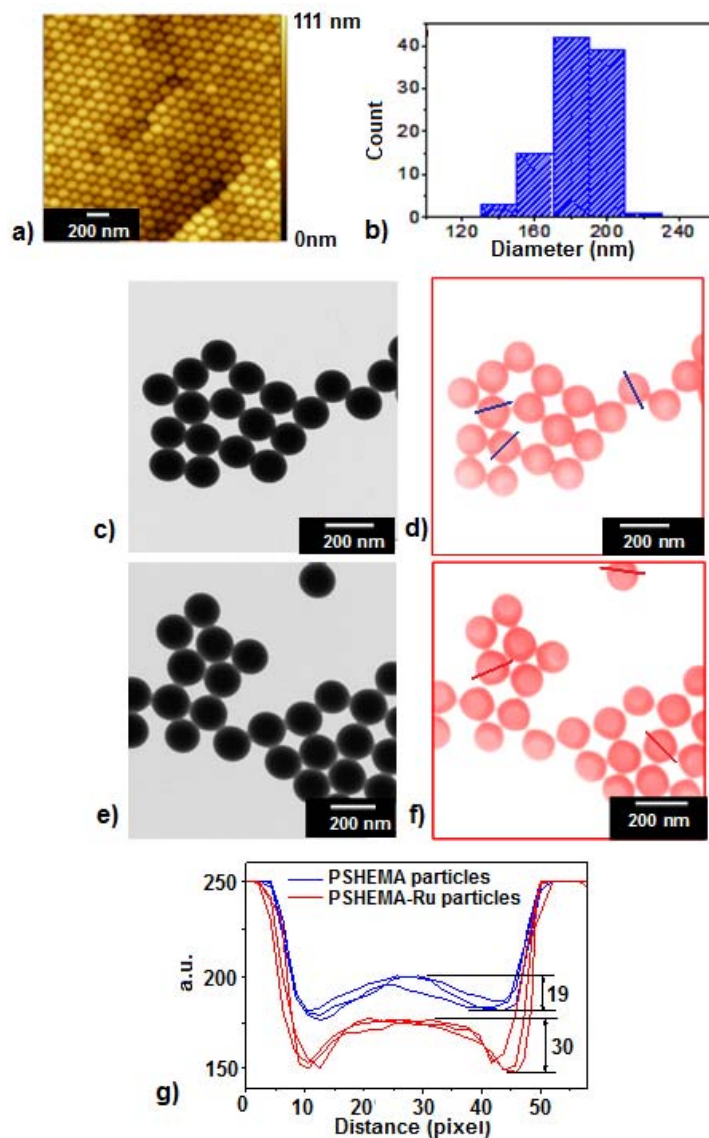


Figure 15. Microscopic characterization of PSHEMA-Ru particles using AFM and TEM. AFM topography image (a) and histogram (b) of diameter distribution of the film surface of PSHEMA-Ru, showing a monodispersed size distribution evidenced by the hexagonal packing. Bright-field and energy loss images at 40 eV (N shell of Ru) for PSHEMA (c and d) and Ru-PSHEMA (e and f). Line profiles of the particles at 40 eV without and with Ru complex, indicating a slight higher contrast between shell and core in presence of Ru than the particles without the complex.

Hexagonal packing caused by high uniformity of particle sizes is observed with low deformation of the particles (Figure 15a). The size distribution of 150 particles yields a diameter of 185 ± 15 nm (Figure 15b). Energy filtered transmission electron microscopy (EFTEM) in combination with electron spectroscopy imaging (ESI-TEM) were used to investigate the Ru complex distribution in the particle (Linares et al., 2011; Valadares et al., 2008). Bright-field images for PSHEMA and Ru-PSHEMA particles (Figure 15c and e) show spherical particles that present slight deformations as necks between the particles, more evident for PSHEMA-Ru. Energy loss TEM images were obtained at 40 eV, which is the N absorption threshold region of Ru (Figures 15d and f). PSHEMA core-shell structure has been already described in the literature using molecular maps at the low energy loss range (0-80eV) (Linares et al., 2009). The images at 40 eV show that the shell of PSHEMA particles with Ru complexes present a slight higher contrast in relation to the core in comparison to PSHEMA particles without Ru complexes, as shown by the line profiles (Figure 16g). More details of image analysis are described in the Chapter 4.

The PSHEMA polymerization is described as a process where monomers are added to the growing chains inside of the polymer swollen particles and the HEMA richer chains are more concentrated at the particle periphery. X-ray photoelectron spectroscopy also indicated that the HEMA component is localized at the shell (Okubo et al., 1989). Thus, considering the hydrophilic structure of Ru complex, it can be expected that the complexes accumulate in the HEMA richer domains, the particle shell. Cardoso and col. (Cardoso et al., 1998) investigated the elemental distribution within PSHEMA particles and showed that the initiator counter ions, K^+ , concentrate in a thin outer particle surface. The positive layer around the particles can have an important role to keep the ruthenium complex in the particle shell.

The Ru complexes concentrate at the particle shell and contribute for further conjugation with biomolecules. In order to demonstrate the potential of the nanoparticles for bioconjugation, biomolecules immobilized on the particle surface and the bioconjugates were applied as detection system for fluorescence microscopy. Monoclonal Dengue virus antibodies for a viral non-structural glycoprotein, NS1, were immobilized on the particle surface and they were used to analyze infected serum samples. A dilution series of the NS1 protein was deposited on the nitrocellulose membrane, forming spots of 0.5 μ L of serum. The resulting analytical curve and the respective luminescent spots (Figure 16a) show a linear range from 200 to 400 ng/mL and a detection limit of 187 ng/mL. More experimental details are described in the chapter 4.

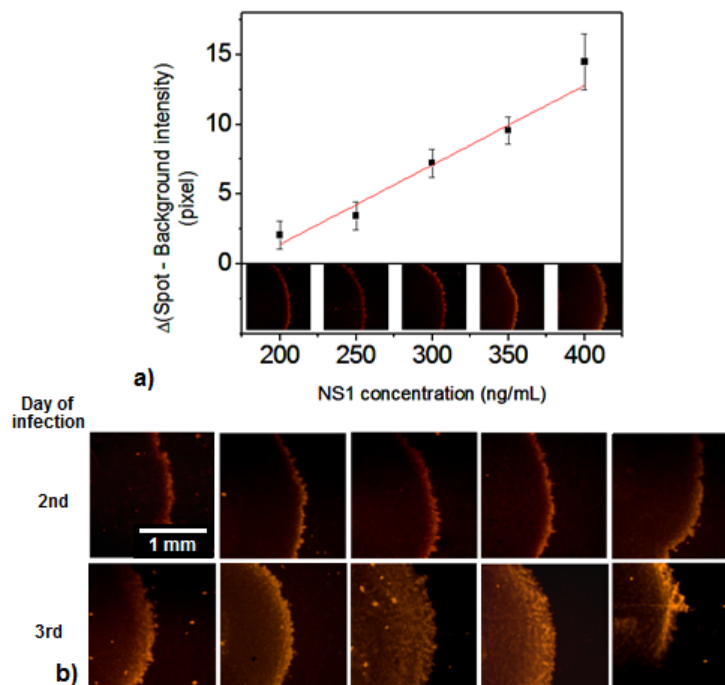


Figure 16. Anti-NS1 coated PSHEMA-Ru particles used to detect Dengue virus NS1 protein. Analytical curve (a) for Dengue virus NS1 performed on nitrocellulose membrane and digital images of serum spots, where NS1 protein was detected by anti-NS1 coated PSHEMA-Ru particles. Values were obtained by subtracting the background intensity from the spot signal. Images from serum positive samples (b) from the second (second row) and third day (first row) of infection from a group of 10 patients. Images were recorded at 10x of magnification.

Serum positive samples (Figure 16b) from the second and third day of the infection of 10 patients were analyzed using PSHEMA-Ru particles and a fluorescence microscope. The test was positive for all samples, proving that the luminescent particles are indeed capable of providing a reliable diagnostic for Dengue fever. The morphology of the serum spots show that the particles tend to accumulate on the edges of the serum spots, where the proteins also concentrate. When a solution of proteins is deposited on a nitrocellulose membrane, the proteins tend to accumulate on the edges of the spot. This is also observed in the Chapter 3, Figure 2g. For the samples from the third day of the infection (Figure 16b, second row), when the NS1 protein concentration is higher, the central part of the spots are also luminescent. It indicates that the particles flowed through the membrane with 450nm of porous size and interacted with the proteins adsorbed in that area.

The PSHEMA-Ru particles showed to have a high potential to be successfully used in biomedical applications. The low agglomeration of the particles allows easy particle flow in the paper based assays, avoiding membrane obstruction and influence in the test performance.

2.4 Colorimetry and fluorescence based detection system

2.4.1 Gold and fluorescent nanoparticle clusters

In the last section (Chapter 5), the detection limit improvement of LFIA and ISAs is taken up by the combination of colorimetry and fluorescence methods. Gold and fluorescent nanoparticles (emission maximum: 605 nm) were combined in small clusters and used as labels for immunoassays. The strategy increases the colorimetric signal because each analyte is recognized by several colored nanoparticles instead of a single nanoparticle. Furthermore, the combination of fluorescent NPs allow decreasing the detection limit by using a simple UV lamp to excite the fluorophores, which also produces an enhanced signal in comparison to single fluorescent NPs used as detection labels. The fluorescence emission is only used in case that the colorimetric signal is not enough to provide a convincing result.

The clusters were prepared by coating the particles with albumin and then combining them by peptide bonds between the albumin layers. The structures were characterized using transmission electron microscopy (Figure 17).

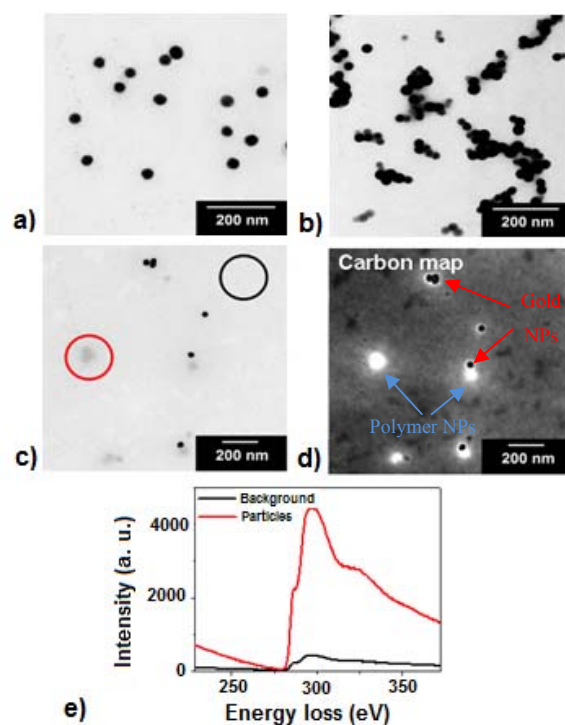


Figure 17. Microscopic characterization of nanoparticles and clusters. Bright-field images of (a) gold nanoparticles, (b) fluorescent beads and (c) cluster of gold and polystyrene nanoparticles. Carbon map (d) of the clusters with red arrows indicating the gold nanoparticles and blue arrows point to the polymer particles. Spectra (e) of the background and the polymer particles.

Bright field image of gold nanoparticles (Figure 17a) shows well dispersed structures with average diameter of 39 ± 5 nm. Image of fluorescent nanoparticles (Figure 17b) shows particles with a mean diameter of 38 ± 8 nm. In the bright field image of the clusters (Figure 17c), the darker particles consist of gold due to its higher atomic number in comparison to fluorescent polystyrene nanoparticles. It is possible to observe small agglomerates consist of gold-gold, gold-fluorescent and fluorescent-fluorescent particles. The carbon map (Figure 17d) indicates all materials containing carbon in their composition as intense bright signal. This image is obtained by an arithmetic procedures on images acquired above and below the energy threshold for the excitation of K shell electrons of carbon (303 eV). Hence, it demonstrates that there is organic material around the gold nanoparticles formed by biomolecules conjugated to the particle surface. The bare gold nanoparticles do not show the bright shell (image not shown here). The fluorescent nanoparticles are evidenced by undefined borders around the particles. The agglomerates consisted of gold and polystyrene show their organic shell of biomolecules in contact, suggesting interactions between them. The carbon map is confirmed by the electron energy loss spectroscopy (EELS) at the K absorption threshold region of carbon. It shows the high intensity of carbon signal for the polystyrene nanoparticles in comparison to the background formed by parlodium, which is a thin film that supports the sample and has carbon in its composition.

Lateral flow immunoassays were developed using gold-fluorescent clusters as labels for Dengue fever detection (Figure 18a).

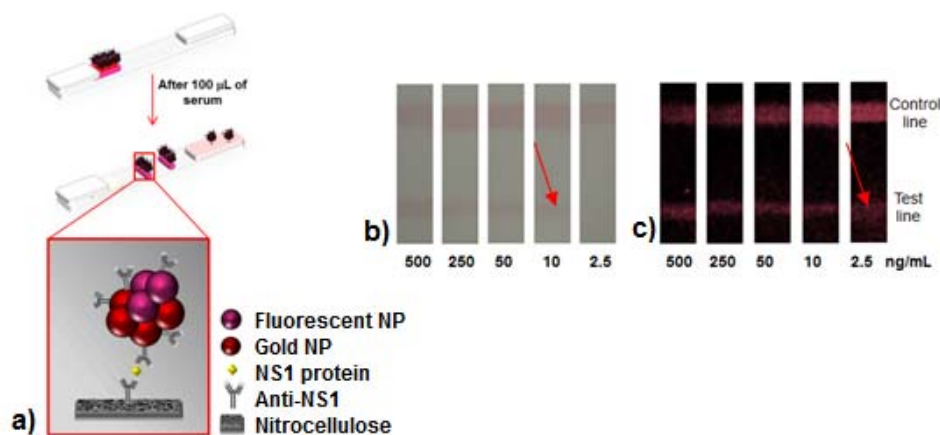


Figure 18. Scheme and pictures of a lateral flow immunoassay based on clusters for Dengue virus NS1 protein. Lateral flow immunoassay (a) based on gold-polystyrene nanoparticles clusters and zoom of the test line showing the cluster bound to the NS1 protein previously immobilized on the nitrocellulose membrane. LFIA pictures at different concentrations of NS1 protein (b) and under UV lamp (c). The detection limits for gold nanoparticles and carbon black alone (indicated by the red arrows) are 500 and 10 ng/mL, respectively.

The test and control lines consist of anti-NS1 capture antibody and biotinylated-albumin. The clusters were separately coated with anti-NS1 detection antibody and streptavidin. A red-fluorescent line indicates positive serum sample for Dengue fever.

Tests were performed with different NS1 protein concentration and the picture of them is shown in the Figure 18b and c. The detection limit of colorimetric signal is 10 ng/mL, but when the strip tests are under UV light, the detection limit is lowered down to 2.5 ng/mL (Figure 18c). Accordingly, gold-fluorescent nanoparticle cluster provides comparable colorimetric sensitivity of the best colored labels, carbon black, and shows additional sensitivity due to the fluorescent nanoparticles, contributing to a more reliable assay.

2.5 Detection limit comparison

In this work, different detection systems based on nanostructures were used in order to develop reliable, sensitive and fast immunoassays for early Dengue fever infection detection based on the viral protein NS1. A summary of the detection systems is described in the Table 4, including characteristics of each system. A comparison between both colored labels indicates that an immunoassay produced with carbon black shows the highest colorimetric signal and represents an interesting option to replace gold nanoparticles (Chapter 2 and 5). Fluorescence is a very sensitive method that provides lower detection limits than colorimetry, as observed for the immunospot assay based on commercial fluorescent nanoparticles (Chapter 3). PSHEMA-Ru particle (Chapter 4) has a core-shell structure and also shows good performance with low particle agglomeration. Although fluorescent labels generally provide lower detection limit, it requires the use of fluorescence readers, which is contrary to the conception of producing a simple assay for impoverished environments. Therefore, clusters with colored and fluorescent nanoparticles were developed. The detection is based on colorimetric signal provided by gold nanoparticles, but an additional signal enhancement can be obtained by using a simple UV lamp or LED. As described above, the detection limit for the cluster showed comparable detection limit to carbon black, but lower values were obtained by exciting fluorescent particles.

In terms of Dengue fever disease detection, all investigated labels detect the DF from the first to the second day of the infection, except for the PSHEMA-Ru particles, which can be used to diagnose from the second to the third day. The performance of those labels is superior to the standard gold nanoparticles currently in use in commercial available assays and the

progress achieved by this thesis in terms of LFIA sensitivity is shown in the Figure 20.

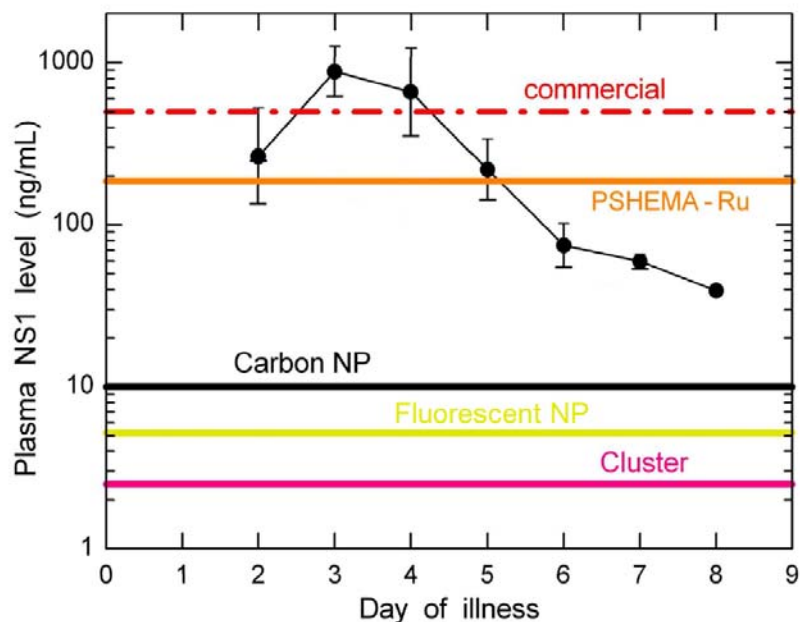
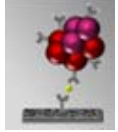


Figure 19. NS1 concentration vs. infection time after symptom onset and detection limits of LFIA. Detection limit of commercial LFIA kits based on gold nanoparticles and the achievements of the detection labels obtained in this thesis (Adapted from Libraty et al., 2002)

The graph clearly shows that commercial tests can only detect the disease from third of the infection, when the patient with hemorrhagic fever is already on risk to develop shock bleeding. However, the proposed labels allow the detection of DF days before than the commercial kits (1st-2nd day). The anticipated diagnostic is essential to provide correct treatment and avoids the progress of the infection. The high sensitivity in immunoassays can be very useful for the development of point-of-care tools that provide early stage diagnostic of other diseases.

Table 4. Summary of the detection systems for Dengue fever diagnostics based on nanoparticles.

Detection system	Assay type	Detection limit (ng/mL)	Duration (min)	Day after the outbreak	References
Gold nanoparticles ("gold standard")	 Lateral flow immunoassay	500	20	3rd	Chapter 2
Carbon black	 Lateral flow immunoassay	10	25	1st-2nd	Chapter 2 and 5
Fluorescent nanoparticles	 Immunospot assay	Optical fiber reader: 5 ELISA reader: 15 UV lamp: 200	45-60	1st-2nd	Chapter 3
Luminescent PSHEMA-Ru particles	 Immunospot assay	Microscope: 190	25	3rd	Chapter 4
Gold-fluorescent nanoparticles clusters	 Lateral flow immunoassay	Visible: 10 Under UV: 2.5	25	1st-2nd	Chapter 5

3. References

- Algar, W.R.; Prasuhn, D. E.; Stewart, M. H.; Jennings, T. L.; Blanco-Canosa, J. B.; Dawson, P. E.; Medintz, I. L. The controlled display of biomolecules on nanoparticles: a challenge suited to bioorthogonal chemistry. *Bioconjugate Chem.* **2011**, 22, 825–858.
- Allwinn, R. Significant increase in travel-associated dengue fever in Germany. *Med. Microbiol. Immunol.* **2011**, 200, 155–159.
- Azzazy, H. M. E.; Mansour, M. M. H.; Kazmierczak, S. C. Nanodiagnostics: A New Frontier for Clinical Laboratory Medicine *Clin. Chem.* **2006**, 52, 1238–1246.
- Bathoorn, E.; Limburg, A.; Bouwman, J. J.; Bossink, A. W.; Thijsen, S. F. Diagnostic potential of an enzyme-linked immunospot assay in tuberculous pericarditis. *Clin. Vaccine Immunol.* **2011**, 18, 874–877.
- Blacksell, S. D.; Jarman, R. G.; Bailey, M. S.; Tanganuchitcharnchai, A.; Jenjaroen, K.; Gibbons, R. V.; Paris, D. H.; Premaratna, R.; Janaka de Silva, H.; Laloo, D. G.; Day, N. P. J. Evaluation of six commercial point-of-care tests for diagnosis of acute dengue infections: the need for combining NS1 antigen and IgM/IgG antibody detection to achieve acceptable levels of accuracy. *Clin. Vaccine Immunol.* **2011**, 18, 2095–2101.
- Blacksell, S. D. Commercial Dengue Rapid Diagnostic Tests for Point-of-Care Application: Recent Evaluations and Future Needs? *J. Biomed. Biotechnol.* **2012**, 2012, 1–12.
- Cardoso, A. H.; Leite, C. A. P.; Zaniquelli, M. E. D.; Galembeck, F. Easy polymer latex self-assembly and colloidal crystal formation: the case of poly[styrene-co-(2-hydroxyethyl methacrylate)]. *Colloids Surf., A* **1998**, 144, 207–217.
- Cardoso, A. H.; Leite, C. A. P.; Galembeck, F. Latex particle self-assembly and particle microchemical symmetry: ps/hema latex particles are intrinsic dipoles. *Langmuir* **1999**, 15, 4447–4453.
- Cardoso, A. H.; Leite, C. A. P.; Galembeck, F. Latex macrocrystal self-assembly dependence on particle chemical heterogeneity. *Colloids Surf., A* **2001**, 181, 49–55.
- Carrilho, E.; Phillips, S.T.; Vella, S.J.; Martinez, A.W.; Whitesides, G.M. Paper Microzone Plates. *Anal. Chem.* **2009**, 81, 5990–5998.
- Cheng, C.-M.; Martinez, A.W.; Gong, J.; Mace, C.R.; Phillips, S.T.; Carrilho, E.; Mirica, K.A.; Cho, J-H.; Paek, S-H. Semiquantitative, bar code version of immunochromatographic assay system for human serum albumin as model analyte. *Biotechnol. Bioeng.* **2001**, 75, 725–732.
- Cole, S. P. C.; Campling, B. G.; Atlaw, T.; Kozbor, D.; Roder, J. C. Human monoclonal antibodies. *Mol. Cell. Biochem.* **1984**, 62, 109–120.

- Cortez-Retamozo, V.; Backmann, N.; Senter, P. D.; Wernery, U.; Baetselier, P. D.; Muyldermans, S.; Revets, H. Efficient cancer therapy with a nanobody-based conjugate. *Cancer Res.* **2004**, *64*, 2853–2857.
- Discher, D. E.; Ahmed, F. Polymersomes. *Ann. Rev. Biomed. Eng.* **2006**, *8*, 323–341.
- Ellerbee, A. K.; Phillips, S. T.; Siegel, A. C.; Mirica, K. A.; Martinez, A. W.; Striehl, P.; Jain, N.; Prentiss, M.; Whitesides, G. M. Quantifying colorimetric assays in paper-based microfluidic devices by measuring the transmission of light through paper. *Anal. Chem.* **2009**, *81*, 8447–8452.
- Falconar, A. K. I.; Young, P. R. Production of dimerspecific and dengue virus group cross-reactive mouse monoclonal antibodies to the dengue 2 virus non-structural glycoprotein NS1. *J. Gen. Virol.* **1991**, *72*, 961–965.
- Flamand, M.; Megret, F.; Mathieu, M.; Lepault, J.; Rey, F. A.; Deubel, V. Dengue virus type 1 nonstructural glycoprotein NS1 is secreted from mammalian cells as a soluble hexamer in a glycosylation-dependent fashion. *J. Virol.* **1999**, *73*, 6104–6110.
- Fortina, P.; Kricka, L. J.; Graves, D. J.; Park, J.; Hyslop, T.; Tam, F.; Halas, N.; Surrey, S.; Waldman, S. A. Applications of nanoparticles to diagnostics and therapeutics in colorectal cancer. *Trends Biotechnol.* **2007**, *25*, 145–152.
- Franci, C.; Ingles, J.; Castro, R.; Vidal, J. Further studies on the ELISA-spot technique. Its application to particulate antigens and a potential improvement in sensitivity. *J. Immunol. Methods* **1986**, *88*, 225–232.
- Gavin, P. J.; Thomson, Jr., R. B. Review of rapid diagnostic tests for influenza. *Clin. Appl. Immunol. Rev.* **2003**, *4*, 151–172.
- Goldman, E. R.; Clapp, A. R.; Anderson, G. P.; Uyeda, H. T.; Mauro, J. M.; Medintz, I. L.; Mattoussi, H. Multiplexed toxin analysis using four colors of quantum dot fluororeagents. *Anal. Chem.* **2004**, *76*, 684–688.
- Gray, R. H.; Makumbi, F.; Serwadda, D.; Lutalo, T.; Nalugoda, F.; Opendi, P.; Kigozi, G.; Reynolds, S. J.; Sewankambo, N. K.; Wawer, M. J. Limitations of rapid HIV-1 tests during screening for trials in Uganda: diagnostic test accuracy study. *Brit. Med. J.* **2007**, *335*, 188–190.
- Gubala, V.; Harris, L. F.; Ricco, A. J.; Tan, M. X.; Williams, D. E. Point of care diagnostics: status and future. *Anal. Chem.* **2010**, *84*, 487–515.
- Gubler, D. J.; Suharyono, W.; Tan, R. Viraemia in patients with naturally acquired dengue infection,” *Bulletin of the World Health Organization* 1981, *59*, 623–630.
- Guo, X.; Szoka, F. C. Chemical approaches to triggerable lipid vesicles for drug and gene delivery. *Acc. Chem. Res.* **2003**, *36*, 335–341.

- Gussenhoven, G. C.; van der Hoorn, M. A.; Goris, M. G.; Terpstra, W. J.; Hartskeerl, R. A.; Mol, B. W.; van Ingen, C. W.; Smits, H. L. LEPTO dipstick, a dipstick assay for detection of *Leptospira*-specific immunoglobulin M antibodies in human sera. *J. Clin. Microbiol.* **1997**, 35, 92–97.
- Haerberle, S.; Zengerle, R. Microfluidic platforms for lab-on-a-chip applications. *Lab on a Chip* **2007**, 7, 1094–1110.
- Jain, K. K. Nanodiagnosics: application of nanotechnology in molecular diagnostics. *Expert. Rev. Mol. Diagn.* **2003**, 3, 153–161.
- Jain, K.K. Nanotechnology in clinical laboratory diagnostics. *Clin. Chim. Acta.* **2005**, 358, 37–54.
- Jain, P. K.; Huang, X.; El-Sayed, I. H.; El-Sayed, M. A. Noble metals on the nanoscale: Optical and photothermal properties and some applications in imaging, sensing, biology and medicine. *Acc. Chem. Res.* **2008**, 41, 1578–1586.
- Jianrong, C.; Yuqing, M.; Nongyue, H.; Xiaohua, W.; Sijiao, L. Nanotechnology and Biosensors. *Biotechnol. Adv.* **2004**, 22, 505–518.
- Juntunen, E.; Myyryläinen, T.; Salminen, T.; Soukka, T.; Pettersson, K. Performance of fluorescent europium(III) nanoparticles and colloidal gold reporters in lateral flow bioaffinity assay. *Anal. Biochem.* **2012**, 428, 31–38.
- Köhler, G.; Milstein, C. Continuous cultures of fused cells secreting antibody of predefined specificity. *Nature* **1975**, 256, 495–497.
- Koraka, P.; Burghoorn-Maas, C. P.; Falconar, A.; Setiati, T. E.; Djaniatun, K.; Groen, J.; Osterhaus, A. D. M. E. Detection of immune-complex-dissociated nonstructural-1 antigen in patients with acute dengue virus infections. *J. Clin. Microbiol.* **2003**, 41, 4154–4159.
- ^a Laitinen, M. P. A.; Sojakka, K. M.; Vuento, M. Thin-Layer Affinity Chromatography in Analysis of Protein-Ligand Affinity. *Anal. Biochem.* **1996**, 243, 279–282.
- ^b Laitinen, M. P. A.; Vuento, M. Affinity immunosensor for milk progesterone: identification of critical parameters. *Biosens. Bioelectron.* **1996**, 11, 1207–1214.
- Leung, V. Development of Paper-based Devices for Diagnostics and Biosensing. Master thesis, University Hamislton, Ontario 2011.
- ^a Leuvering, J. H. W.; Thal, P. J. H. M.; Van Der Waart, M.; Schuurs, A. H. W. M. Sol particle immunoassay (SPIA). *J. Immunoassay* **1980**, 1, 77–91.
- ^b Leuvering, J. H. W.; Thal, P. J. H. M.; Waart, M.; Schuurs, A. H. W. M. Sol particle agglutination immunoassay for human chorionic gonadotrophin. *Fresenius' J. Anal. Chem.* **1980**, 301, 132.
- Leuvering, J. H. W.; Goverde, B. C.; Thal, P. J. H. M.; Schuurs, A. H. W. M. A homogeneous sol particle immunoassay for human chorionic gonadotrophin using monoclonal antibodies. *J.*

- Immunol. Meth.* **1983**, 60, 9–23.
- Libraty, D. H.; Young, P. R.; Pickering, D.; Endy, T. P.; Kalayanarooj, S.; Green, S.; Vaughn, D. W.; Nisalak, A.; Ennis, F. A.; Rothman, A. L. High circulating levels of the dengue virus nonstructural protein NS1 early in dengue illness correlate with the development of dengue hemorrhagic fever. *J Infect. Dis.* **2002**, 186, 1165–1168.
- Liddell, E.; Weeks, I. In *Antibody technology; Therapeutic application of antibodies*, Chapter 7. Bios Scientific Publisher: Oxford, United Kingdom, 1995; pp. 103–119.
- Lin, W.; Zheng, Y.; Zhang, J.; Wan, X. Fabrication of core shell nanostructures from near-infrared electrochromic amphiphilic diblock copolymers containing pendant dinuclear ruthenium group through assembly and their optical, electrochemical, and electrooptical properties. *Macromolecules* **2011**, 44, 5146–5154.
- Linares, E. M.; Valadares, L. F.; Silva, C. A.; Rezende, C. A.; Galembeck, F. Molecular mapping by low-loss-energy EFTEM imaging. *Anal. Chem.* **2009**, 81, 2317–2324.
- Linares, E. M.; Jannuzzi, S. A. V.; Galembeck, F. Electrostatic contributions in the increased compatibility of polymer blends. *Langmuir* **2011**, 27, 15199–15205.
- ^a Linares, E. M.; Kubota, L. T.; Michaelis, J.; Thalhammer, S. Enhancement of the detection limit for lateral flow immunoassays: evaluation and comparison of bioconjugates *J. Immunol. Methods* **2012**, 375, 264–270.
- ^b Linares, E. M.; Pannuti, C.S.; Kubota, L.T.; Thalhammer, S. Immunospot assay based on fluorescent nanoparticles for Dengue fever detection. *Biosens. Bioelectron.* **2012**, *in press*.
- Lipman, N. S.; Jackson, R. L.; Trudel, L. J.; Weis-Garcia, F. Monoclonal versus polyclonal antibodies: distinguishing characteristics, applications, and information resources. *ILAR J.* **2005**, 46, 258–268.
- Liu, C.; Jia, Q.; Yang, C.; Qiao, R.; Jing, L.; Wang, L.; Xu, C.; Gao, M. Lateral flow immunochromatographic assay for sensitive pesticide detection by using Fe₃O₄ nanoparticle aggregates as color reagents. *Anal. Chem.* **2011**, 83, 6778–6784.
- Lönnerberg, M.; Carlsson, J. Quantitative detection in the attomole range for immunochromatographic tests by means of a flatbed scanner. *Anal. Biochem.* **2001**, 293, 224–231.
- Lou, S.; Patel, C.; Ching, S.; Gordon, J. One-step competitive immunochromatographic assay for semiquantitative determination of lipoprotein(a) in plasma. *Clin. Chem.* **1993**, 39, 619–624.
- Mark, D.; Haerberle, S.; Roth, G.; von Stetten, F.; Zengerle, R. Microfluidic lab-on-a-chip platforms: requirements, characteristics and applications. *Chem. Soc. Reviews* **2010**, 39, 1153–1182.

- Martin-Rodriguez, A.; Cabrerizo-Vilchez, M. A.; Hidalgo-Alvarez, R. Surface characterization of latexes with different interfacial Properties *Colloids Surf., A* **1996**, 108, 263–271.
- Martinez, A.W.; Phillips, S.T.; Whitesides, G.M.; Carrilho, E. Diagnostics for the Developing World: Microfluidic Paper-Based Analytical Devices. *Anal. Chem.* **2010**, 82, 3–10.
- Masoodi, R.; Pillai, K. M. Darcy's law-based model for wicking in paper-like swelling porous media. *AIChE Journal* **2010**, 56, 2257–2267.
- Mukhopadhyay S.; Kuhn R. J.; Michael Rossmann, M. G. A structural perspective of the flavivirus life cycle. *Nat. Rev. Microbiol.* **2005**, 3, 13–22.
- Murray, C. K.; Gasser, Jr., R. A.; Magill, A. J.; Miller, R. S. Update on Rapid Diagnostic Testing for Malaria. *Clin. Microbiol. Rev.* **2008**, 21, 97–110.
- Najioullah, F.; Combet, E.; Paturel, L.; Martial, J.; Koulmann, L.; Thomas, L.; Hatchuel, Y.; Cabié, A.; Cesaire, R. Prospective evaluation of nonstructural 1 enzyme-linked immunosorbent assay and rapid immunochromatographic tests to detect dengue virus in patients with acute febrile illness. *Diagn. Microbiol. Infect. Dis.* **2011**, 69, 172–178.
- Näreoja, T.; Vehniäinen, M.; Lamminmäki, U.; Hänninen, E. P.; Härmä, H.; Study of nonspecific of an immunoassy using Eu-doped polystyrene nanoparticle labels. *J. Immunol. Methods* 2009, 345, 80–89.
- O'Keefe, M.; Crabbe, P.; Salden, M.; Wichers, J.; van Peteghem, C.; Kohen, F.; Pieraccini, G.; Moneti, G. Preliminary evaluation of a lateral flow immunoassay device for screening urine samples for the presence of sulphamethazine. *J. Immunol. Methods* **2003**, 278, 117–126.
- Okubo, M.; Suzuki, T.; Fukuhara, Y. Estimation of heterogeneous surface structure of submicron-sized, composite polymer particles consisting of hydrophobic and hydrophilic components by atomic force microscopy. *Colloid Polym. Sci.* **2003**, 281, 569–574.
- Osorio, L.; Ramirez, M.; Bonelo, A.; Villar, L. A.; Parra, B. Comparison of the diagnostic accuracy of commercial NS1- based diagnostic tests for early dengue infection. *Viol. J.* **2010**, 361.
- Parolo, C.; Escosura-Muñiz, A.; Merkoçi, A. Enhanced lateral flow immunoassay using gold nanoparticles loaded with enzymes. *Biosens. Bioelectron.* **2012**, *in press*.
- Peer, D.; Karp, J. M.; Hong, S.; Farokhzad, O. C.; Margalit, R.; Langer, R. Nanocarriers as an emerging platform for cancer therapy. *Nat. Nanotechnol.* **2007**, 2, 751–760.
- Pok, K. Y.; Lai, Y. L.; Sng, J.; Ng, L. C. Evaluation of nonstructural 1 antigen assays for the diagnosis and surveillance of dengue in Singapore. *Vector-Borne Zoonotic Dis.* **2010**, 10, 1009–1016.
- Ponti, J. S.; Brown, M. C.; Chun, P.; Mansfield, M. A. In Lateral flow immunoassay. Wong, R.; Tse, H., Ed.; Material platform for the assembly of LFIA test strips/ Antibodies: key to a robust

- LFIA/ Colloidal gold and other labels for LFIA/ Nitrocellulose membrane for LFIA: a technical treatise. Chapters 3-6; Human Press: New York, US, 2009; pp 51–114.
- Posthuma-Trumpie, G. A.; Korf, J.; van Amerongen, A. Lateral flow (immuno)assay: its strengths, weaknesses, opportunities and threats. A literature survey. *Anal. Bioanal. Chem.* **2009**, 393, 569–582.
- Posthuma-Trumpie, G. A.; Wichers, J. H.; Koets, M.; Berendsen, L. B. J. M.; van Amerongen, A. Amorphous carbon nanoparticles: a versatile label for rapid diagnostic (immuno)assays. *Anal. Bioanal. Chem.* **2012**, 402, 593–600.
- Rayev, M.; Shmagel, K. Carbon-protein covalent conjugates in non-instrumental immunodiagnostic systems. *J. Immunol. Methods* **2008**, 336, 9–15.
- Rodenhuis-Zybert, I. A.; Wilschut, J.; Smit, J. M. Dengue virus life cycle: viral and host factors modulating infectivity". *Cell. Mol. Life Sci.* **2010**, 67, 2773–86.
- Schubert-Ullrich, P.; Rudolf, J.; Ansari, P.; Galler, B.; Führer, M.; Molinelli, A.; Baumgartner, S. *Anal. Bioanal. Chem.* **2009**, 395, 69–81.
- Schwarz, J. P.; Spackman, J. R.; Fahey, D. W.; Gao, R. S.; Lohmann, U.; Stier, P.; Watts, L. A.; Thomson, D. S.; Lack, D. A.; Pfister, L.; Mahoney, M. J.; Baumgardner, D.; Wilson, J. C.; Reeves, J. M. Coatings and their enhancement of black carbon light absorption in the tropical atmosphere. *J. Geophys. Res.* **2008**, 113, D03203.
- Skoog, D. A.; West, D. M.; Holler, F. J.; Crouch, S. R. In *Fundamentals of Analytical Chemistry, Introduction to spectrochemical methods; Instruments for optical spectrometry; Molecular absorption spectrometry; Molecular fluorescence spectroscopy*, Chapter 24-27, 8th ed Thomson, Brooks/Cole: Toronto, Canada, 2004; pp 710–838.
- Snowden, K.; Hommel, M. Antigen detection immunoassay using dipsticks and colloidal dyes. *J. Immunol. Methods* **1991**, 140, 57–65.
- Torchilin, V. P. Multifunctional nanocarriers. *Adv. Drug Delivery Rev.* **2006**, 58, 1532–1555.
- Valadares, L. F.; Linares, E. M.; Braganca, F. C.; Galembeck, F. Electrostatic adhesion of nanosized particles: the cohesive role of water. *J. Phys. Chem. C* **2008**, 112, 8534–8544.
- Vaughn, D. W.; Green, S.; Kalayanarooj, S.; Innis, B. L.; Nimmannitya, S.; Suntayakorn, S.; Endy, T. P.; Raengsakulrach, B.; Rothman, A. L.; Ennis, F. A.; Nisalak, A. Dengue viremia titer, antibody response pattern, and virus serotype correlate with disease severity," *J. Infect. Dis.* **2000**, 181, 2–9.
- Verheijen, R.; Stouten, P.; Cazemier, G.; Haasnoot, W. Development of a one step strip test for the detection of sulfadimidine residues. *Analyst* **1998**, 123, 2437–2441.
- Xia, X.; Xu, Y.; Zhao, X.; Li, Q. Lateral flow immunoassay using europium chelate-loaded silica

- nanoparticles as labels. *Clin. Chem.* **2009**, 179–182.
- Zaytseva, N. V.; Montagna, R. A.; Lee, E. M.; Baeumner, A. J. Multi-analyte single-membrane biosensor for the serotype-specific detection of Dengue virus. *Anal. Bioanal. Chem.* **2004**, 380, 46–53.
- Zhang, C.; Zhang, Y.; Wang, S. Development of Multianalyte Flow-through and Lateral-Flow Assays Using Gold Particles and Horseradish Peroxidase as Tracers for the Rapid Determination of Carbaryl and Endosulfan in Agricultural Products. *J. Agric. Food Chem.* **2006**, 54:2502–2507.
- Yang, Q.; Gong, X.; Song, T.; Yang, J.; Zhu, S.; Li, Y.; Cui, Y.; Li, Y.; Zhang, B.; Chang, J. Quantum-dot based immunochromatography test strip for rapid, quantitative and sensitive detection of alpha fetoprotein. *Biosens. Bioelectron.* **2011**, 30, 145–150.
- Young, P. R.; Hilditch, P. A.; Bletchly, C.; Halloran, W. An antigen capture enzyme-linked immunosorbent assay reveals high levels of the dengue virus protein NS1 in the sera of infected patients. *J. Clin. Microbiol.* **2000**, 38, 1053–1057.
- Watts, R.J. Ruthenium Polypyridyls: A Case Study. *J. Chem. Educ.* **1983**, 60, 834–842.
- Whitesides, G.M. Paper-Based ELISA. *Angew. Chem. Int. Ed.* **2010**, 49, 4771–4774.

Web references:

(Last access:December 2012)

Web ref. 1, ASTM E2456

<http://www.astm.org/Standards/E2456.htm>

Web ref.2, Millipore tutorial:

<http://www.millipore.com/immunodetection/id3/antibodiestutorial>

Web ref. 3, Abcam protocol:

<http://www.abcam.com/index.html?pageconfig=resource&rid=11269&pid=11287>

Web ref. 4, WHO:

<http://www.who.int/tdr/publications/documents/bl7-annual-report-2008.pdf>

Web ref. 5, Millipore protocol:

<http://www.millipore.com/techpublications/tech1/tb500en00> (last access date: 9/2012).

Web ref. 6:

<http://www.lasalle.edu/~prushan/IC-articles/IC%20exp%204.pdf>

Web ref. 7:

WHO: http://whqlibdoc.who.int/publications/2010/9789241564090_eng.pdf (last access date:

9/2012). *World Health Organization, 2010.*

Web ref. 8:

WHO: <http://www.who.int/mediacentre/factsheets/fs117/en/> -(last access date: 9/2012). *World Health Organization, 2012.* Fact Sheet 117.

Web ref. 9:

<http://drrajivdesaimd.com/290/drrajivdesai/dengue/>

CHAPTER 2

*Enhancement of the detection limit for lateral
flow immunoassays: Evaluation and comparison
of bioconjugates*



Contents lists available at SciVerse ScienceDirect

Journal of Immunological Methods

journal homepage: www.elsevier.com/locate/jim

Technical note

Enhancement of the detection limit for lateral flow immunoassays: Evaluation and comparison of bioconjugates

Elisângela M. Linares ^a, Lauro T. Kubota ^b, Jens Michaelis ^c, Stefan Thalhammer ^{a,*}

^a Helmholtz Zentrum München, German Research Center for Environmental Health, Ingolstädter Landstrasse 1, 85764 Neuherberg, Germany

^b Institute of Chemistry, University of Campinas, Cidade Universitária s/n, 13083-970, Campinas, São Paulo, Brazil

^c Department of Chemistry, Ludwig-Maximilians-Universität München, Butenandtstr. 11, Haus E, 81377 München, Germany

ARTICLE INFO

Article history:

Received 25 September 2011

Received in revised form 2 November 2011

Accepted 3 November 2011

Available online 10 November 2011

Keywords:

Lateral flow immunoassay

Dengue fever

Carbon black

Gold nanoparticles

ABSTRACT

There is an increasing demand for convenient and accurate point-of-care tools that can detect and diagnose different stages of a disease in remote or impoverished settings. In recent years, lateral flow immunoassays (LFIA) have been indicated as a suitable medical diagnostic tool for these environments because they require little or no sample preparation, provide rapid and reliable results with no electronic components and thus can be manufactured at low costs and operated by unskilled personnel. However, even though they have been successfully applied to acute and chronic disease detection, LFIA based on gold nanoparticles, the standard marker, show serious limitations when high sensitivity is needed, such as early stage disease detection. Moreover, based on the lack of comparative information for label performance, significant optimization of the systems that are currently in use might be possible. To this end, in the presented work, we compare the detection limit between the four most used labels: colloidal-gold, silver enhanced gold, blue latex bead and carbon black nanoparticles. Preliminary results were obtained by using the biotin–streptavidin coupling as a model system and showed that carbon black had a remarkably low detection limit of 0.01 µg/mL in comparison to 0.1 µg/mL, 1 µg/mL and 1 mg/mL for silver-coated gold nanoparticles, gold nanoparticles and polystyrene beads, respectively. Therefore, as a proof of concept, carbon black was used in a detection system for Dengue fever. This was achieved by immobilizing monoclonal antibodies for the nonstructural glycoprotein (NS1) of the Dengue virus to carbon black. We found that the colorimetric detection limit of 57 ng/mL for carbon black was ten times lower than the 575 ng/mL observed for standard gold nanoparticles; which makes it sensitive enough to diagnose a patient on the first days of infection. We therefore conclude that, careful screening of detection labels should be performed as a necessary step during LFIA development in order to enhance the detection limit in a final test system.

© 2011 Elsevier B.V. All rights reserved.

1. Introduction

There is an increasing demand for convenient and accurate point-of-care tools that can detect and diagnose different stages of a disease in remote or impoverished settings.

In recent years, lateral flow immunoassays (LFIA) have been indicated as a suitable medical diagnostic tool for these environments and are used as an appropriate technology for a wide variety of point-of-care or field applications ranging from: uses in the health sector to diagnose diseases and prove the absence of pathogenic organisms in food or feed, to aiding law enforcement in the fight against drugs of abuse and bio-warfare (Posthuma-Trumpie et al., 2009). This chromatographic device contains labeled detection proteins, e.g. nanoparticle–antibody conjugates, which will react with a specific analyte. This mobile phase is pulled through the stationary by the capillary effect

* Corresponding author at: Helmholtz Zentrum München, P.O. Box 6154-13084-971, München, Germany. Tel.: +49 89/3187 2893; fax: +49 89/3187 3323.

E-mail address: stefan.thalhammer@helmholtz-muenchen.de (S. Thalhammer).

and passes through a capture zone, e.g. of immobilized target molecules, where the trapped labels accumulate in concentration until visually detectable. The advantages of such a system are numerous and mostly lie in its compact design, speed, simplicity of use and long and robust storage time. Indeed, they require little or no sample preparation, have no electronic components and can solely rely on a binary visual detection. This presents the needed result in a rapid and reliable form, so that an unskilled operator can interpret it, at a low manufacturing cost. However, even though LFIA have been successfully applied to numerous systems, including acute and chronic disease detection, they show serious limitations in high sensitivity applications; which is especially important in the early stage diagnostics of diseases. Here, the detection limit is related to the labels used for detection, and in many cases coupling nanoparticles to the detection molecule is considered to be one of the most powerful techniques for an immediate and clearly resolved test. While colloidal gold is currently the most commonly used label, other detection systems mainly based on fluorescent nanoparticles, dyed latex, and carbon black have been used in an effort to improve the detection limit (Näreoja et al., 2009; Lönnberg and Carlsson, 2001).

Recent works have compared and evaluated LFIA with different detection systems for a variety of applications (Gordon and Michel, 2008; Posthuma-Trumpie et al., 2009). However, a systematic evaluation of the label performance in dependence on the detection limit was not presented. For instance: Colloidal gold was used as detection system for pesticide residues of carbaryl and endosulfan in extracts of cereals and vegetables, showing a detection limit of 100 µg/L and 10 µg/L respectively (Zhang et al., 2006). On the other hand, the same label was applied to detect human serum albumin in urine and it showed a detection limit of 30 mg/L (Cho and Paek, 2001). Furthermore, colloidal carbon labels were used in LFIA to detect the residue of antibiotic sulfametazine (O'Keffe et al., 2003) and erythropoietin (Lönnberg et al., 2008) in 200 µL of urine, revealing detection limits of 6.3 µg/L and 0.035 ng/L, respectively. Nevertheless, the sample for erythropoietin determination was pretreated with filtration and desalting steps, whereas the urine for sulfametazine determination was used without pretreatment. So, although the characteristics of many tests can be found, they are performed in different systems, device structures, sample pretreatments and volumes. Therein, a comparison of the performance and sensitivities of different labels could be used to significantly optimize the detection limit of the end product.

A current example related to the inadequate detection limit for LFIA has been reported for early stage detection of Dengue fever (DF). DF is a mosquito-borne viral infection that, in recent decades, has become a major international public health concern. Dengue hemorrhagic fever (DHF), a potentially lethal complication, has become a leading cause of hospitalization and death. Indeed, the World Health Organization (2009) estimated that two fifths of the world's population was at risk with an annual 50 million reported cases worldwide. For DHF, early detection and medical care can decrease mortality rates from more than 20% to less than 1%. More than 20 rapid tests based on LFIA principles for DF are commercially available, but most of them show limited application due to their low sensitivity and specificity. This was recently exemplified when 8 commercial

kits for DF based on IgG/IgM detection were evaluated and only one showed the necessary specificity (97.6%) and sensitivity (65.3%) to be considered of clinical use (>50%) (Blacksell et al., 2006). It means that only one test had the proportion of actual positives correctly identified (sensitivity) higher than 50% and the proportion of negatives correctly identified (specificity) higher than 50%. Currently, a highly conserved viral non-structural glycoprotein (NS1) of the Dengue virus has been used as a high potential analyte target for early Dengue detection (Datta and Wattal, 2010). During the acute phase, the virus produces high NS1 levels in membrane-associated and secretory forms, which are both demonstrated to be immunogenic (Alcon et al., 2002; Lima et al., 2010). Commercial LFIA tests based on NS1 detection are available and show a high variability in sensitivity (between 37% and 98.9%), which can be partially explained by the fact that the sensitivity has been reported to decrease with time both during the infection and with secondary infections (Osorio et al., 2010).

Based on the lack of comparative information available for label performance, in the light that optimization could yield the necessary sensitivity for LFIA to be used as an early stage diagnostic tool, we identified and evaluated the four most used labels: gold, silver-enhanced gold, dyed latex bead and carbon black nanoparticles. Preliminary results, in the terms of a systematic comparison of the detection limit, were obtained by using the well-known biotin–streptavidin coupling as a model system. Once established, a proof of concept was made by comparing carbon black against the standard colloidal gold to diagnose DF.

2. Materials and methods

2.1. Chemicals and materials

Streptavidin-labeled carboxylate-modified polystyrene blue latex beads with a mean diameter of 250 nm, bovine serum albumin (BSA) powder, biotin-NHS, streptavidin, boric acid, glycine, anti-mouse IgG antibody-alkaline phosphatase, nitroretazolium blue chloride, 5-bromo-4-chloro-3-indolyl phosphate disodium salt, potassium phosphate mono- and dibasic were purchased from Sigma-Aldrich (Milwaukee, USA). Glutaraldehyde 25% was obtained from Calbiochem (Darmstadt, Germany). Gold nanoparticles with a mean diameter of 40 nm, streptavidin-labeled gold nanoparticles and a silver enhancer kit were purchased from British Biocell International (Cardiff, United Kingdom). Carbon black 100 and nitrocellulose AC99 membranes were obtained from Degussa (Essen, Germany) and Whatman (Maidstone, United Kingdom), respectively. Purified Dengue virus NS1 glycoprotein and Dengue Virus NS1 glycoprotein mouse monoclonal antibody (NS1mAb) supernatant were obtained from Abcam (Cambridge, United Kingdom) and Thermo Scientific (Rockford, United States), respectively. 1 mL Hitrap protein G HP column for affinity chromatography and a PD10 desalting column were purchased from GE Healthcare (Uppsala, Sweden). Sample of DF serum was provided by Clinical Hospital at State University of Campinas in Brazil and the presence of the DF virus NS1 protein was confirmed by the use of a sandwich ELISA from Standard Diagnostics (Hagal-Dong, Korea).

2.2. Antibody purification

The NS1mAb was purified by protein G affinity chromatography. The supernatant was slowly passed through the protein G column using an ÄKTApurifier 100 (GE Healthcare, Uppsala, Sweden). The NS1mAb was eluted from the column in a total volume of 10 mL of 0.1 mol/L glycine at pH 2.8. The volume was additionally reduced to 1 mL by ultrafiltration, using a 100 k Amicon ultra-4 centrifugal filter (Millipore, Billerica, USA), centrifuged at 4000 rpm for 13 min and then the buffer was exchanged to $1 \times$ PBS using a desalting column.

2.3. Nanoparticle–protein conjugate preparation

Blue latex bead nanoparticles were purchased with streptavidin covalently bound in a buffered aqueous suspension and, therefore, only needed to be diluted.

Carbon black–streptavidin and carbon black–NS1mAb covalently bound particle–conjugates were prepared according to Rayev et al. (Rayev and Shmagel, 2008). Purifying the protein-coated nanoparticles was achieved through centrifugation at 13 000 rpm for 10 min, carefully removing the clear supernatant and dispersing. This washing step was repeated 5 times. Protein-coated nanoparticles were stored in 0.01 M phosphate buffer solution containing 5% BSA and 20% glycerol at pH 7.5 and stored at 4 °C. In order to optimize the immobilization reaction, the buffer concentration and pH were varied from 1 to 0.001 M and from 6 to 8, respectively. For all other reactions 0.01 M borate buffer, pH 8, and phosphate buffer were used. The final solid content was 1% (w/w).

Gold nanoparticles were purchased with streptavidin already covalently bound in a buffered aqueous suspension and, therefore, only needed to be diluted.

Gold nanoparticle–NS1mAb conjugate preparation was performed according to the following protocol: Gold nanoparticle dispersions were adjusted to pH 8 with a 0.01 M solution of NaOH. 10 μ L of 0.01 mg/mL NS1mAb solution was added to 0.1 mL of the adjusted gold dispersion and stirred for 30 min. Purification of the gold nanoparticle–NS1mAb conjugates was achieved by centrifugation at 5000 rpm for 15 min at 4 °C. The clear supernatant was carefully removed, and the precipitated gold conjugates were dispersed in 100 μ L of phosphate buffer and stored at 4 °C, containing 1% (w/w) of solid contents. The optimum pH for conjugation was found by making a series composed of solutions adjusted to pH 7, 8, and 9 and evaluated by dot blot tests.

2.4. Streptavidin coated nanoparticle characterization by atomic force microscopy (AFM)

Topographical analysis of the different nanoparticle labels was performed by AFM. Each particle–dispersion was sonicated for 10 min at room conditions and deposited on glass slides resulting in a 0.01% (w/v) dispersion of solid components. Particles were analyzed using an AFM (JPK Nanowizard 1, Berlin Germany) in intermittent contact mode with 100 μ m xy-scan range and 15 nm z-scan range and Si tips NSC 15 (40 N/m spring constant) (Mikromasch, Las Rozas de Madrid Spain). Images were processed and analyzed using JPK SPM v3.1 and Gwyddion v2.19. Size distribution

histograms were obtained by measuring the diameter of 150 particles of each material.

2.5. Dot blot tests

2.5.1. The streptavidin–biotin system

BSA was biotinylated according to Guesdon et al. (1979) and purified by dialysis. Biotin functionalization of the nitrocellulose membrane was achieved by slowly pipetting 2 μ L spots, each of different concentrations ranging from 0.01 μ g/mL to 10 mg/mL of the biotinylated BSA onto different locations of the membrane. The remaining non-specific sites were blocked by submersing the membrane into a deactivation solution 5% (w/v) BSA in 0.1 M phosphate buffer at pH 7. Washing steps were performed by dipping the membranes 3 times during 5 min each into a 0.01 M phosphate buffer solution, at pH 7.4. Gold, blue latex and carbon black particle–streptavidin conjugate dispersions were diluted in 0.01 M phosphate buffer at pH 7.4 to a content of 0.5% (w/v) solids. Each of the biotin functionalized membranes was submerged into different particle–streptavidin conjugate dispersions for 20 min. The particles passed through the membranes and particles in excess were absorbed by a cellulose absorbent pad located on the other membrane extremity. Subsequently, the membranes were washed with 0.01 M phosphate buffer at pH 7.4, air-dried and scanned.

2.5.2. Silver enhancement

The gold nanoparticle labeled membrane was additionally enhanced by submersing it into silver solution with reducing agent. A curve of gold nanoparticle–conjugates being enhanced with silver was obtained by adding a 2 μ L droplet of gold nanoparticle–streptavidin solution, containing 0.5% (w/v) of solids, onto an untreated nitrocellulose membrane. This was in turn submerged into silver solution with reducing agent and the signal enhancement was measured by taking consecutive pictures with a Sony 230 of 7.3 megapixel camera and analyzing the results with Gwyddion v2.19.

2.5.3. Antibody–protein system

NS1 protein concentration was determined, from a serum sample of a patient with clinical diagnosis of acute DF, by enzyme linked immunosorbent assay. NS1 protein functionalization of the nitrocellulose membrane was achieved by diluting the serum samples in 0.01 M phosphate buffer at pH 7.4 and then slowly pipetting 2 μ L spots, each of different concentrations ranging from 0.06 to 5.75 μ g/mL, of the NS1-protein onto different locations of the membrane. The remaining non-specific sites were blocked by submersing the membrane into a solution 5% (w/v) BSA in 0.1 M phosphate buffer at pH 7. Each of the NS1 functionalized membranes were submerged into either carbon black–NS1mAb or gold–NS1mAb conjugate dispersions with a concentration of 1% (w/v) solids in 0.01 M phosphate buffer at pH 7.4 and incubated at RT for 20 min. The particles flowed through the membranes and particles in excess were absorbed by a cellulose absorbent pad located on the other membrane extremity. Subsequently, the membranes were washed with 0.01 M phosphate buffer at pH 7.4 and air-dried. Gray scale optical analysis was performed from scanned images.

2.6. Digitalization of the dot blot test

48-bit images of the dot blot tests, that included a gray scale reference chart in each scan, were acquired with a Hewlett-Packard 3800 Scanjet scanner (Palo Alto, USA). The images were processed with Image-J v1.42 where a 5×1.2 mm area was selected for analysis of each image and the mean background, calculated from three different points in close proximity to the relevant dot blot, was subtracted. The processed image RGB channels were then split using Adobe Photoshop CS3, and the most intense channel was converted into 8-bit gray scale. Each dot blot was now represented by a number from 0 to 255, corresponding to white and black, respectively, and the data quantified in blackness percentage.

3. Results and discussion

An initial study, by topographical analysis, of the different nanoparticle labels was performed to make a firsthand comparison of the systems. This was of particular importance since the silver-enhanced gold particle system was uncharacterized. The AFM micrographs are depicted in Fig. 1 together

with the corresponding cross section graph defined by a white line. The gold nanoparticles, shown in Fig. 1a, have a very sharp size distribution with a mean diameter of 39 ± 5 nm. This particle size was chosen since it is well-known to provide the best performance for gold nanoparticles in LFA (Posthuma-Trumpie et al., 2009). Moreover, silver enhancement is a well-practiced method of additionally improving the signal from gold nanoparticle systems. To this end, the autometallography method (Danscher et al., 1993), which is based on the reduction of a silver salt at the surface of gold particles, was used to enlarge the gold particle size by forming a core-shell structure. As it transpired, the resulting silver coated gold nanoparticles had grown up to 5 times larger than the gold core, which can be seen in Fig. 1b. The size distribution curve can be seen in Fig. 1e and reveals a bimodal mean diameter distribution of 55 ± 9 nm and 187 ± 22 nm. This inhomogeneity in growth may be caused by the steric hindrance of neighboring particles. In order to find the optimum exposure time in dependence on visual signal enhancement, gold nanoparticle-conjugates were deposited onto a nitrocellulose membrane and exposed to silver reducing solution. The measured Δ blackness was plotted in dependence on

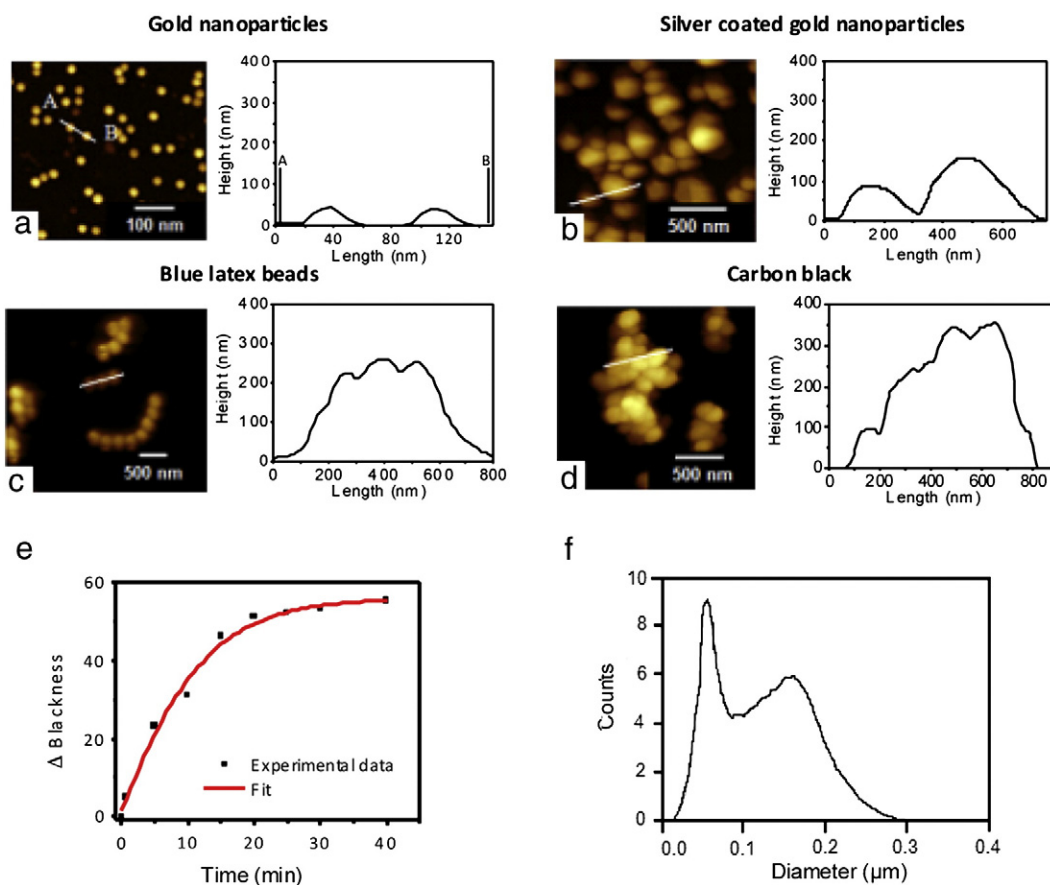


Fig. 1. Particle characterization using AFM. Topography images and line profiles were obtained for particle dispersions dried on glass slides for: a) gold nanoparticles, b) silver enhanced gold nanoparticles, c) blue latex beads and d) carbon black. e) The variation of blackness is plotted in dependence on exposure time for gold nanoparticles added to silver reducer solution. f) Size distribution curve calculated from AFM images of gold nanoparticle after 20 min of exposure to silver reducer solution.

time and is depicted in Fig. 1f. We found that 20 min was the best choice since it is the shoulder value between a fast increase in intensity and the start of non-specific silver reduction increasing the background signal. Blue latex beads, Fig. 1c, were found to have a slightly larger average diameter, than the 250 nm defined by the manufacture, of 293 ± 9 nm and form strip like agglomerates. Carbon black, Fig. 1d, has a large distribution with an average particle diameter of 150 ± 50 nm and form extensive aggregates ranging between 0.5 and $2 \mu\text{m}$.

It can be seen that the labels show different degrees of agglomeration that even occur after ultrasonic treatment, as a result of the high affinity of similar particles and the differences in structure. The density and size of these agglomerates could impede a direct comparison of performance among the labels for LFIA, due to the difficulty of attributing the signals to differences in absorptivity, particle concentration in agglomerates or density of immobilized biomolecules. However, each system was chosen according to the literature, using the most appropriate label characteristics for LFIA, optimized biomolecule immobilization and particle excess to ensure saturation in the nitrocellulose. For instance, gold nanoparticles with 40 nm diameter provides the most efficient flow through the membranes and high signal to noise ratio in comparison to bigger gold particles. On the other hand, due to its low density, carbon black can be used with larger diameters without dramatically preventing its flow through the membranes in which pore size is 8–12 times the carbon black agglomerate diameter.

Evaluation of the nanoparticles as labels was done by dot blot tests. Here, the nanoparticles were directly bound to the detection proteins as represented in Fig. 2a. In this work we used

both NS1mAb and streptavidin to target the NS1 protein and biotin, respectively. A nitrocellulose membrane was functionalized with a concentration series of the target molecules in the form of $2 \mu\text{L}$ dots placed in different locations along the membrane. The remaining non-specific sites were blocked and then the membrane was exposed to a solution of the labeled detection proteins, as depicted in Fig. 2b, and the signal intensity interpreted.

Preliminary results, in the terms of a systematic comparison of the detection threshold and saturation values, were obtained by using the well-known biotin–streptavidin coupling as a model system. To this end, dot blot tests were prepared with a dilution series of biotinylated-BSA spots ranging from 10 mg/mL to $0.01 \mu\text{g/mL}$ and exposed to the nanoparticle–streptavidin conjugates. Curves comparing the signal intensity, for each label in dependence on the concentration of deposited biotinylated-BSA, are presented in Fig. 2c–d. Absorbance saturation curves are presented in Fig. 2c showing plateau values of 3, 6, 17 and 58% for blue latex bead, gold, silver enhanced gold and carbon black nanoparticles, respectively. The same data set is plotted in Fig. 2d with the concentration on a \log_{10} scale to identify the visible detection thresholds of 1 mg/mL, $1 \mu\text{g/mL}$, $0.1 \mu\text{g/mL}$ and $0.01 \mu\text{g/mL}$ for blue latex bead, gold, silver enhanced gold and carbon black nanoparticles, respectively. Spots were visible by naked eye above 5% of blackness percentage (represented by the dashed line in Fig. 2d). Thus, carbon black has unmistakably the highest signal performance in relation to the other tested labels with 100 times greater detection limit and 10 times higher signal intensity than the standard gold system. In addition, it is readily available in several forms

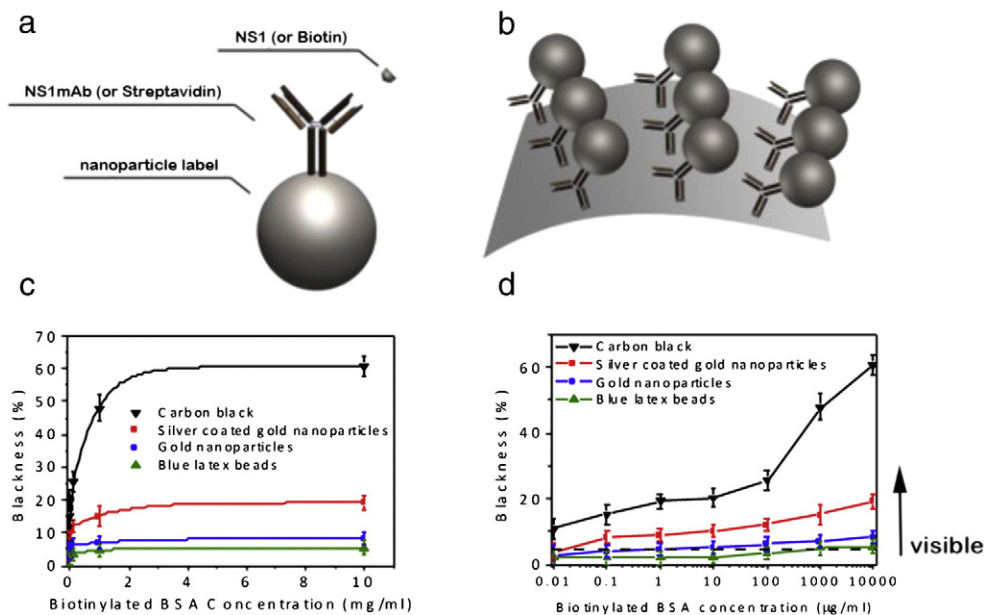


Fig. 2. Illustration of the system and a comparison of the blackness after 20 min of exposure in dependence on biotinylated-BSA concentration for the four different labels: carbon black, silver coated gold, gold, and blue polystyrene bead nanoparticles. a) An illustration of a nanoparticle labeled detection protein. b) Illustration of a target protein functionalized membrane exposed to labeled detection protein conjugates. c) A linear plot emphasizing the saturation point of the different labels; carbon black showing by far the strongest signal. d) The same data set is plotted with the concentration on a \log_{10} scale to identify the detection threshold for the different systems (a dashed line shows the visible limit observed by naked eye).

and particle sizes useful for different detection ranges (Lönnberg and Carlsson, 2001).

Based on these results, carbon black was chosen as detection label for DF using the viruses NS1 glycoprotein, which is used in early detection methods, as a target molecule. Since the standard LFIA tests are based on gold nanoparticles and are clinically known to provide limited sensitivity for diagnosis during the first days of the disease: Carbon black was directly compared with the gold system to find out if it can overcome this limitation.

Thus, dot blot tests were prepared with a dilution series of NS1 protein spots ranging from 0.06 to 5.75 $\mu\text{g}/\text{mL}$ and separately exposed to the nanoparticle–NS1mAb conjugates prepared at the same solid contents. Fig. 3a shows an image of the scanned spots and the carbon black–antibody conjugates are clearly visible at 57 ng/mL, whereas the gold nanoparticle signal can only be clearly interpreted at 575 ng/mL. This detection limit is according to the concentration that is required to produce a signal greater than three times the standard deviation of the noise level. The difference in detection threshold is more clearly shown in Fig. 3b–c. The blackness and the spot area reduce when the protein concentration is decreased and the detection limit depends on the compromise of both parameters. The area reduction is due to the high affinity of the protein to the nitrocellulose membrane, avoiding the protein spreading during the solution deposition. The results reveal that carbon black conjugates are approximately 10 times more sensitive than gold nanoparticles for NS1 protein detection. According to Libraty et al. (2002), plasma levels of secreted NS1 protein from free Dengue-2 virus may vary between 150 and

250 ng/mL per day of illness for the second day of contracting the disease for patients that are both DHF and secondary infections. Therein, the carbon black system is indeed capable of providing a visual signal bellow the NS1 concentration that exists in infected patients on the first days of the disease. This sensitivity enhancement is decisive for early DF detection based on the NS1 protein and can be vital for the rapid assessment of patients developing more severe cases of the disease.

4. Conclusion

We compared the detection limit and signal intensity between the four most used labels: gold, silver enhanced gold, blue latex bead and carbon black nanoparticles. Preliminary results were obtained by using the biotin–streptavidin coupling as a model system and showed that carbon black had a remarkably lower detection limit of 0.01 $\mu\text{g}/\text{mL}$ in comparison to 0.1 $\mu\text{g}/\text{mL}$, 1 $\mu\text{g}/\text{mL}$ and 1 mg/mL for silver-enhanced gold, gold, and latex bead nanoparticles, respectively. Moreover, carbon black was used as a detection system for Dengue fever where a colorimetric detection limit of 57 ng/mL for carbon black was found to be ten times lower than the 575 ng/mL for standard gold nanoparticles. This improvement, that makes the system sensitive enough to diagnose a patient on the first day of infection, can be crucial to overcome the limitations of LFIA in regard to early diagnosis of Dengue fever. We therefore conclude that, careful screening of detection labels should be performed as a necessary step during LFIA development in order to enhance the detection limit in a final test system and we hope that these results can facilitate the development of

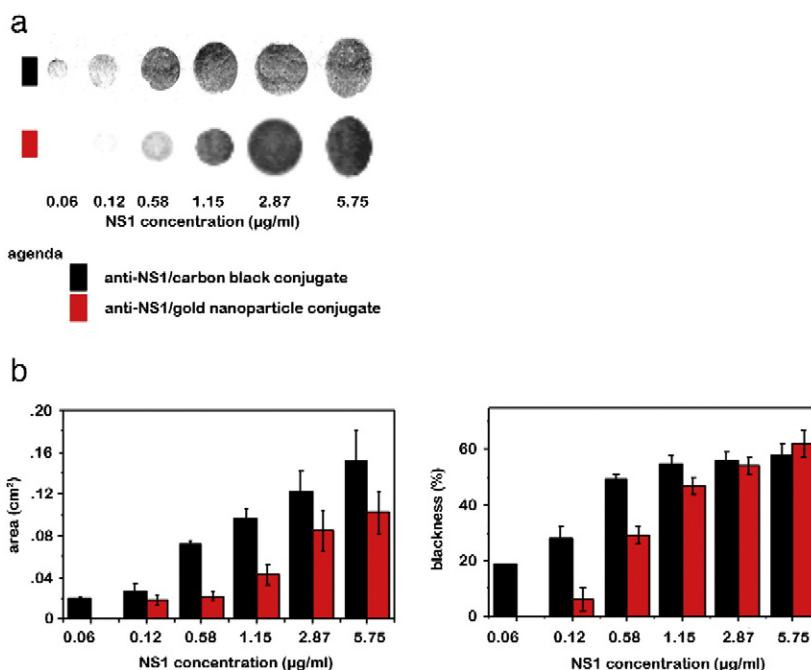


Fig. 3. Detection limit for the Dengue virus NS1 protein based on gold and carbon black nanoparticles coated with anti-NS1 monoclonal antibodies. a) Scanned dot blot tests showing the dilution series of NS1 protein after being exposed to carbon black and gold nanoparticle NS1mAb detection conjugates. b) Shows the same data set as blackness intensity and spot area in dependence on concentration.

LFIA in terms of the suitable label choice for the detection system in order to achieve a specific sensitivity.

Acknowledgments

The authors would like to thank the Clinical Hospital at State University of Campinas, Brazil, which kindly provided the serum sample. EML acknowledges the fellowship from the International Doctorate Program NanoBioTechnology (IDK-NBT) funded by the Elite Network of Bavaria (ENB) and John Howgate for assistance and proof reading. This work was supported by the cluster of excellence Nano Initiative Munich (NIM), the Center of Nanoscience (CeNS), DAAD and CAPES.

References

- Alcon, S., Talarmin, A., Debruyne, M., Falconar, A., Deubel, V., Flamand, M., 2002. An antigen capture enzyme-linked immunosorbent assay reveals high levels of the dengue virus protein NS1 in the sera of infected patients. *J. Clin. Microbiol.* 40, 376.
- Blacksell, S.D., Newton, P.N., Kelley, J., Mammen Jr., M.P., Vaughn, D.W., Wuthiekanun, V., Sungkakum, A., Nisalak, A., Day, N.P.J., 2006. The comparative accuracy of 8 commercial rapid immunochromatographic assays for the diagnosis of acute dengue virus infection. *Clin. Infect. Dis.* 42, 1127.
- Cho, J.-H., Paek, S.-H., 2001. Semiquantitative, bar code version of immunochromatographic assay system for human serum albumin as model analyte. *Biotechnol. Bioeng.* 75, 725.
- Danscher, G., Hacker, G.W., Grimelius, L., Rytter, J.O., 1993. Autometallographic silver amplification of colloidal gold. *J. Histochem. J.* 16, 201.
- Datta, S., Wattal, C., 2010. Dengue NS1 antigen detection: a useful tool in early diagnosis of Dengue virus infection. *Indian J. Med. Microbiol.* 28, 107.
- Gordon, J., Michel, G., 2008. Analytical sensitivity limits for lateral flow immunoassays. *Clin. Chem.* 54, 1250.
- Guesdon, J.L., Ternynck, T., Avrameas, S., 1979. The use of avidin-biotin interaction in immunoenzymatic techniques. *J. Histochem. Cytochem.* 27, 1131.
- Libraty, D.H., Young, P.R., Pickering, D., Endy, T.P., Kalayanarooj, S., Green, S., Vaughn, D.W., Nisalak, A., Ennis, F.A., Rothman, A.L., 2002. High circulating levels of the Dengue virus nonstructural protein NS1 early in Dengue illness correlate with the development of Dengue hemorrhagic fever. *J. Infect. Dis.* 186, 1165.
- Lima, M.R.Q., Nogueira, R.M.R., Schatzmayr, H.G., Santos, F.B., 2010. Comparison of three commercially available Dengue NS1 antigen capture assays for acute diagnosis of Dengue in Brazil. *PLoS Neglected Trop. Dis.* 4, e738.
- Lönnerberg, M., Carlsson, J., 2001. Quantitative detection in the attomole range for immunochromatographic tests by means of a flatbed scanner. *Anal. Biochem.* 293, 224.
- Lönnerberg, M., Drevin, M., Carlsson, J., 2008. Ultra-sensitive immunochromatographic assay for quantitative determination of erythropoietin. *J. Immunol. Methods* 339, 236.
- Näreoja, T., Vehniäinen, M., Lamminmäki, U., Hänninen, E.P., Härmä, H., 2009. Study of nonspecific of an immunoassay using Eu-doped polystyrene nanoparticle labels. *J. Immunol. Methods* 345, 80.
- O'Keffe, M., Crabbe, P., Salden, M., Wichers, J., van Peteghem, C., Kohen, F., Pieraccini, G., Moneti, G., 2003. Preliminary evaluation of a lateral flow immunoassay device for screening urine samples for the presence of sulphamethazine. *J. Immunol. Methods* 278, 117.
- Osorio, L., Ramirez, M., Bonelo, A., Villar, L.A., Parra, B., 2010. Comparison of the diagnostic accuracy of commercial NS1-based diagnostic tests for early dengue infection. *Virology* 403, 361.
- Posthuma-Trumpie, G.A., Korf, J., Amerongen, A., 2009. Lateral flow (immuno)assay: its strengths, weakness, opportunities and threats. A literature survey. *Anal. Bioanal. Chem.* 393, 569.
- Rayev, M., Shmagel, K., 2008. Carbon-protein covalent conjugates in non-instrumental immunodiagnostic systems. *J. Immunol. Methods* 336, 9.
- Zhang, C., Zhang, Y., Wang, S., 2006. Development of multianalyte flow-through and lateral-flow assays using gold particles and horseradish peroxidase as tracers for the rapid determination of carbaryl and endosulfan in agricultural products. *J. Agric. Food Chem.* 54, 2502.

Web references

- World Health Organization, 2009. Dengue and dengue haemorrhagic fever—Fact Sheet 117 <http://www.who.int/mediacentre/factsheets/fs117/en/print.html>2009-(last access date: 08/2010).

CHAPTER 3

Immunospot assay based on fluorescent nanoparticles for Dengue fever detection



ELSEVIER

Contents lists available at [SciVerse ScienceDirect](http://SciVerse.Sciencedirect.com)

Biosensors and Bioelectronics

journal homepage: www.elsevier.com/locate/bios

Immunospot assay based on fluorescent nanoparticles for Dengue fever detection

Elisângela M. Linares^a, Claudio S. Pannuti^b, Lauro T. Kubota^c, Stefan Thalhammer^{a,*}

^a Helmholtz Zentrum München, German Research Center for Environmental Health, Ingolstädter Landstrasse 1, 85764 Neuherberg, Germany

^b Laboratory of Virology, Instituto de Medicina Tropical de São Paulo e Faculdade de Medicina, Universidade de São Paulo. Eneas de Carvalho Aguiar 470, 05403-000, São Paulo, Brazil

^c Institute of Chemistry, State University of Campinas, Cidade Universitária s/n, 13083-970, Campinas, São Paulo, Brazil

ARTICLE INFO

Article history:

Received 14 June 2012

Received in revised form

25 July 2012

Accepted 3 August 2012

Keywords:

Immunospot assay

Dengue fever

Fluorescent nanoparticles

ELISA

ABSTRACT

Dengue fever is one of the most neglected tropical diseases and of highest international public health importance, with 50 million cases worldwide every year. Early detection can decrease mortality rates from more than 20% to less than 1% and the relevant early diagnosis analyte is the viral non-structural glycoprotein, NS1. Currently, enzyme linked immunosorbent assay (ELISA) is the method of choice to detect NS1. However, this is a time consuming method, requiring 3–5 h, and it is the bottleneck for routine of clinical analysis laboratory in epidemic periods, when hundreds of samples should be tested. Here we describe an easy method combining principles of fluorophore linked immunosorbent assay (FLISA) and enzyme linked immunospotting (ELISPOT). For detection, we used mouse anti-NS1 IgG labeled with fluorescent nanoparticles. The presented procedure needs only 4 μ L of serum samples and requires 45–60 min. The detection limit, 5.2 ng/mL, is comparable to ELISA tests. The comparison of 83 samples with a commercial ELISA revealed a sensitivity of 81% and specificity of 88%. The use of fluorescent nanoparticles provides a higher sensitivity than an assay using usual fluorescent dye molecules, besides avoiding bleaching effects. Based on the results, the proposed method provides fast, specific and sensitive results, and proves to be a suitable method for Dengue NS1 detection in impoverished regions or epidemic areas.

© 2012 Elsevier B.V. All rights reserved.

1. Introduction

Neglected tropical diseases (NTD) are a multiple of diverse diseases strongly associated with poverty, flourishing in impoverished environments and thriving best in tropical areas. Due to these characteristics, they have low visibility in the rest of the world and limited access to support services. Among the NTD, Dengue fever (DF) has emerged as a rapidly spreading vector-borne disease affecting mainly poor, urban populations and it is also the leading cause of hospital admissions in several countries (WHO, 2010). DF results from infection with a virus transmitted mainly by *Aedes aegypti*, a species of mosquito with a global distribution. The incidence of DF has dramatically grown over the world in recent decades. Over 2.5 billion people are now endangered from Dengue. The World Health Organization (WHO, 2012) currently estimates 100 million cases of Dengue fever, 500,000

cases of Dengue hemorrhagic fever (DHF) and resulting in 2.5% of annual mortality. The disease is now endemic in more than 100 countries in Africa, America, Eastern Mediterranean, South-east Asia and Western Pacific. The threat of a possible outbreak of DF now exists in Europe and local transmission of DF was reported for the first time in 2010. For DHF, medical care can save lives, decreasing mortality rates from more than 20% to less than 1% (Allwinn, 2011).

To provide medical care, DF diagnosis should be fast, specific, sensitive and with low cost. Nowadays, there are different tools used for diagnosis by isolating the virus, detecting viral antigen or RNA in serum or tissues (Levi et al., 2007), and detecting specific antibodies or proteins in the serum (Guzman and Kouri, 1996). Serologic tests have been routinely used for diagnosis of DF due to their simplicity and rapidity in comparison to the other methods. Enzyme linked immunosorbent assay, ELISA, has become the most widely used serologic test for DF diagnosis in the past few years due to its simplicity and little sophisticated equipment (Gubler, 1998). These assays are predominantly based on the detection of immunoglobulin, which consists of IgM and IgG antibodies produced against the virus at day 5 or 6 of illness (Vaughn et al., 1997). Due to the necessity of diagnosing DF in

* Correspondence to: Ingolstädter Landstraße 1, 85764 Neuherberg, Germany. Tel.: +49 89 3187 2893; fax: +49 89 3187 3323.

E-mail addresses: elisangela.linares@helmholtz-muenchen.de (E.M. Linares), cpannuti@usp.br (C.S. Pannuti), kubota@iqm.unicamp.br (L.T. Kubota), stefan.thalhammer@helmholtz-muenchen.de (S. Thalhammer).

early stages, a highly conserved viral non-structural glycoprotein (NS1) of the Dengue virus has been used as a high potential analyte target for early Dengue detection (Datta and Wattal, 2010; Linares et al., 2012). Dengue NS1 antigen has been detected in the serum of DF infected patients as early as one day post onset of symptoms. During acute phase, high NS1 level exists as membrane-associated and secretory forms by the virus; both forms are demonstrated to be immunogenic (Lima et al., 2010).

NS1 detection using ELISA is based on the principle of a solid phase sandwich enzyme-linked immunosorbent assay with colorimetric detection. A monoclonal antibody is adsorbed on the solid phase and works as capture antibody for binding the antigen. Another monoclonal antibody conjugated to an enzyme is used to detect the antigen through a colorimetric enzymatic reaction (Najjoulah et al., 2011). Although Dengue NS1 ELISA offers a sensitive approach with detection in the low ng/ml range, the technique also shows some disadvantages. ELISA tests require a large number of incubation and washing steps. These make the procedure difficult to automate for screening large sample number, and significantly prolong the time up to 5 h to get the results (Alcon et al., 2002; Young et al., 2000). In addition, in many cases, efficient antibody adsorption on microplates requires overnight incubation time. For routine tests in clinical analysis laboratories during epidemic periods, the test duration is relatively long, as hundreds of samples should be tested at the same day (Liu et al., 2003; Velappan et al., 2008).

Analogous to ELISA principles, another technique has been used for DF detection, which are based on enzyme-linked immunospot (ELISPOT). The term immunospot has been used to refer to a method, where antibodies are immobilized on membrane, compounds secreted by cells are captured and an enzyme conjugated antibody provides the colorimetric detection (Bathoorn et al., 2011; Franci et al., 1986). The use of paper, such as nitrocellulose membranes, has provided an useful and simple base for fast and low cost tests (Liu et al., 2011; Martinez et al., 2010). Cardoso et al. (1988, 1995) reported the development of a dot enzyme immunoassay for the detection of Dengue antibodies. This formed the basis of a commercial Dengue blot kit in which the viral antigens are bound to nitrocellulose membranes instead of microplates. The antibodies are visualized using protein A, which is labeled with horseradish peroxidase (Lam et al., 1996). Although this assay allows field application with diagnosis in peripheral health settings due to the use of membrane as solid support, the tests also involve several time consuming steps, which turns to the same practical disadvantages observed for ELISA.

While efforts have been described to overcome ELISA limitations (Chunglok et al., 2011; Pião et al., 2009; Piletsky et al., 2001; Wan et al., 2012), fluorophore linked immunosorbent assays (FLISAs) have been proven to be a powerful alternative that uses fluorescence rather than enzymatic activity for detection and thus overcome some of the disadvantages of ELISA (Cummins et al., 2006; Liu et al., 2003; Velappan et al., 2008). Compared to sandwich ELISA, this assay has several advantages: rapidity (the time is reduced from 5 to 1.5 h), simplicity and lower costs due to the use of fewer reagents. FLISA still shows similar specificity and sensitivity as the sandwich ELISA (Liu et al., 2003). New approaches have also been described to improve FLISA performance. Miller et al. (2006) used fluorescent dyes conjugated to antibody coated polystyrene beads to detect the analyte on the focus plane by confocal laser scanning microscopy. High sensitive assays have been also described using quantum dot-based fluorescence-linked immunosorbent assays, enhancing the fluorescence signal provided by high intensity of a particle in comparison to a dye (Zhu et al., 2011; Peng et al., 2009).

In this work, we present an immunospot test for Dengue detection, combining FLISA advantages with principles of ELISPOT

as an alternative method to replace sandwich ELISA in impoverished regions or epidemic areas. The advantage of combining both techniques is the development of a sensitive and fast sensor. Spot tests based on fluorescence detection have already shown useful combinations of high sensitivity and low complexity (Linares et al., 2007). In the proposed test, a low volume of serum sample is applied onto a nitrocellulose membrane and mouse anti-NS1 IgG labeled with fluorescent nanoparticles are used for Dengue detection. The test takes less time and the fluorescent signal can be measured with a fluorometer or alternatively with an UV-lamp. The possibility of applying the sample directly to a high surface area nitrocellulose membrane allows the use of low volume of samples and avoids the necessity of two antibodies for capture and detection. The use of fluorescent nanoparticles provides lower detection limit in comparison to conventional FLISA, additionally avoiding bleaching effects. As a general view, the immunospot test allows diagnosing DF in less than one hour with high specificity and sensitivity, less complexity and using conventional apparatus in clinical analysis laboratories.

2. Materials and methods

2.1. Chemicals and materials

Bovine serum albumin (BSA), glycine, *N*-(3-Dimethylamino-propyl)-*N*'-ethylcarbodiimide hydrochloride (EDC), anti-mouse IgG-FITC antibody, dialysis membranes (MWCO 100 kDa and 130 kDa), Tween 20, sodium carbonate and bicarbonate, potassium phosphate mono- and dibasic were purchased from Sigma-Aldrich (Munich, Germany). FluoSpheres carboxylate-modified microspheres, 5% (w/w), [yellow-green (505/515 nm), orange (540/560 nm) and red (580/605 nm)], 0.04 μm , were obtained from Invitrogen (Carlsbad, United States). Nitrocellulose AC100 membrane and absorbent pad were purchased from Whatman (Maidstone, United Kingdom). ELISA microplate, F96 MicroWell™ plates, was obtained from NUNC (Roskilde, Denmark).

Dengue Virus NS1 glycoprotein mouse monoclonal antibody was obtained from Abcam (Cambridge, United Kingdom). Purification procedure is described in Supplementary Information. NS1 Ag ELISA kits were purchased from Standard Diagnostics (Hagal-Dong, Korea) and Biorad Laboratories (Marnes-La-Coquette, France).

2.2. Serum samples

A total of 83 serum samples were obtained by the São Paulo Institute of Tropical Medicine, University of São Paulo. The tests were approved by the ethics committee from the university. The samples were analyzed for NS1 using the commercial kit Platelia™NS1 (Biorad Laboratories, Marnes-La-Coquette, France). Dengue diagnostic is described in the supplementary information.

2.3. Synthesis of polystyrene nanoparticle-albumin conjugates

An aliquot of 1 mg of albumin at 3 mg/mL was dissolved in phosphate buffer 0.01 mol/L, pH 7.4. Then, 500 μL of a 2% aqueous suspension of carboxylate-modified sphere was added and incubated at RT for 30 min. Subsequently, 0.5 mg of EDC was added and mixed by vortexing and the pH was adjusted to 6.5 ± 0.2 with diluted NaOH. The dispersion was incubated on a shaker for 3 h at RT. To remove unbound proteins, dialysis was performed through a membrane with MWCO of 100 kDa against phosphate buffer 0.01 mol/L, pH 7.4, during 24 h and 5-times change of the external solution.

2.4. BSA-coated particle functionalization with monoclonal dengue NS1 antibody

A 500 μL particle aqueous dispersion 1% (w/w) was added to 0.09 mL of a 0.5 mg/mL solution of antibody dissolved in phosphate buffer 0.01 M, pH 6. In principle, the conjugate has 9 μg of NS1 antibody per mg of nanoparticles. The suspension was incubated for 30 min at RT. Briefly after, 1 mg of EDC was added and mixed by vortexing. The dispersion was constantly stirred for 1 h at RT. To separate the protein-labeled conjugates from unbound antibodies, a dialysis membrane with MWCO of 130 kDa was used against phosphate buffer 0.01 mol/L, pH 7.4 for 24 h and 5-times change of the external solution. The conjugates were stored at 4 $^{\circ}\text{C}$.

2.5. Immunospot tests

For single analysis, the strip test contains the reaction membrane and the absorbent pad. Nitrocellulose membrane (10 mm \times 60 mm) was pasted on a polyvinyl back (10 mm \times 100 mm) and an absorbent pad (10 mm \times 45 mm) was fixed on the opposite side. Four microliters of serum were slowly spotted on the center area of the nitrocellulose membrane. After drying the serum droplet, 40 μL of BSA 3% in phosphate buffer 0.01 mol/L, pH 7.4, was added directly on the dried serum spot and the excess of liquid was absorbed by the absorbent pad. Subsequently, 30 μL of fluorescent conjugates 1% in phosphate buffer 0.01 mol/L, pH 7.4, was added to the membrane and the excess was absorbed with the absorbent pad. To remove unbound particles, 100 μL of washing buffer (phosphate buffer 0.01 mol/L, pH 7.4, Tween 20 0.01% and NaCl 0.05 mol/L) was added to the membrane.

For multiple tests, 4 μL of serum was deposited on the nitrocellulose membrane (7 cm \times 10 cm) with 15 mm spacing between each spot to avoid contamination and checking the alignment between them to fit on the wells of an ELISA microplate. This sample volume was the minimum volume necessary to observe a clear result. After 10 min, a blocking solution containing BSA 3% in phosphate buffer 0.01 mol/L, pH 7.4 was added to cover the entire membrane for 15 min at RT. Subsequently, the blocking solution was removed and 3 mL fluorescent conjugates 1% in phosphate buffer 0.01 mol/L, pH 7.4 was added and incubated for 30 min.

2.6. Fluorescence spectroscopy

The spectrofluorometric measurements were performed with a LS-55 Perkin-Elmer luminescence spectrometer (Connecticut, USA) coupled to an optical fiber accessory. The negative control consisted of a membrane blocked with BSA, treated with fluorescent particles and rinsed with washing buffer. Protein NS1 from the Standard Diagnostics NS1 Ag ELISA kit was used as positive control. To compare the fluorescence measurements with an ELISA reader, measurements were performed using SAFIRE II Multimode Microplate Reader (Männedorf, Switzerland). For the measurement, nitrocellulose membranes were deposited on an ELISA microplate (F96 MicroWellTM plates, NUNC, Roskilde, Denmark) and enclosed with a microplate cover. Data was obtained using XFluorTM software version 4.62n. To perform qualitative fluorescence measurements, an UV-Lamp Biometra T1 (Foster, USA) was used.

2.7. Fluorophore linked immunosorbent assay for dengue fever detection

FLISA test was performed following the steps as described in 2.5; however, nanoparticles were replaced by not conjugated antibodies and only three serum samples with known NS1 concentration (see Supplementary information) were used in

different diluted solutions with phosphate buffer, pH 7.4. Subsequently, the membrane was washed three times with phosphate buffer 0.01 mol/L, pH 7.4, and incubated with anti-mouse IgG-FITC antibody 1:64, following the manufacturer instructions, for 30 min in a dark chamber at RT. After washing with phosphate buffer 0.01 mol/L, the fluorescence was measured.

2.8. Transmission electron microscopy (TEM)

For electron microscopy analysis, samples were prepared by drying a suspension droplet of particles at 0.1% (w/w) on carbon-coated parlodio films supported in 200-mesh copper grids. Particles were analyzed using a Carl Zeiss Libra 120 kV TEM equipped with omega filter to obtain bright-field images with low chromatic aberration when the energy slit was selected to zero. The images were recorded using iTEM Universal TEM Imaging Platform.

3. Results and discussion

The accessibility to sensitive and fast assays to detect diseases for routine or emergency diagnostics in non-well equipped laboratories is still a challenge. The presented work is driven by the current limitations to combine the speed of analysis, ease of use and the sensitivity for Dengue fever detection. This will lead to the development of a reliable assay based on fluorescence detection devices. To achieve the high detection sensitivity, a fluorescence intensity screening of three different fluorescent particles was performed and the spectra are depicted in Fig. 1a. Fluorophores incorporated in polymer particles were chosen to

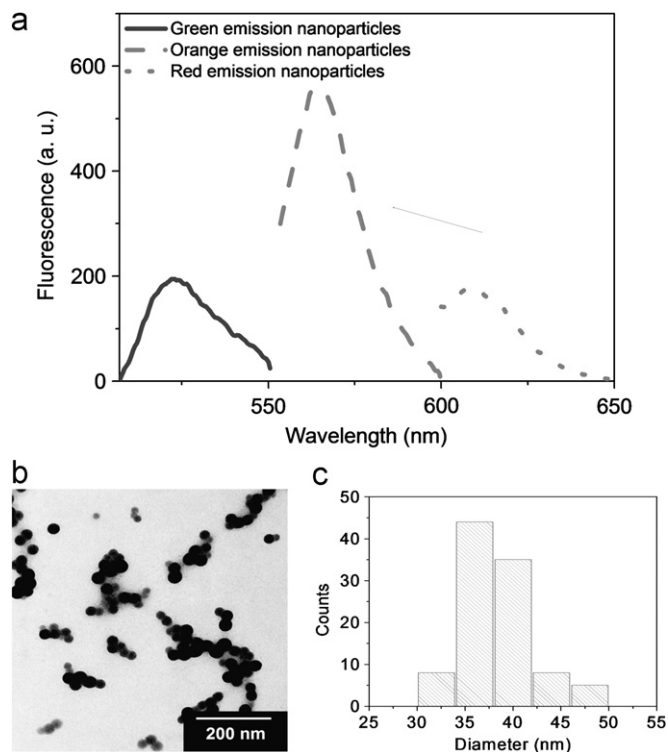


Fig. 1. Comparison of fluorescence for three different labels and microscopic characterization. Fluorescence spectra (a) from three different fluorescent particles at 5% (w/w) of solid content: orange, red and yellow carboxylated nanoparticles. Arrow indicates the chosen orange nanoparticles for immunospot development. Bright-field (TEM) images (b) from the orange nanoparticles. The diameter histogram (c) reveals the monomodal dispersion of the particles in 37 ± 5 nm.

overcome bleaching effects generally observed with fluorescent dyes. The particles consist of polystyrene containing multiple carboxylic acids for covalent ligand attachment. The emission wavelengths of the fluorophores covered a spectrum range from 450 to 600 nm. The spectra comparison clearly shows that the particles with emission in 567 nm (orange, see arrow in Fig. 1a) present up to 3.2-times higher intensity than the other particles and was therefore chosen as the label of choice for the immunospot development.

Monodispersity and uniform morphology are prerequisites for adequate particles in immunospot applications. These characteristics directly affect the performance and repeatability of the tests. Therefore, particle morphology was analyzed by TEM, which is a well-known tool for particle characterization (Linares et al., 2009, 2010). A bright field image of the particle dispersion, dried on parlodion film, is shown in Fig. 1b. The particles show a round shape of polymer latex and form aggregates on the nanoscale, which do not exceed 300 nm in the x - or y -axis. The aggregation does not affect the flow through the membrane, due to the fact that their size is hundreds times smaller than the nitrocellulose membrane pores (8 μm). The size histogram, obtained by measuring 100 particles (Fig. 1c), shows that the particles are monodispersed and have a mean diameter of 37 ± 5 nm. Due to uniform morphology, high fluorescence emission and monodispersity, the particles were used to develop the immunoassay. Focusing on rapidity and ease of use by concurrent high sensitivity, we present single and multiple tests using common available materials and equipment in clinical laboratories. The single tests, or strip tests, were constructed combining cellulose

and nitrocellulose membranes in a layer-by-layer structure, as show in Fig. 2a.

This test requires only 4 μL of serum sample and could be performed in 1 h. In case of multiple sample analysis, parallel tests can be performed by applying the 4 μL samples directly on the same nitrocellulose membrane with sufficient 15 mm spacing between each spot to avoid contamination. After the serum application area onto the membrane being already saturated, other protein molecules from the sample will laterally migrate through the membrane and will form a defined spot area. The molecules in the spot are pulled out of solution by the membrane and stick to the paper avoiding cross contamination between neighboring spots. This also remains stable after several washing steps. Experiments comparing the fluorescence intensity of the same samples analyzed in single and multiple tests revealed a variation lower than 16%. The presented direct sample application is analogous to indirect ELISA tests, with the advantage of a shorter incubation time and no further washing steps. These steps are time consuming and need higher sample volume, dependent on antibody-solid phase absorption. By using nitrocellulose, the high membrane-protein affinity assures the retaining of the analyte into the membrane and only a single sample deposition step is necessary and some minutes for drying are enough for detection.

Versatility was also achieved for the fluorescence measurement. Considering that laboratories around the world have different equipment availability and even lack of instruments, three different instruments were used and evaluated: simple fluorometer coupled to an optical fiber (Fig. 2b); ELISA reader, which allows the measurement fitting the membrane in a ELISA microplate

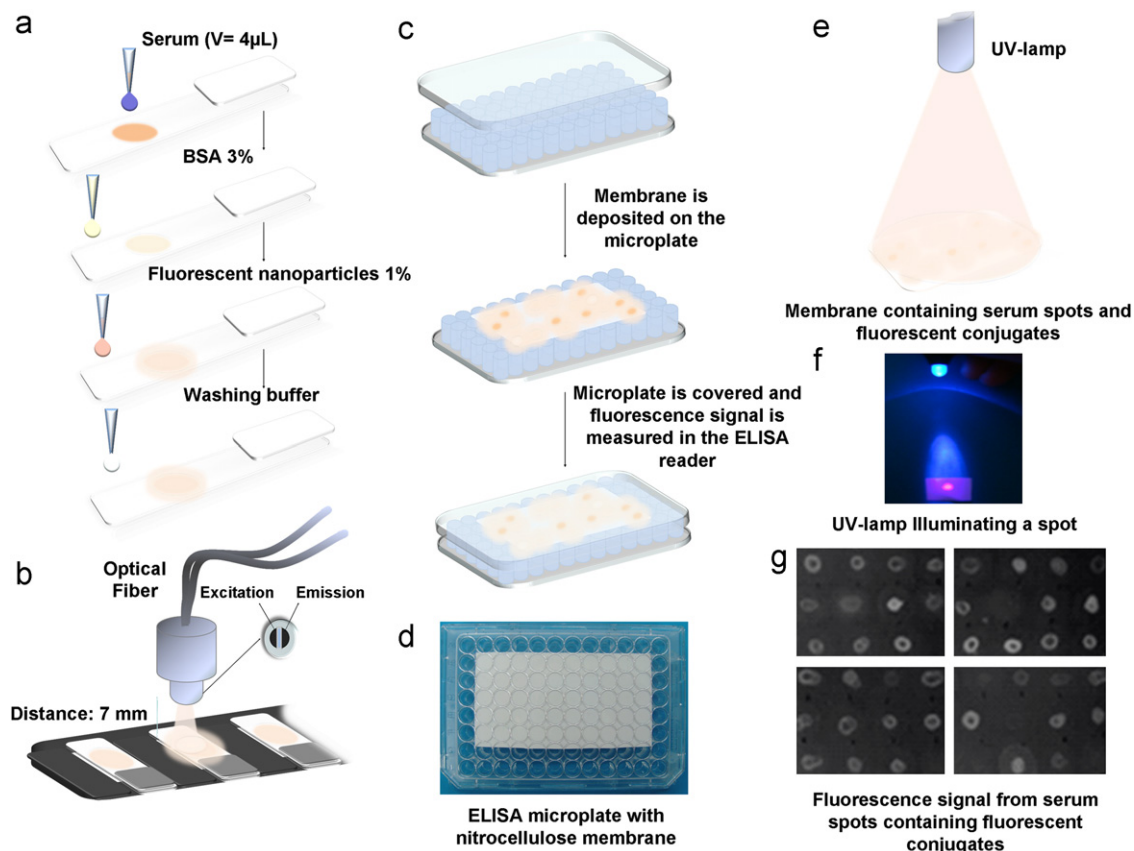


Fig. 2. Scheme of three different possible detection tools for immunospot based on fluorescent particles for Dengue NS1 protein determination. (a) Four steps for sample preparation including serum deposition, blocking of unspecific site, anti-NS1 nanoparticle conjugate and washing steps; (b) use of optical fiber to measure quantitatively fluorescence signal from the tests; (c) quantitative multiple tests performed on a single nitrocellulose membrane placed in a ELISA microplate and measured using an usual ELISA-reader; (d) picture of the membrane positioned in the microplate; (e) scheme of UV-lamp used to show fluorescent spots of serum samples applied on a nitrocellulose membrane; (f) cheap LED on UV range used for fluorescent nanoparticles excitation; (g) multiple tests analyzed under UV-lamp.

(Fig. 2c and d); and UV-lamp (Fig. 2e and f) that can be used in unequipped laboratories and that can provide qualitative results (Fig. 2g). Although, UV-lamp can only perform qualitative tests, it is a very cheap apparatus and can be easily obtained, besides the fact that many tests only need a yes/no diagnostics, such as for Dengue fever detection. We chose a lamp in the UVB range due to the fact that they are mostly used in clinical laboratories and the emission is capable to excite the band-tail of the fluorophore. Besides that, the lamp emission in the visible excitation range would be so close to the fluorophore emission that would be very difficult to distinguish the signal of the lamp and from the labels.

To compare the performance and consequently the detection limits for measurements performed with these three apparatus, a NS1 protein dilution series from 5–500 ng/mL was analyzed by all of them (Fig. 3). The fluorescent spots under UV-lamp (Fig. 3a) can be easily visualized from 200 ng/mL NS1 protein. Below this concentration, it is not possible to precisely confirm the positive NS1 protein serum signal. A positive and negative control is used to provide the limits for yes/no definition by comparison with the sample spot (Fig. 3c). The measurements performed by the fluorometer coupled to an optical fiber revealed a lower detection limit compared to the ELISA reader (Fig. 3b).

The detection limits were calculated for optical fiber coupled to fluorometer and ELISA reader measurements, showing 5.2 and 11.5 ng/mL, respectively. The relative standard deviation of the proposed method was evaluated by performing ten successive determinations of two serum samples. The calculation was performed dividing the standard deviation by the mean of the measurements. The values, 17% and 12%, were low considering that the tests are performed on membranes, where the pore structure is not totally homogeneous like ELISA substrate.

Although these two instruments showed different sensitivities for NS1 protein detection, both are adequate to be used for the diagnostics. According to Libraty et al. (2002), plasma levels of secreted NS1 protein may vary between 150 and 250 ng/mL for the second day of contracting the disease for patients that are both Dengue hemorrhagic fever and secondary infections. The concentration for the first day is scarce and variable, due to the difficulty to get samples from patients in this infection stage. Therein, the immunospot is indeed capable of providing a reliable diagnostic below the NS1 concentration that exists in infected patients on the second day of the disease. The low detection limit is decisive for early Dengue fever detection based on the NS1 protein and can be vital for the rapid assessment of patients developing more severe cases of the disease. When an UV-lamp is the only available tool, Dengue fever can be detected at the third day of infection. Lateral flow immunoassays are faster than the

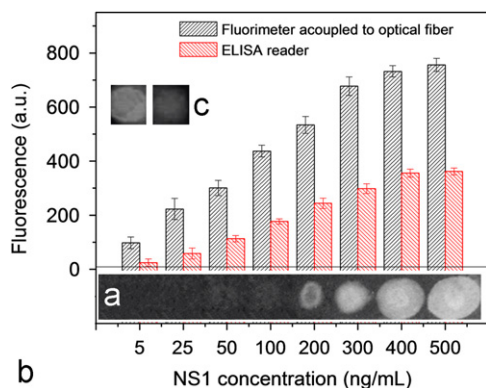


Fig. 3. Comparison between quantitative and qualitative detection. Fluorescent spots from infected serum dilution with anti-NS1 coated fluorescent particles measured under UV-lamp (a), by fluorometer coupled with optical fiber and ELISA reader (b). Positive (left) and negative (right) controls are shown in (c).

presented immunospot assay, but they require 25-times more sample volume, two antibodies for capture and detection of the analyte and they provide a visual signal emanating from a very small physical area, which often causes doubtful evaluation due to heterogeneous flow of particles.

In order to evaluate the gain in performance of the proposed method in comparison to classical FLISA, analytical curves for NS1 antibody coated fluorescent particles and anti-mouse IgG FITC antibodies were obtained on nitrocellulose. Fig. 4 shows that higher signals were recorded when particles were used, resulting therefore in a more sensitive assay. Besides avoiding bleaching effects, the use of particles permits to concentrate the fluorophores and contribute to a higher fluorescence signal per antibody bound to the antigen, unlike FLISA.

Precisely, considering the concentration range between 2 and 100 ng/mL, the particles used as enhancers resulted in a curve slope of 0.758 a.u. mL/ng, which is higher than the assay using only FITC (0.539 a.u. mL/ng). It means that the proposed assay is more sensitive to detect variations on the concentration axis.

In order to verify the potential of the proposed methodology in the biological analysis, 83 blood serum samples from infected patients were analyzed and compared to a commercial NS1 ELISA. Analysis provided satisfactory results compared to the commercial test (Table 1). The fluorescence measurements performed in ELISA reader revealed sensitivity of 81% and specificity of 88%. However, the qualitative measurements using UV-lamp showed low sensitivity, 59%, and specificity of 83%. The low sensitivity is justified by the difficulty to establish visual limits for considering a positive or a negative result. The limit was defined by the negative control, in which non-infected serum was analyzed and non-specific interaction provided background intensity. Thus, the diagnostic was obtained by comparing visually the sample spots

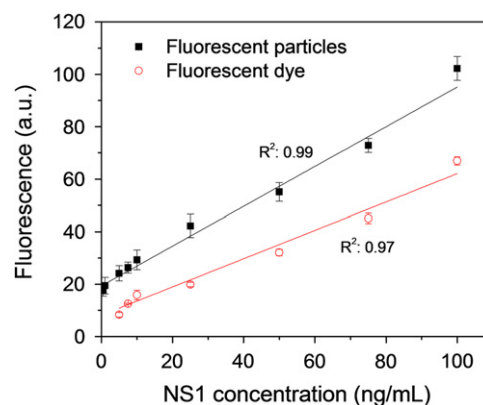


Fig. 4. Comparison of sandwich fluorescent immunolinked sorbent assay using fluorescent particles and fluorescent molecules as the detection label. Dengue NS1 antibody conjugated to orange particle signal is compared to anti-mouse IgG FITC antibody.

Table 1

Dengue NS1 detection using the proposed method with reference to a commercial NS1 ELISA in 83 serum samples from infected patients.

NS1 status	Immunospot (ELISA reader)		Immunospot (UV-lamp)		Total
	Positive	Negative	Positive	Negative	
Positive	48	11	35	24	59
Negative	3	21	4	20	24
Total	51	32	39	44	83
Sensitivity	81%		59%		
Specificity	88%		83%		

with the established limit. Furthermore, the fluorophores were not excited in their maximum wavelength, which reduces the emission intensity and consequently the sensitivity. After comparing the values obtained with commercial NS1 ELISA and fluorescent measurements in ELISA reader (paired *t*-test), no significant statistical differences were found. Based on the exposed results, the proposed test described using particles and fluorescence readers shows high potential to be applied as detection tool for Dengue NS1.

This test has the advantage of being performed during 45–60 min in comparison to classical ELISA or FLISA, which usually take 3–5 h. Thus, it is possible to save time and keep good sensitivity in routine procedures of clinical analysis laboratories. In addition, those tests based on UV-lamp detection can provide qualitative diagnostics in laboratories with lack of adequate infrastructure. Although, they showed low sensitivity, it is still acceptable as a diagnostic tool due to its sensitivity be superior to 50%.

4. Conclusion

We present the development of an immunospot assay for Dengue fever diagnosis based on anti-NS1 fluorescent nanoparticle conjugates, combining principles of fluorescence linked immunosorbent assay and enzyme linked immunospot. The use of fluorescent nanoparticles allowed high sensitivity and ease detection using different laboratory equipment. In addition, the application of reagents and samples on nitrocellulose membrane provided easy manipulation, low volume samples and lower costs. We proved that the combination of principles of different assays can produce a fast and high sensitive test to be applied to Dengue fever detection, mainly in impoverished environments and epidemic areas, where sensitivity, speed and simplicity are essentials. Furthermore, this method can be easily applied to the diagnosis of other neglected tropical diseases, which require fast and alternative detection tools.

Acknowledgments

The authors would like to thank the Sao Paulo Institute of Tropical Medicine for kindly providing the serum panel, especially Lucy Santos Vilas Boas and Clara Felix for the sample organization. We also thank Prof. Axel K. Walch for microscopy apparatus. EML acknowledges the fellowship from the International Doctorate Program NanoBioTechnology (IDK-NBT) funded by the Elite Network of Bavaria (ENB). This work was supported by the cluster of excellence Nano Initiative Munich (NIM), the Center of Nanoscience (CeNS), DAAD and CAPES.

Appendix A. Supporting information

Supplementary data associated with this article can be found in the online version at <http://dx.doi.org/10.1016/j.bios.2012.08.005>.

References

Alcon, S., Talarmin, A., Debruyne, M., Falconar, A., Deubel, V., Flamand, M., 2002. *Journal of Clinical Microbiology* 40, 376–381.

- Allwinn, R., 2011. *Medical Microbiology and Immunology* 200, 155–159.
- Bathoorn, E., Limburg, A., Bouwman, J.J., Bossink, A.W., Thijsen, S.F., 2011. *Clinical and Vaccine Immunology* 18, 874–877.
- Cardosa, M.J., Tio, P.H., Noor Sham, S., 1988. *Journal of Virological Methods* 22, 81–88.
- Cardosa, M.J., Baharudin, F., Hamid, S., Tio, P.H., Nimmannitya, S., 1995. *Clinical and Diagnostic Virology* 3, 343–350.
- Chunglok, W., Wuragil, D.K., Oaew, S., Somasundrum, M., Surareungchai, W., 2011. *Biosensors and Bioelectronics* 26, 3584–3589.
- Cummins, C.M., Koivunen, M.E., Stephanian, A., Gee, S.J., Hammock, B.D., Kennedy, I.M., 2006. *Biosensors and Bioelectronics*, 1077–1085.
- Datta, S., Wattal, C., 2010. *Indian Journal of Medical Microbiology* 28, 107–110.
- Franci, C., Ingles, J., Castro, R., Vidal, J., 1986. *Journal of Immunological Methods* 88, 225–232.
- Gubler, D., 1998. *Clinical Microbiology Reviews* 11, 480–496.
- Guzman, M.G., Kouri, G., 1996. *Clinical and Diagnostic Laboratory Immunology* 3, 621–627.
- Lam, S.K., Fong, M.Y., Chungue, E., Doraisingham, S., Igarashi, A., Khin, M.A., Kyaw, Z.T., Nisalak, A., Roche, C., Vaughn, D.W., Vorndam, V., 1996. *Clinical and Diagnostic Virology* 7, 93–98.
- Levi, J.E., Tateno, A.F., Machado, A.F., Ramalho, D.C., de Souza, V.A., Guilarde, A.O., de Rezende Feres, V.C., Martelli, C.M., Turchi, M.D., Siqueira Jr., J.B., Pannuti, C.S., 2007. *Journal of Clinical Microbiology* 45, 1893–1897.
- Libraty, D.H., Young, P.R., Pickering, D., Endy, T.P., Kalayanaraj, S., Green, S., Vaughn, D.W., Nisalak, A., Ennis, F.A., Rothman, A.L., 2002. *Journal of Infectious Diseases* 186, 1165–1168.
- Lima, M.R.Q., Nogueira, R.M.R., Schatzmayr, H.G., Santos, F.B., 2010. *PLoS Neglected Tropical Diseases* 4, e738.
- Linares, E.M., Trombetta, L.P., Moreira, A.B., Sotomayor, P., Kubota, L.T., 2007. *Analytical Letters* 40, 573–583.
- Linares, E.M., Leite, C.A.P., Valadares, L.F., Silva, C.A., Rezende, C.A., Galembeck, F., 2009. *Analytical Chemistry* 81, 2317–2324.
- Linares, E.M., Rippel, M.M., Galembeck, F., 2010. *ACS Applied Materials and Interfaces* 2, 3648–3653.
- Linares, E.M., Kubota, L.T., Michaelis, J., Thalhammer, S., 2012. *Journal of Immunological Methods* 375, 264–270.
- Liu, C., Jia, Q., Yang, C., Qiao, R., Jing, L., Wang, L., Xu, C., Gao, M., 2011. *Analytical Chemistry* 83, 6778–6784.
- Liu, S.W., Boyer-Chatenet, L., Lu, H., Jiang, S.B., 2003. *Journal of Biomolecular Screening* 8, 685–693.
- Martinez, A.W., Phillips, S.T., Whitesides, G.M., Carrilho, E., 2010. *Analytical Chemistry* 82, 3–10.
- Miller, D.K., Menke, J.D., Hayes, N.S., Uzieblo, A., Tew, D., Hayashi, Y., Guan, Y., Zhao, A., Cummings, R.T., Park, Y.-W., Yamin, T.-T.D., 2006. *Analytical Biochemistry* 349, 129–135.
- Najjioullah, F., Combet, E., Paturol, L., Martial, J., Koulmann, L., Thomas, L., Hatchuel, Y., Cabié, A., Cesaire, R., 2011. *Diagnostic Microbiology and Infectious Disease* 69, 172–178.
- Peng, C., Li, Z., Zhu, Y., Chen, W., Yuan, Y., Liu, L., Li, Q., Xu, D., Qiao, R., Wang, L., Zhu, S., Jin, Z., Xu, C., 2009. *Biosensors and Bioelectronics* 24, 3657–3662.
- Piào, Y., Lee, D., Lee, J., Hyeon, T., Kim, J., Kim, H.-S., 2009. *Biosensors and Bioelectronics* 25, 906–912.
- Piletsky, S.A., Piletska, E.V., Bossi, A., Karim, K., Lowe, P., Turner, A.P.F., 2001. *Biosensors and Bioelectronics* 16, 701–707.
- Vaughn, D.W., Green, S., Kalayanaraj, S., Innis, B.L., Nimmannitya, S., Suntayakorn, S., Rothman, A.L., Ennis, F.A., Nisalak, A., 1997. *Journal of Infectious Diseases* 17, 322–330.
- Velappan, N., Clements, J., Kiss, C., Valero-Aracama, R., Pavlik, P., Bradbury, A.R.M., 2008. *Journal of Immunological Methods* 336, 135–141.
- Wan, Y., Qi, P., Zhang, D., Wu, J., Wang, Y., 2012. *Biosensors and Bioelectronics* 33, 69–74.
- Young, P.R., Hilditch, P.A., Bletchly, C., Halloran, W., 2000. *Journal of Clinical Microbiology* 38, 1053–1057.
- Zhu, K., Li, J., Wang, Z., Jiang, H., Beier, R.C., Xu, F., Shen, J., Ding, S., 2011. *Biosensors and Bioelectronics* 26, 2716–2719.

Web references

- World Health Organization, 2010. <http://whqlibdoc.who.int/publications/2010/9789241564090_eng.pdf> (accessed 05.12).
- World Health Organization, 2012. Fact Sheet 117. <<http://www.who.int/media/centre/factsheets/fs117/en/>> (accessed 05.12).

Supplementary Information

Immunospot assay based on fluorescent nanoparticles for Dengue fever detection

Elisângela M. Linares^a, Claudio S. Pannuti^b, Lauro T. Kubota^c and Stefan Thalhammer^{a,}*

^aHelmholtz Zentrum München - German Research Center for Environmental Health, Ingolstädter Landstrasse 1, 85764 Neuherberg, Germany; elisangela.linares@helmholtz-muenchen.de, stefan.thalhammer@helmholtz-muenchen.de;

^bLaboratory of Virology, Instituto de Medicina Tropical de São Paulo e Faculdade de Medicina, Universidade de São Paulo. Eneas de Carvalho Aguiar 470, 05403-000, São Paulo, Brazil.

cpannuti@usp.br

^cInstitute of Chemistry, State University of Campinas, Cidade Universitária s/n, 13083-970, Campinas, São Paulo, Brazil

kubota@iqm.unicamp.br

CORRESPONDING AUTHOR FOOTNOTE

*Stefan Thalhammer, P.O. Box 6154 – 13084-971 – München – Germany. Phone: +49-089/3187-2893. Fax: +49-089/3187-3323. stefan.thalhammer@helmholtz-muenchen.de

Antibody purification

The NS1mAb (Abcam, Cambridge UK) was purified by Protein G affinity chromatography. One ml Hitrap protein G HP column for affinity chromatography and the PD10 desalting column were purchased from GE Healthcare (Uppsala, Sweden). The supernatant was slowly passed through the protein G column using Äktapurifier 100 (GE Healthcare, Uppsala, Sweden). The NS1mAb was eluted from protein G in 10 ml of 0.1 mol/L glycine, pH 2.8. The eluent was concentrated to 1 ml by centrifugation at 5000 rpm and buffer exchange into 1x PBS, pH 7.4, using a desalting column at RT.

Dengue diagnostics

The samples belong to a repository collection obtained during previous studies conducted by the Virology Laboratory of the Instituto de Medicina Tropical de São Paulo of the University of São Paulo, and stored at -20°C. Aliquots were prepared from samples with laboratory-confirmed acute DF infection, defined by detection of DF RNA by qPCR, and/or anti-DF IgM antibodies (Dengue ELISA IgM, Focus Technologies, Cypress, USA), and/or dengue NS1 antigen. Commercial kits were used as described by the manufacturers instructions.

Sandwich enzyme linked immunosorbent assay for NS1 protein quantification:

The NS1 protein determination in serum samples was performed adapting a SD NS1 Ag ELISA kit for quantification analysis. Microplate wells were coated with NS1 monoclonal antibodies from Abcam at a concentration of 5 µg/ml in a 0.01 M carbonate/bicarbonate buffer, pH 9.6. The plate was covered with an adhesive plastic and incubated overnight at 4°C. The coating solution was then removed and the wells were washed, by filling with 200 µl of washing buffer (0.01 M phosphate buffer containing 0.01% of Tween 20, pH 7.4). The remaining protein-binding sites in the coated wells were blocked by adding 200 µl of a 5% albumin solution in 0.01 M phosphate buffer, pH 7.4. The plate was covered with an adhesive plastic and incubated for 2 h at RT. After washing the wells twice with 200 µl of washing buffer, NS1 protein solutions and samples were added. For the standard curve, 100 µl of diluted NS1 protein solutions, 1, 50, 100, 250, 500, 650 and 800 ng/mL were added to the wells, using a triplicate for each concentration and incubated for 90 min at 37°C. For the standard curve and the positive control, NS1 protein from the SD NS1 Ag ELISA kit was used. NS1 protein concentration was determined using UV method. Three different samples were also incubated in triplicate. Subsequently, the wells were washed twice, by filling with 200 µl of washing buffer. After washing, 100 µl of 0.01µg/mL mouse monoclonal detection antibody conjugated with horseradish peroxidase was added to each well and the plate was covered with an

adhesive plastic and incubated for 2 h at room temperature. The plates were then washed six times with washing buffer. The substrate for the enzyme was prepared by mixing 1:1 of substrate A (sodium acetate, hydrogen peroxide and gentamicin) and B (tetramethylbenzidine and hydrochloric acid) from the kit. Finally, 100 µl of substrate was added in each well and the solutions were measured after 30 min using an ELISA reader.

Sensitivity and specificity calculation

Sensitivity measures the proportion of actual positives which are correctly identified and it is calculated using the equation SI-1:

$$\text{sensitivity} = \frac{\text{number of true positives}}{\text{number of true positives} + \text{number of false negatives}} \quad \text{Equation SI-1}$$

And specificity measures the proportion of negatives which are correctly identified and the percentage is calculated using the equation SI-2:

$$\text{specificity} = \frac{\text{number of true negatives}}{\text{number of true negatives} + \text{number of false positives}} \quad \text{Equation SI-2}$$

Fluorescence spectroscopy

The spectrofluorometric measurements were performed with a LS-55 Perkin-Elmer luminescence spectrometer (Connecticut, USA) equipped with a xenon discharge lamp (20 kW, 8 ms), a Hamamatsu photomultiplier, a reference photodiode and a bifurcated optical fiber bundle of quartz (4.0 mm diameter at the common end) coupled to an optical fiber accessory. The excitation and emission of fluorescent nanoparticles were monitored at 542 and 565 nm, respectively. In order to compare the fluorescence measurements between fluorometer coupled to an optical fiber and an ELISA reader, measurements were performed using SAFIRE II Multimode Microplate Reader (Männedorf, Switzerland), setting excitation and emission slits to 10 nm and 20 nm, respectively. The UV-Lamp Biometra T1 emits at UV-A and B lamp (280-400 nm). For fluorometer coupled with optical fiber and ELISA readers, the influence of the variables that potentially affect the fluorescence intensity was investigated in order to optimize the measurement conditions. Besides the excitation and emission slit and the monochromator scan rate, the distance between the optical fiber tip and the irradiated surface was optimized. An important parameter is the acceptance angle when optical fibers are used, which is the angle at which the maximum amount of light goes back

into the optical fiber through total internal reflectance. Thus it is very important to find the distance between the optical fiber tip and the irradiated surface, in order to reach the maximum signal. Figure SI-1 shows that the best sensitivity was attained with the distance varying from 1-10 mm. Therefore, for further experiments a distance of 7 mm was used.

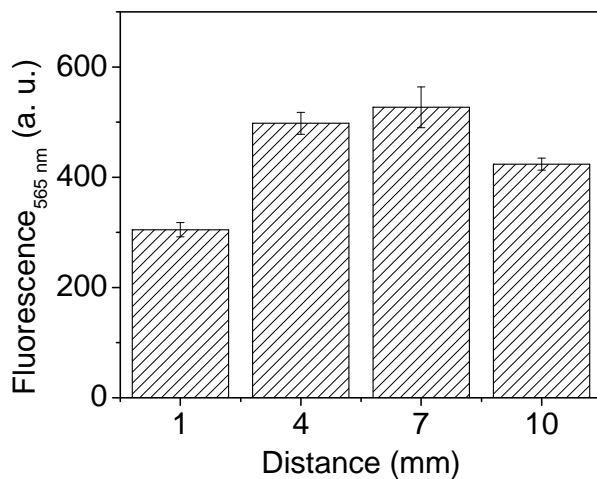


Figure SI-1. Influence of instrument variable on the fluorescence intensity. Effect of the distance between optical fiber and the sample on the nitrocellulose membrane obtained for the fluorescent orange nanoparticles covered with Ab-NS1; $C_{\text{particles}}$: 2 % (w/w).

CHAPTER 4

*One step synthesis polymer core-shell particles
with carboxylated Ruthenium complex:
potential tool for biomedical applications*

One step synthesis of polymer core-shell particles with carboxylated Ruthenium complex: potential tool for biomedical applications

*Elisângela M. Linares^a, André Formiga^b, Lauro T Kubota^b, Fernando Galembeck^b, Stefan
Thalhammer^{a*}*

^a Helmholtz Zentrum München - German Research Center for Environmental Health, Ingolstädter
Landstrasse 1, 85764 Neuherberg, Germany

^b Institute of Chemistry, State University of Campinas, Cidade Universitária s/n, 13083-970,
Campinas, São Paulo, Brazil

CORRESPONDING AUTHOR FOOTNOTE

Stefan Thalhammer, Helmholtz Zentrum München, P.O. Box 6154 – 13084-971 – München –
Germany. Phone: +49 089/3187-2893. Fax: +49 089/3187-3323. stefan.thalhammer@helmholtz-
muenchen.de

Abstract

Luminescent core-shell particles are structures widely applied to biomedical purposes with the potential of combining multiple features within one single particle. The development of particles that are easily synthesized and tunable for each application, combining biocompatibility, easy bioconjugation and high detection signal as a label, is highly desired. In this work, we describe one-step synthesis of poly[styrene-*co*-(2-hydroxyethyl methacrylate)], PSHEMA, core-shell particles containing [Ru(4,4'-dicarboxylate-2,2'-bpy)₃] luminescent complexes. These particles show monodispersity, biocompatibility, easy functionalization and dye incorporation to focus on bioapplications, such as cell-tracking and diagnostics. The natural monomer self-assemble during the polymerization produces core-shell structure with hydrophilic-hydrophobic character. It allows the concentration of hydrophilic ruthenium complexes into the particle due to HEMA hydrophilic character and incorporation of hydrophobic molecules (e. g. diphenylanthracene) due to the styrene hydrophobic character. The incorporation of Ru complex into the particle resulted in higher photostability than the free dye. Furthermore, carboxylic groups on the particle surface originated from carboxylated ligands of Ru complexes were used to immobilize biomolecules. The particles were successfully used as a diagnostic label for an immunospot assays for Dengue fever (DF) detection, which is a viral infection transmitted by mosquito that lacks in early reliable detection tools. The immunospot assay for viral Dengue non-structural glycoprotein detection provided a detection limit (DL) of 187 ng/mL. The particles are promising for paper based assays due its high stability and low agglomeration. The particles showed a considerable decrease in DL and allowed the infection diagnosis 24h before in comparison to current assays based on gold nanoparticles. In addition, the particle biocompatibility was demonstrated with an adherent grown fibroblast cell line.

Introduction

Core-shell particles play an important role in life science applications ranging from drug delivery¹ and biosensing for diagnosis to therapeutic use^{2,3} and contrast agent for multimodality imaging.²⁻⁵ Particles with specific features are required for these wide range of applications. Due to the vast variety of morphologies and molecular compositions, polymer latex particles are considered as the first choice to fulfill the requirements for each use. Numerous structures involving polymers have been described, including polymer shell-polymer core,⁶ polymer shell-silica core,⁷ polymer shell-quantum dot core⁸ and polymer shell-magnetic core^{9,10}. Among these, special interest is given to core-shell particles with hydrophobic core and hydrophilic shell. This assembly provides functional groups for bioconjugation and a protective coating between the core and the external medium, which make it especially suitable for hydrophobic drug delivery systems or nanoreactors.^{11,12} In addition, hydrophilic shells are produced to avoid hydrophobic particle aggregation in aqueous medium¹³ and for improving the photostability of incorporated luminescent dyes.⁷

Among latexes with hydrophobic properties, polystyrene particles (PS) are predominantly applied to biomedical purposes and have been extensively used as a specific carrier for diagnostic reagents, detection labels, agglutination tests and other applications.¹⁴ Unfortunately, PS particles show low colloidal stability and problems with bioconjugation step.¹⁵ Its low stability causes particle agglomeration, which affects its use in flow tests, such as paper based assays. Accordingly, poly[styrene-*co*-(2-hydroxyethyl methacrylate)] (PSHEMA) polymer particles are used as a suitable material for bioapplications substituting PS particles.¹⁵ PSHEMA particles consist of a hydrophilic/hydrophobic heterogeneous surface, providing high colloidal stability, insensitive non-specific agglutinability, free-emulsifier polymerization and high monodispersity. The particles are characterized as core-shell structures, where the HEMA richer chains are more concentrated at the particle periphery.¹⁶ In addition and due to the structural array, the surface modification allows the functionalization with biomolecules and the incorporation of different molecules into the hydrophobic core and/or the hydrophilic shell, i.e. as luminescent (fluorescent, phosphorescent) dyes.

The incorporation of luminescent dyes into the PSHEMA particles makes them potential candidates for bioapplications such as detection system in diagnostics or living cell imaging. Luminescent transition metal complexes can provide high emissive particles due to high quantum yields and long luminescence lifetimes in comparison with most organic fluorophores. In addition, luminescent transition metals show large Stokes shifts eliminating self-quenching processes, intense

absorption in the visible spectral range as well as thermal, chemical and photochemical stability.¹⁷ Hence particles with luminescent transition metal complexes are capable to overcome the typical limitations of organic fluorophores, such as poor brightness, fast photobleaching, non-specific quenching and solvatochromic effects.¹³

Ruthenium (Ru) complexes show many advantages over other transition metal complexes and have been extensively investigated both from the fundamental and technological point of view.^{18,19} To use Ru complexes in biological applications and take advantage from their luminescent properties, they should be incorporated into a matrix to avoid non-specific binding to proteins and membranes. A recent work by Lin and coworkers²⁰ described the fabrication of core-shell nanostructures from near-infrared electrochromic amphiphilic diblock copolymers containing a pendant dinuclear ruthenium group. Although this work produced stable micelles and vesicles, the copolymer of styrene and the ruthenium complex requires very complicated and time-consuming sequential steps for the polymer synthesis.

Here we describe one step synthesis of core-shell particles composed of PSHEMA, containing high luminescent [Ru(4,4'-dicarboxylate-2,2'-bpy)₃] complex. These particles combine photostability and high luminescence intensity from the transition metal complex with the stable monodispersed PSHEMA core-shell structure. The ruthenium complex has a hydrophilic nature that results in an accumulation into the particle shell, which also has a hydrophilic character. The presence of 2,2'-bipyridine-4,4'-dicarboxylic acid ligands provide carboxylate groups anchored on the particle surface that allow further biofunctionalization. Single step reactions produce core-shell particles with luminescent dye and functional groups incorporated on the surface. It overcomes the current challenge of probe conjugation to target biomolecules, which usually involves additional polymerization steps to incorporate functional groups. The concentration of Ru complexes into the shell allows further molecule incorporation in the hydrophobic core. Furthermore, the surfactant free polymerization avoids desorption of surfactant molecules, producing stable dispersions without undesired interactions of emulsifiers with biomolecules. The PSHEMA-Ru particle architecture results in the improvement of various properties, such as reduced photobleaching, minimized solvatochromic shift, and increased luminescence efficiency relative to a free dye in aqueous solution and allows colocalization of multiple fluorophores/molecules within a single particle.

In order to demonstrate the potential of Ru-PSHEMA bioconjugates as detection system, we developed a paper based immunospot assay for the ambitious task of early Dengue fever detection. Dengue fever is a viral infection transmitted by mosquito that in recent decades has become a major international public health concern,²¹ which has a lack in early reliable detection tools. The stability

and low agglomeration produce more homogeneous spots on the membrane. While efficient approaches to control the insect vector are ongoing²², there is an increase necessity for sensitive and reliable tools for Dengue fever detection. Furthermore, we show the use of these particles for hydrophobic fluorescent dye incorporation, resulting in successful hydrophobic molecule entrapment inside the particles. Biocompatibility tests are also reported, which illustrate the potential use in cell-tracking applications.

Experimental Procedures

Materials and reagents

Styrene, 2-Hydroxyethyl methacrylate, ruthenium(III) chloride trihydrate, 2,2'-bipyridine-4,4'-dicarboxylic acid, sodium persulfate, sodium bicarbonate, bovine serum albumin (BSA) powder, *N*-(3-Dimethylaminopropyl)-*N'*-ethylcarbodiimide hydrochloride (EDC), 9,10-Diphenylanthracene (DPA), dichloromethane and potassium phosphate, mono- and dibasic, were purchased from Sigma-Aldrich (Milwaukee, USA). Dimethylformamide and ethanol were obtained from Merck (Darmstadt, Germany). Dengue Virus NS1 glycoprotein mouse monoclonal antibody (supernatant) was obtained from Abcam (Cambridge, United Kingdom). RPMI media and Vectashield were purchased from Biochrom AG (Berlin, Germany) and Vector Laboratories (Burlingame, USA), respectively. Aminosilane coated glass slides were purchased from Schott (Mainz, Germany). The fluorescent dyes Hoechst 33342 and DiI12(3) perchlorate were purchased from Invitrogen (Eugene, USA) and Enzo Life Sciences (Lörrach, Germany), respectively. Hitrap protein G HP column for affinity chromatography and the PD10 desalting columns were purchased from GE Healthcare (Uppsala, Sweden). Nitrocellulose membrane (8 μ m) was obtained from Whatman (Maidstone, United Kingdom).

Synthesis of $Na_4[Ru(4,4'$ -dicarboxylate-2,2'-bpy) $_3] \cdot 13 H_2O$

Tris-chelated complex of Ru(II) was synthesized according to the protocol described by Nazeeruddin et al.²³ with slight modifications. In a three-necked round bottomed flask, linked to a reflux condenser, 50 mL of *N,N'* dimethylformamide was deaerated with N₂ for 10 minutes at RT. Then, 0.214 g of Ruthenium (III) chloride trihydrate and 0.610 g of 2,2'-bipyridine-4,4'-dicarboxylic acid were added. The mixture was heated to 150°C for 3 hours at reflux with vigorous stirring. Shortly after, 9.6 mL of 0.5 mol/L NaHCO₃ aqueous solution was added and the reflux was

kept at 150°C for additional 4 hours. The reaction procedure was monitored by checking the reaction solution color. The initial blue-green starting solution turned immediately into pink after adding NaHCO₃, then red, and finally orange at the end of the reaction. The solid produced was directly collected on a sintered glass filter and washed three times with 20 mL DMF at RT. The material was recrystallized using methanol and diethylether. The final product was dried under vacuum, resulting in a 79% yield. NMR-¹H analysis of the complex is shown in the Electronic Supporting Information (ESI-1).

Synthesis of the poly[styrene-co-(2-hydroxyethyl methacrylate)] latex, PSHEMA

The latex was prepared by batch surfactant-free emulsion copolymerization of styrene (S) and 2-hydroxyethyl methacrylate (HEMA) adapting procedures described by Tamai et al.²⁴ and Cardoso et al.²⁵ The polymerization was carried out in a 500 mL three-neck round-bottom flask connected to a condenser, a Teflon paddle stirrer and a gas inlet providing a constant flow of nitrogen gas. Five reactions were performed containing different monomer percentages: 1.5, 2.5, 4.2, 5.5 and 7.3 wt. % of HEMA. Only the high HEMA concentration is described herein. Initially, the reaction flask was filled with 220 mL of water. The system was purged with nitrogen gas and kept at 70 °C. After stirring for 30 minutes, 31.5 g styrene and 2.5 g 2-hydroxyethyl methacrylate were added. In a subsequent step, 0.0543g of sodium persulfate was dissolved in 5 mL of water and was added to the reaction after 1 h. The reaction was kept for 10 h at 70 °C under constant stirring at 450 rpm. The latex was filtered with a mesh steel sieve, to remove coagulated latex. In order to eliminate monomers and initiator, the dispersion was centrifuged twice at 13 000 rpm for 10 minutes at RT. The zeta potential measurement indicated -43 mV for PSHEMA particles.

Synthesis of PSHEMA latex containing Na₄[Ru(4,4'-dicarboxylate-2,2'-bpy)₃].13 H₂O, PSHEMA-Ru

The reaction was performed in the same reactor and conditions (nitrogen atmosphere, stirring at 450 rpm and temperature at 70°C) as used for the poly[styrene-co-(2-hydroxyethyl methacrylate)] synthesis. The flask was filled with 220 mL of water, heated up to 70°C and stirred during 30 min in a nitrogen atmosphere. Subsequently, 31.5 g styrene and 2.5 g 2-hydroxyethyl methacrylate were added. In a subsequent step, 0.0543g of sodium persulfate dissolved in 5 mL of water was added after 1 h. After a reaction time of 7 h at 70°C, a solution of ruthenium complex containing 7.5 mg in 10 mL water was added to the flask. The reaction was kept up to 10h at 70 °C under constant

stirring at 450 rpm. Finally, the latex was filtered to remove coagulated latex and centrifuged twice at 13 000 rpm for 10 minutes at RT in order to eliminate monomers, initiator and non-incorporated complexes. The PSHEMA-Ru particles have a zeta potential of -54 mV.

9,10-Diphenylanthracene incorporation in PSHEMA-Ru particles

The DPA incorporation was performed Allard and Larpent²⁶. Dye loading was performed in an aqueous suspension containing 0.4% (w/v) of PSHEMA-Ru particles. An aliquot of 20 μ L of DPA 23 mM in dichloromethane was added to 1 mL of the PSHEMA-Ru particles. The sample was stirred at RT, in the dark for 48 h, to allow the diffusion of dye within the polymer matrix and the progressive evaporation of dichloromethane. Subsequently, the dispersion was centrifuged to remove non-incorporated DPA from the dispersion and the water was replaced by phosphate buffer 0.01M, pH 7.4. The incorporation was evaluated by acquiring an emission spectrum (λ_{ex} : 350nm).

Antibody purification

The NS1mAb (Abcam, Cambridge UK) was purified by Protein G affinity chromatography. The supernatant was slowly passed through the protein G column using Aektapurifier 100 (GE Healthcare, Uppsala, Sweden). The NS1mAb was eluted from protein G in 10 ml of 0.1 mol/L glycine, pH 2.8. The eluent was concentrated to 1 ml by centrifugation at 5000 rpm during 5 min and buffer exchange into 1x PBS, pH 7.4, using a desalting column at RT.

Biomolecule immobilization on the PSHEMA-Ru particles

Bovine serum albumin was covalently bound to the PSHEMA-Ru particles as a spacer for further biomolecule immobilization. Water-soluble carbodiimide activates the surface carboxyl groups originated from the complex on the particle surface. An aliquot of 1 mg of albumin was dissolved at 3 mg/mL using 0.1 mol/L PBS buffer, pH 6.5. Then, 500 μ L of a 0.3 % aqueous suspension of particles was added and incubated for 30 min at RT. Subsequently, 1.5 mg of EDC was added and mixed by vortexing. The dispersion was incubated on a shaker for 3 hours at RT. To separate the protein-labeled microsphere particles from unbound protein and EDC molecules, the dispersion was centrifuged at 10 000 rpm for 10 min at RT. The suspension was stored at 4°C with phosphate buffer 0.01M, pH 7.4, until being used for biomolecule conjugation.

Immunospot assay for Dengue virus NS1 protein detection

For single analysis, the strip test contains the reaction membrane and the absorbent pad. Nitrocellulose membrane (5mm x 60mm) was placed glass slide and an absorbent pad (5mm x 45mm) was fixed on the opposite side. An aliquot of 0.5 μ L of serum was slowly spotted on the center area of the nitrocellulose membrane. After drying the serum droplet, 20 μ L of BSA 3% in phosphate buffer 0.01 mol/L, pH 7.4, was added directly on the dried serum spot and the excess of liquid was absorbed by the absorbent pad. Subsequently, 20 μ L of fluorescent conjugates 1% in phosphate buffer 0.01 mol/L, pH 7.4, was added to the membrane and the excess was absorbed with the absorbent pad. To remove unbound particles, 100 μ L of washing buffer (phosphate buffer 0.01 mol/L, pH 7.4, Tween 20 0.01% and NaCl 0.05 mol/L) was added to the membrane. NS1 concentration was detected using sandwich ELISA. The membrane was analyzed by fluorescence microscopy.

Dengue virus infected serum samples

The samples belong to a repository collection of the Virology Laboratory of the Instituto de Medicina Tropical de São Paulo, University of São Paulo. The serum samples were stored at -20°C until the analysis. Aliquots of positive samples were used for detection of DF RNA by qPCR, and/or anti-DF IgM antibodies (Dengue ELISA IgM, Focus Technologies, Cypress, USA), and/or dengue NS1 antigen. Commercial kits were used as described by the manufacturers instructions.

Cell staining and particle incorporation

L929 mouse fibroblasts were grown on glass slides for testing the particle biocompatibility and cellular uptake of PSHEMA-Ru particles. L929 were cultured to a confluent layer in RPMI media with 10% fetal calf serum, 1% antibiotic–antimycotic solution and incubated at 37° C in a humidified 95% air and 5% CO₂ atmosphere. PSHEMA-Ru particles without coating treatment were added to the cell medium in two concentrations, 7 and 15 μ g/mL, and the cells were incubated for 24h. For each concentration, 3 samples were prepared after 24h, 48h and 72h of particle incubation and a fourth sample for negative control. Firstly, RPMI medium was removed and cells were incubated with DilC12(3) perchlorate in RPMI for 20min at 37°C. Secondly, the medium with Dil was removed and cells were fixed with 2% paraformaldehyde for 15min at RT. Fixation was

stopped by washing the cells twice with 1mol/L PBS at RT. The nucleus was stained with the incorporating dye Hoechst 33342 1% by incubating for 10min at RT. Finally the samples were washed with 1mol/L PBS, sealed with 10 μ l Vectashield mounting medium and covered with a cover slide. The samples were kept in the dark at 4°C until use.

Confocal microscopy

For confocal images, a Carl Zeiss LSM 510 NLO (Göttingen, Germany) confocal microscope equipped with 10x and 63x water objective was used. Images were obtained by depositing 0.5% (w/v) of particle dispersion on a glass slide. The serum analyses were performed by pasting the nitrocellulose membrane on a glass slide. Images were recorded using the software LSM 510 version 4.2 SP1. Instrument parameter for the spatial distribution analysis of each dye of the stained cells is shown in the Electronic Supporting Information (ESI-2). More information about the image analyses of the serum spots is described in the (ESI-3). Stacks with 0.1 μ m z steps were obtained and images were processed using the software LSM Image Examiner and Adobe Photoshop CS3.

Spectroscopy

Measurements were performed using SAFIRE II Multimode Microplate Reader (Männedorf, Switzerland), setting the excitation and emission slits to 10 nm and 20 nm. The excitation and emission of luminescent particles were monitored at 470 and 630 nm, respectively. For the measurement, an ELISA microplate (F96 MicroWell™ plates, NUNC, Roskilde, Denmark) was used. Data were obtained using the XFluor™ software version 4.62n.

Atomic force microscopy analysis

For high resolution atomic force microscopy (AFM) analysis each particle dispersion was diluted to a 0.05% dispersion of solid components and deposited onto freshly cleaved mica. Particles were analyzed using an AFM (JPK Nanowizard 1, Berlin, Germany) in intermittent contact mode using Si tips NSC 15 with 40 Nm⁻¹ spring constant from Mikromasch (Las Rozas de Madrid, Spain). Images were processed using JPK DP Data Processing Software 4.0 and Gwyddion 2.2.

Transmission electron microscopy

Images were acquired using a Carl Zeiss Libra 120 kV transmission electron microscope (TEM)

equipped with an omega filter. Energy-filtered transmission electron microscopy (EFTEM) was used to obtain bright-field images with low chromatic aberration when the energy slit was set to zero. Elemental maps were acquired by imaging inelastically scattered electrons using electron spectroscopy imaging (ESI). Energy selecting slits of 5eV were set at energy loss of Ru (43 eV). The images were recorded using a CCD camera and iTEM Universal TEM Imaging Platform. Samples were prepared by drying an aqueous suspension droplet of PSHEMA with and without Ru on carbon-coated parlodion films supported in 400-mesh copper grids (SPI supplies, West Chester, USA).

Photostability

Photostability measurements were performed to a Ru complex aqueous solution at 0.0808 g/mL and an aqueous Ru-PSHEMA dispersion at 0.1 g/mL, using a Photon Technology International, PTI, (Birmingham, USA) spectrofluorometer, with a photomultiplier detection system (model 810/814), operated in the emission mode. Samples were irradiated at 470 nm wave-length for 3400 seconds and the emission maximum of the Ru complex was monitored at 630 nm. All samples were continuously stirred during the measurements and kept under room conditions.

Results and Discussion

In order to assure reproducibility in different uses, the particles were characterized in terms of luminescence intensity, monodispersity and morphology using microscopies. Particles and agglomerates are shown in Figure 1a and appear as highly intense luminescent spots in the luminescence digital image in Figure 1b. Particles were excited at 470 nm and the spectrum in the Figure 1c shows the emission band of the Ru complex with maximum emission at 630 nm.

Particle morphology was analyzed by AFM and the results are depicted in Figure 1d and f. Hexagonal packing caused by high uniformity of particle sizes is observed with low deformation due to high glass temperature of PSHEMA (PS: 104°C and PHEMA: 85°C).²⁷ This kind of arrangement has been described in the literature for colloidal latex particles in dry films with highly ordered structures.^{28,29} Additionally, these structures are also attributed to a peculiar distribution of the chemical elements in particles by electrical dipole formation.³⁰ PSHEMA particles have a smooth surface also for particles without ruthenium complex. This is contrary to the description in the literature, where particles contain convoluted protrusions like in a “raspberry-like” particle model.²⁸ We attribute the smooth character of the particles to a lower 2-hydroxyethylmethacrylate

concentration in the synthesis than the procedures described in the literature. This is based on the results described by Martin-Rodriguez and co-authors,³¹ which indicated that the surface roughness is proportional to the HEMA percentage in the polymerization process. In order to determine the size distribution, 150 particles were measured and an average diameter of 183 ± 16 nm and 185 ± 15 nm (Figures 1e and g) were obtained for PSHEMA and PSHEMA-Ru, respectively. The similar diameter indicates that the addition of Ru complex after 7 hours of reaction did not notably affect the polymerization process and the stabilization, and monodispersity is maintained.

Five reactions were performed using additional concentration of HEMA. The first three reactions containing 1.5, 2.5 and 4.2 wt. % of monomers produced unstable system forming agglomerates in the first 3h of reaction, probably caused by insufficient HEMA to stabilize the particles. The last two reactions with 5.5 wt. % and 7.3wt. % provide stable colloidal dispersions, but only the highest HEMA concentration yields highly luminescent particles.

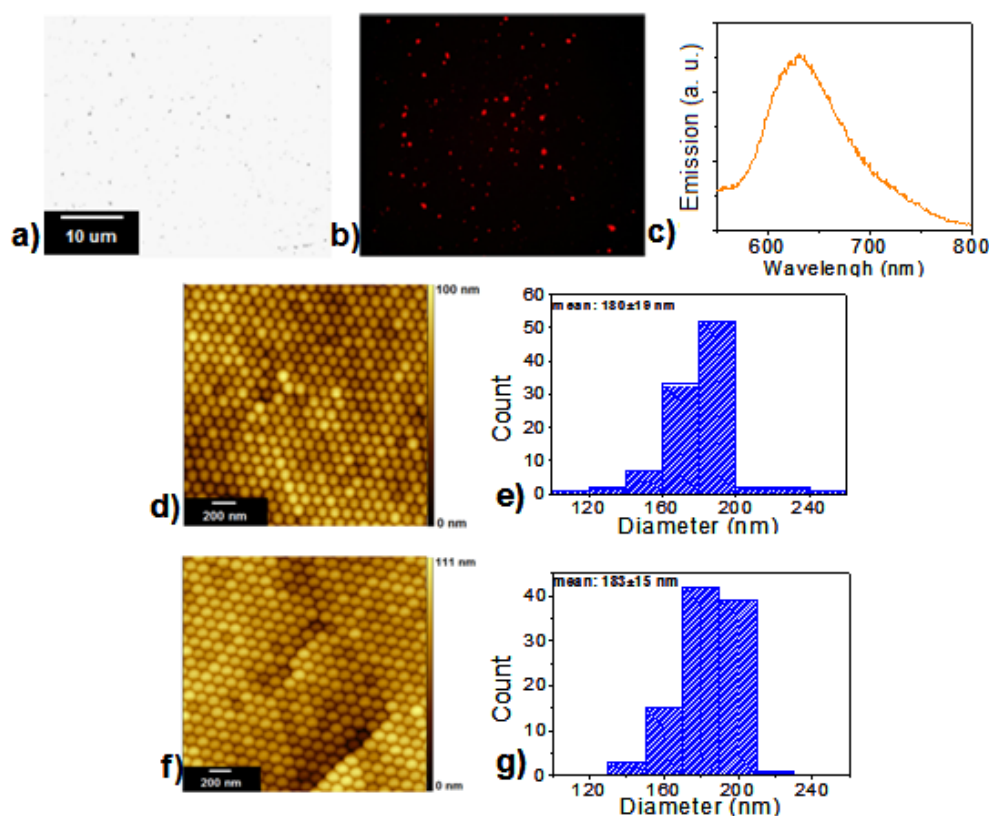


Figure 1. Microscopic characterization of PSHEMA and Ru-PSHEMA particles. Optical (a) and digital fluorescence (b) images from a PSHEMA-Ru particles dried on glass slide (630 x magnification). (c) Emission spectrum of the ruthenium complex. AFM topography images and histograms of diameter distribution from the film surface of PSHEMA (d and e) and PSHEMA-Ru (f and g) particles, showing a monodispersed size distribution evidenced by the particle homogeneous hexagonal packing.

The incorporation of a hydrophobic dye inside of the particle is demonstrated by the entrapment of the hydrophobic 9,10-diphenylanthracene, DPA, using the soaking technique.²⁶ The swelling of the polymer particle with a dichloromethane solution of DPA allowed the hydrophobic dye to diffuse into the polymer matrix. After evaporation of the organic solvent, the dye molecules remain entrapped within the particles. The PSHEMA-Ru-DPA particle spectrum (Figure 2) shows that the particles could incorporate a high percentage of DPA, revealed by the emission band intensity close to the free DPA in dichloromethane.

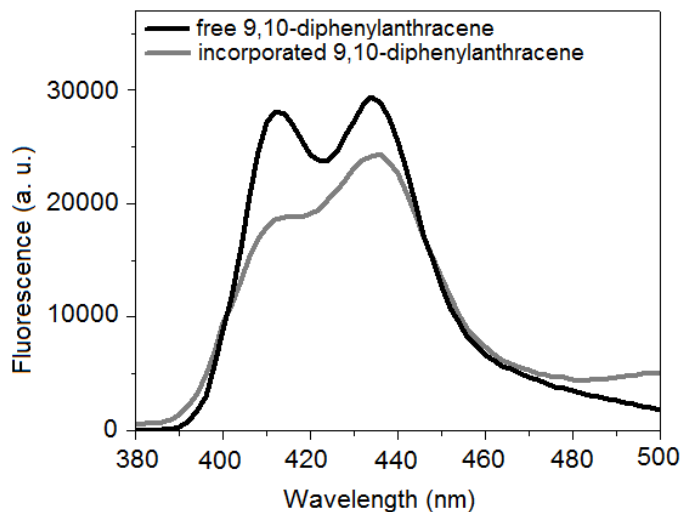


Figure 2. Hydrophobic dye incorporation. Fluorescence spectra of 9,10-diphenylanthracene in dichloromethane and incorporated in PSHEMA-Ru particles by soaking technique (λ_{ex} : 350 nm).

Many methods are used to probe the detailed internal structure of core-shell latex particles. Recently, energy filtered TEM (EFTEM) in the low-energy-loss spectral region was successfully used to observe and distinguish domains with sizes in the nanometer range and with small differences in the chemical composition.^{32,33} Hence, energy filtered transmission electron microscopy (EFTEM) in combination with electron spectroscopy imaging (ESI-TEM) were used to investigate the Ru complex distribution in the particle structure.^{34,34} Bright-field images for PSHEMA and Ru-PSHEMA particles (Figure 3a and c) confirm the smooth spherical particles that present slight deformations as necks between the particles, even more evident for PSHEMA-Ru. Energy loss TEM images were obtained at 40 eV, which is the N absorption threshold region of Ru (Figures 3b and d). Image series from 30 to 50 eV are shown in the Supporting Information (ESI – 3). PSHEMA core-shell structure has been already described in the literature using molecular maps at the low energy loss range (0-80eV).³⁵ The PSHEMA polymerization is described as a process with growing chains in the polymer-swollen particles and the HEMA richer chains are more

concentrated at the particle periphery.²⁵ X-ray photoelectron spectroscopy also indicated that the HEMA component is localized at the surface.³⁶ The images at 40 eV in the Figure 3d show that shell presents a higher contrast in comparison to the core for PSHEMA particles without Ru (Figure 3b). Thus, considering the hydrophilic structure of Ru complex, it can be expected that the complexes are more concentrated into the shell due to its higher hydrophilicity. Cardoso and col.²⁵ investigated the elemental distribution within PSHEMA particles and showed that the initiator counter ions, K^+ , concentrate in a thin outer particle surface. The positive layer around the particles can have an important role to keep the ruthenium complex attached to the particle shell.

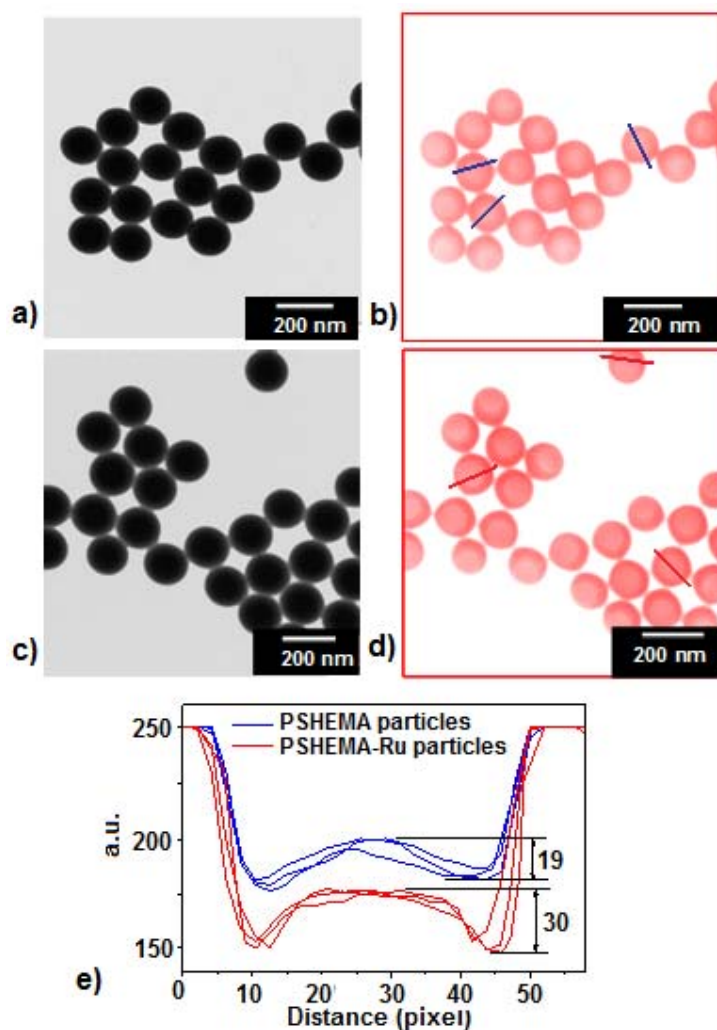


Figure 3. TEM images from PSHEMA and Ru-PSHEMA particles showing core-shell structure with Ru complex in the shell. Bright-field and energy loss images at 40 eV (N shell of Ru) for PSHEMA (a and b) and Ru-PSHEMA (c and d). Line profile (e) from a Ru-PSHEMA particle at 40 eV revealing the contrast difference between shell and core in presence of Ru.

According to the energy image and the line profile (Figure 3e), the thickness of the shell containing ruthenium is approximately 27 ± 9 nm, which corresponds to the HEMA-rich polymer shell observed in the Figure 3b. It is possible to observe that the shell structure is not symmetric around the hydrophobic core.

The time-dependence of the emission, and consequently the photostability, for the free and the incorporated Ru complex dye is shown in Figure 4.

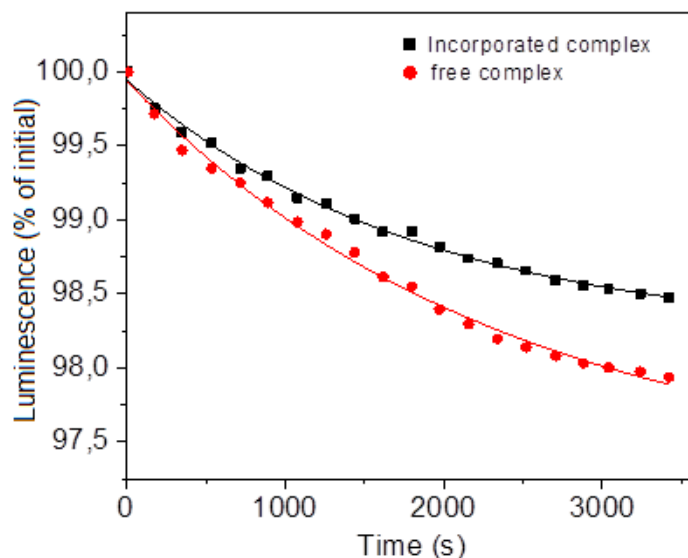


Figure 4. Photostability of Ru complex and Ru complex incorporated in PSHEMA particles. Measurements were performed during 3400 seconds, exposing the sample to $\lambda_{ex}= 470\text{nm}$ and measuring at $\lambda_{em}= 630\text{nm}$. Fluorescence decays show that bleaching effects on fluorescent Ru complex is reduced after incorporation in PSHEMA polymer particles.

The values are shown as a percentage in comparison to the initial intensity. The time-dependence for the incorporated dye is slightly lower than the free dye, indicating higher luminescence stability. The decay for the incorporated dye after 3400 seconds of irradiation was 98.5% in comparison to 97.9% for the free dye. Although the difference is low, it may be significant for the detection limit in diagnostic applications and in long time storage. It can be explained by the diffusional limitations of oxygen molecules inside of the polymer shell. It avoids that singlet state oxygen molecules decompose dye molecules in their excited state.^{37,38} Therefore, immobilization or encapsulation of the complex in polymeric material is necessary and provides possibilities for increasing photostability, besides of minimization of toxicity and invasive perturbation of biological systems.

Besides the TEM images, experiments were performed to verify the character of interaction in

the bioconjugation, showing the availability of carboxylate groups for covalent bond on the particle surface. Two bioconjugate systems with streptavidin were prepared, one in the presence and the other in the absence of *N*-(3-Dimethylaminopropyl)-*N'*-ethylcarbodiimide hydrochloride, EDC, which activates carboxylate groups for further reaction with amines. The conjugate without EDC showed very slight emission after interaction with a biotin spot, whereas the conjugates with EDC revealed much higher luminescent spot (Electronic Supporting Information 4, ESI – 4). This is an indirect indication that carboxylate groups are available on the particle surface and play an important role in the biofunctionalization step.

In order to demonstrate the potential of the particles for bioconjugation, biomolecules were immobilized on the particle surface (ESI – 5) and the bioconjugates were applied as detection system for microscopy. Monoclonal Dengue virus antibodies for a viral non-structural glycoprotein, NS1, were conjugated to the PSHEMA-Ru particles and they were used to analyze infected serum samples. The resulting analytical curve and the respective luminescent spots (Figure 5a and b) show a linear range from 200 to 400 ng/mL and a detection limit of 187 ng/mL. The image analysis is described in the (ESI – 6). Libraty and coworkers³⁹ investigated the plasma levels of secreted NS1 protein from free Dengue-2 virus during the infection. They demonstrated that the concentration may vary between 150 and 250ng/ml per day of illness for the second day of the disease for patients that suffer from Dengue haemorrhagic fever.

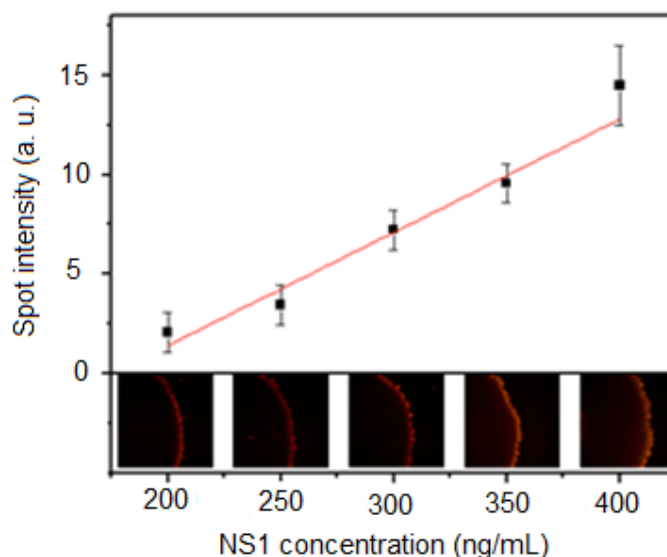


Figure 5. Anti-NS1 coated PSHEMA-Ru particles used to detect Dengue virus NS1 protein. Analytical curve (a) for Dengue virus NS1 performed on nitrocellulose membrane and digital fluorescent images from each spot. Values were obtained by subtracting the background intensity from the spot signal. Images were recorded at 10x of magnification.

Serum positive samples from the second and third day of infection from a group of 10 patients were analyzed using PSHEMA-Ru particles and microscope (Digital images are shown in the Electronic Supporting Information 7, ESI – 7). The test was positive for all samples, proving that the luminescent particles are indeed capable of providing a reliable diagnostic below the NSI concentration that exists in infected patients at the first days of the disease. Immunospot assay based on gold nanoparticles are able to detect after the third to fourth days of the disease (detection limit: 575 ng/mL)²¹. Using PSHEMA-Ru particles, it is possible to detect the disease from the second day. This can help in the rapid assessment of patients developing more severe cases of the disease.

Due to the high stability of these core-shell particles, current agglomeration problems of polymer particles related to flow in the membrane were not observed for PSHEMA-Ru (ESI – 7).

The PSHEMA-Ru particles can also provide a useful tool for cell tracking by immobilizing proteins specific for receptors on cell surface, following examples described in the literature.^{40,41} To verify this possible application, the biocompatibility of PSHEMA-Ru particles for fibroblast cells was evaluated. Polymer based on HEMA monomer is known as biocompatible.⁴² Fibroblasts are the most common cells of connective tissue in animals and are responsible for the extracellular matrix and collagen synthesis. After incubating for 24, 48 and 72 h with PSHEMA-Ru particles, the cells were stained and analyzed in a confocal microscope. The pseudo-colored fluorescence images were overlaid and Figure 6 shows a combined image of the fibroblasts after 72 h cultivated in presence of the PSHEMA-Ru particles.

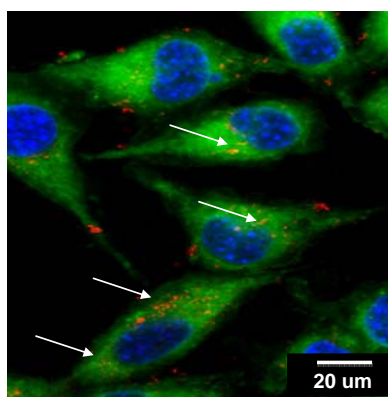


Figure 6. Biocompatibility of PSHEMA particles with fibroblast cells. Confocal fluorescent microscopic image of fibroblast cells grown and stained on a glass surface in the presence of PSHEMA-Ru particles after 72 h of incubation, as indicated by the white arrows. The cell membrane was labelled with Dil and the nuclei were counterstained with Hoechst 33342.

The stained membrane and nucleus shows that the cell morphology was maintained. Moreover,

the particles concentrate on the surface and are not incorporated by the cells, as indicated by the white arrows. This result shows that the PSHEMA-Ru particles are biocompatible and could be used for cell-surface antigen detection, neutral retrograde tracers, sensitive diagnostic reagents and for blood flow measurements.

Supernatant luminescence measurements were performed during ten weeks with no measurable luminescence and the biocompatibility is an indirect confirmation of the stability of the luminescent particles, in terms of ruthenium leaching.

Conclusions

In this work, we described one-step synthesis of surface-functional, [Ru(4,4'-dicarboxylate-2,2'-bpy)₃] labeled poly[styrene-*co*-(2-hydroxyethyl methacrylate)] particles. Particles present a core-shell structure that allows the incorporation of hydrophilic ruthenium complexes and hydrophobic molecules. The special design with carboxylate groups on the surface, surfactant-free and high monodispersity makes them appropriate for biomedical applications. A real system composed by Dengue virus non-structural protein antibody was used for Dengue fever detection utilizing microscopy, which also showed homogeneous luminescent spots with low particle agglomeration. Moreover, the particles are biocompatible expanding the application range to cell-based assays. We show that PSHEMA-Ru particles have a high potential to be successfully used in life science and biomedical applications. The ease conjugation with biomolecules and the vast diversity of molecules to be incorporated, given the structural characteristics of the PSHEMA particles, enable the easy development of particles with a broad range of precisely controlled characteristics and, consequently, vast applications.

Acknowledgement

The authors would like to thank the Sao Paulo Institute of Tropical Medicine for kindly providing the serum panel, especially Lucy Santos Vilas Boas and Clara Felix for the sample organization, Norbert Menzel and Anahi Philippart for laboratory support and Prof. Axel K. Walch for microscopic equipment. EML acknowledges the fellowship from the International Doctorate Program NanoBioTechnology (IDK-NBT) funded by the Elite Network of Bavaria (ENB). This work was supported by the cluster of excellence Nano Initiative Munich (NIM), the Center of Nanoscience (CeNS), and a DAAD/CAPES travel grant.

Electronic Supporting Information

Electronic Supplementary Information (ESI) available: (ESI-1) Characterization of the ruthenium complex; (ESI-2) Parameters used in the confocal microscope to analyze cells and serum spot; (ESI-3) Calculation of the spot intensities for plotting the analytical curve; (ESI-4) TEM bright-field and low energy loss (30 to 50 eV) images for PSHEMA particles without and with ruthenium complex; (ESI-5) Digital fluorescence images of serum sample spots after interacting with PSHEMA-Ru particles coated with anti-NS1 protein antibodies through absorption and covalent coupling; (ESI-6) Procedure and digital fluorescence image series of the bioassay on glass slide based on biotin-streptavidin interaction from 1 mmol/L to 0.01 nmol/L of biotin immobilized on the amine coated glass slide; and (ESI-7) Digital fluorescence images of ten serum sample spots after interacting with PSHEMA-Ru particles covalently coated with anti-NS1 protein antibodies.

References

- 1 D. K. Bonner, C. Leung, J. Chen-Liang, L. Chingozha, R. Langer and P. T. Hammond, *Bioconjugate Chem.*, 2011, **22**, 1519.
- ² M. Lessard-Viger, M. Rioux, L. Rainville and D. Boudreau, *Nano Lett.*, 2009, **9**, 3066.
- 3 D. E. Achatz, F. J. Heiligtag, X. Li, M. Link and O. S. Wolfbeis, *Sens. Actuators, B* 2010, **150**, 211.
- 4 W. Di, S. K. P. Velu, A. Lascialfari, C. Liu, N. Pinna, P. Arosio, Y. Sakka and W. Qin, *J. Mater. Chem.*, 2012, **22**, 20641.
- 5 M. A. Rocco, J-Y. Kim, A. Burns, J. Kostecky, A. Doody, U. Wiesner and M. P. DeLisa, *Bioconjugate Chem.*, 2009, **20**, 1482.
- 6 S. Gu, N. Anzai, D. Nagao, Y. Kobayashi and M. Konno, *e-Polymers*, 2005, **64**, 1.
- 7 F. Chen, X. Jiang, R. Liu, J. Yin, *ACS Appl. Mater. Interfaces*, 2010, **2**, 1031.
- 8 R. Mukthavaram, W. Wrasidlo, D. Hall, S. Kesari and M. Makale, *Bioconjugate Chem.* **2011**, **22**, 1638.
- 9 L. Zhou, L., J. Yuan and Y. Wei, *J. Mater. Chem.*, 2011, **21**, 2823.
- 10 W. Fang, X. Chen and N. Zhen, *J. Mater. Chem.*, 2010, **20**, 8624–8630.
- 11 J. L. Chávez, J. L. Wong and R. S. Duran, *Langmuir*, 2008, **24**, 2064.
- 12 F. Zeng, H. Lee and C. Allen, *Bioconjugate Chem.*, 2006, **17**, 399.
- 13 S. Dembski, M. Milde, M. Dyrba, S. Schweizer, C. Gellermann and T. Klockenbring, *Langmuir*,

- 2011, **27**, 14025.
- 14 T. C. J. Grinbnau, J. W. Leuvering and H. Hell van, *J. Chromatogr. Biomedical Appl.*, 1986, **376**, 175.
- 15 M. Okubo, Y. Yamamoto, M. Uno, S. and T. Matsumoto, *Colloid Polym. Sci.*, 1987, **265**, 1061.
- 16 M. Okubo, Y. Yamamoto and S. Kamei, *Colloid Polym. Sci.*, 1989, **267**, 861.
- 17 M. P. Coogan, J. B. Court, V. L. Gray, A. J. Hayes, S. H. Lloyd, C. O. Millet, S. J. A. Pope and D. Lloyd, *Photochem. Photobiol. Sci.*, 2010, **9**, 103.
- 18 K. Segala, R. L. Dutra, C. V. Franco, A. S. Pereira and T. Trindade, *J. Braz. Chem. Soc.*, 2010, **21**, 1986.
- 19 M. Hara J. T. Lean and T. E. Mallouk, *Chem. Mater.*, 2001, **13**, 4668.
- 20 W. Lin, Y. Zheng, J. Zhang and X. Wan, *Macromolecules*, 2011, **44**, 5146.
- 21 E. M. Linares, L. T. Kubota, J. Michaelis and S. Thalhammer, *J. Immunol. Methods*, 2012, **375**, 264.
- 22 A. Sooresh, H. Kwon, R. Taylor, P. Pietrantonio, M. Pine and C. M. Sayes, *ACS Appl. Mater. Interfaces*, 2011, **3**, 3779.
- 23 M. K. Nazeeruddin, K. Kalyanasundaran, M. Grätzel, B. P. Sullivan and K. Morris, In *Inorganic Syntheses*. Chapter 3; M. Y. Darensbourg, Ed.; John Wiley & Sons, Inc.: New York, 1998; Vol. 32, p 181.
- 24 H. Tamai, A. Fujii, T. Suzawa, T. *J. Colloid Interface Sci.*, 1987, **116**, 37.
- 25 A. H. Cardoso, C. A. P. Leite and F. Galembeck, *Langmuir*, 1998, **14**, 3187.
- 26 E. Allard and C. Larpent, *J. Polym. Sci. A*, 2008, **46**, 6206–6213.
- 27 M. Okubo, T. Suzuki and Y. Fukuhara, *Colloid Polym. Sci.*, 2003, **281**, 569.
- 28 A. H. Cardoso, C. A. P. Leite and F. Galembeck, *Colloids Surf., A*, 2001, **181**, 49.
- 29 A. H. Cardoso, C. A. Leite, M. E. D. Zaniquelli, and F. Galembeck, *Colloids Surf., A*, 1998, **144**, 207.
- 30 A. H. Cardoso, C. A. P. Leite and F. Galembeck, *Langmuir*, 1999, **15**, 4447.
- 31 A. Martin-Rodriguez, M. A. Cabrerizo-Vilchez and R. Hidalgo-Alvarez, *Colloids Surf., A*, 1996, **108**, 263.
- 32 E. M. Linares, L. F. Valadares, C. A. Silva, C. A. Rezende, and F. Galembeck, *Anal. Chem.*, 2009, **81**, 2317.
- 33 E. M. Linares, M. M. Rippel and F. Galembeck, *ACS Appl. Mater. Interfaces*, 2010, **2**, 3648.
- 34 E. M. Linares, S. A. Jannuzzi and F. Galembeck, *Langmuir*, 2011, **27**, 15199.
- 35 L. F. Valadares, E. M. Linares, F. C. Braganca and Galembeck, *J. Phys. Chem. C*, 2008, **112**,

- 8534.
- 36 M. Okubo, Y. Yamamoto and S. Kamei, *Colloid Polym. Sci.*, 1989, **267**, 861.
- 37 Y. Kobayashi, K. Misawa, M. Kobayashi, M. Takeda, M. Konno, M. Satake, Y. Kawazoe, N. Ohuchi, and A. Kasuya, *Colloids Surf., A*, 2004, 24247.
- 38 D. Chen, Y. Yu, F. Huang, H. Lin, P. Huang, A. Yang, Z. Wangab and Y. Wang, *J. Mater. Chem.*, 2012, **22**, 2632.
- 39 D. H. Libraty, P. R. Young, D. Pickering, T. P. Endy, S. Kalayanarooj, S. Green, D. W. Vaughn, A. Nisalak, F. A. Ennis, A. L. Rothman, *J. Infect. Dis.*, 2002, **186**, 1165.
- 40 V. I. Slaveykova, K. Startchev and J. Roberts, *J. Environ. Sci. Technol.*, 2009, **43**, 5117.
- 41 P. Voisin, E. J. Ribot, S. Miraux, A-K. Bouziers-Sore, J-F. Lahitte, V. Bouchaud, S. Mornet, E. Thiaudiere, J-M. Franconi, L. Raison, C. Labrugere and M-H. Delville, *Bioconjugate Chem.*, 2007, **18**, 1053.
- 42 K. Kejlová, J. Labský, D. Jírová, H. Bendová, *Toxicol. In Vitro*, 2005, **19**, 957.

Electronic Supporting Information

One step synthesis of polymer core-shell particles with carboxylated Ruthenium complex: potential tool for biomedical applications

Elisângela M. Linares^a, André Formiga^b, Lauro T Kubota^b, Fernando Galembeck^b, Stefan Thalhammer^{a}*

^a Helmholtz Zentrum München - German Research Center for Environmental Health, Ingolstädter Landstrasse 1, 85764 Neuherberg, Germany

^b Institute of Chemistry, State University of Campinas, Cidade Universitária s/n, 13083-970, Campinas, São Paulo, Brazil

CORRESPONDING AUTHOR FOOTNOTE

Stefan Thalhammer, Helmholtz Zentrum München, P.O. Box 6154 – 13084-971 – München – Germany. Phone: +49 089/3187-2893. Fax: +49 089/3187-3323. stefan.thalhammer@helmholtz-muenchen.de

List of Contents

The supporting information contains four sub-sections:

ESI-1 Characterization of the ruthenium complex

ESI-2 Parameters used in the confocal microscope to analyze cells and serum spot;

ESI-3 Calculation of the spot intensities for plotting the analytical curve.

ESI-4 Calculation of the spot intensities for plotting the analytical curve. **ESI-3** TEM bright-field and low energy loss (30 to 50 eV) images for PSHEMA particles without and with ruthenium complex;

ESI-5 Digital fluorescence images of serum sample spots after interacting with PSHEMA-Ru particles coated with anti-NS1 protein antibodies through absorption and covalent coupling;

ESI-6 Digital fluorescence image series of the bioassay on glass slide based on biotin-streptavidin interaction from 1 mmol/L to 0.01 nmol/L of biotin immobilized on the amine coated glass slide;

ESI-7 Digital fluorescence images of ten serum sample spots after interacting with PSHEMA-Ru particles covalently coated with anti-NS1 protein antibodies.

ESI-1 Characterization of the ruthenium complex

Comparative analysis between ^1H NMR spectra of tris-chelated complex of Ru(II), obtained using a Bruker Avance II 250 MHz spectrometer in D_2O

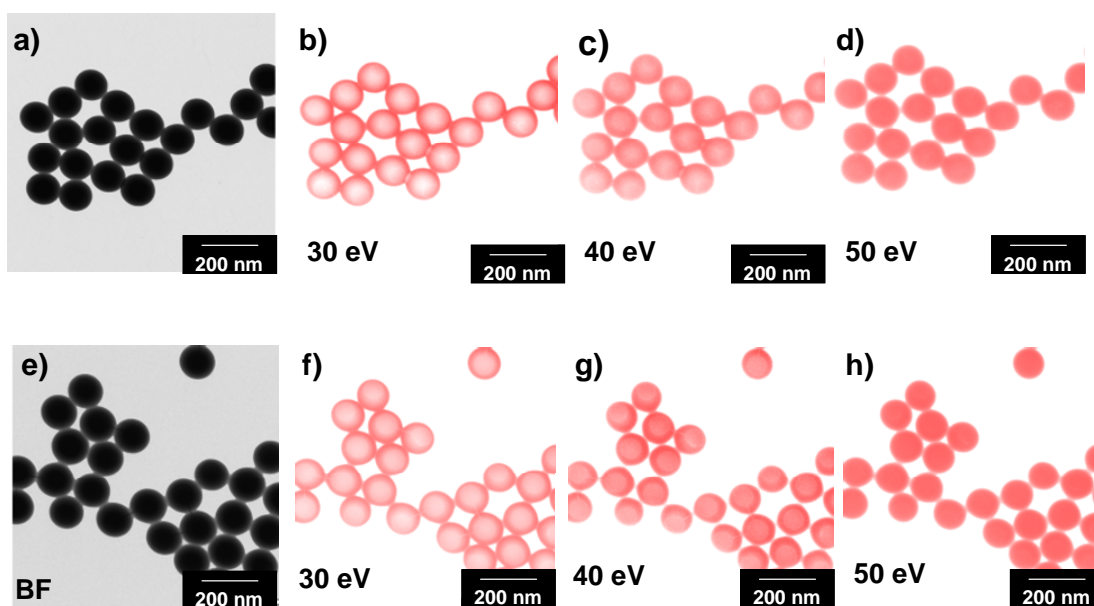
	<i>Literature</i> ¹	<i>Synthesis</i>
<i>C-H (1)</i>	7,93 (d)	7,58 (d)
<i>C-H (2)</i>	7,73 (d)	7,67 (d)
<i>C-H (3)</i>	8,94 (s)	8,79 (s)

(1) Nazeeruddin, M. K.; Kalyanasundaran, K.; Grätzel, M.; Sullivan, B. P. and Morris, K. (1998) One-Pot Synthesis of Tetrahydronium Tris(4,4'-Dicarboxylato-2,2'-Bipyridine)-Ruthenium(II) Dihydrate. *Inorganic Syntheses. Volume 32: Transition metal complexes and precursors* (Darensbourg, M.Y. (Ed.) pp 181-186, Chapter 3, John Wiley & Sons, Inc., New York.

ESI-2 Parameters used in the confocal microscope to analyze cells and serum spot.

Material	Dye	Excitation and emission wavelength (nm)	Laser	Filter configuration
Nucleus	Hoechst 33342	350/460	Argon (488)	HFT KP700/514, mirror, mirror, BP 435-485
Membrane	DilC	549/565	543	NT80/20/543, BG39, LP560
Particles (cells)	Ruthenium complex	470/630	Argon (488)	HFT488/543, mirror, BG39, KP685
Particles (serum spots)	Ruthenium complex	470/630	Argon (488)	HFT488, mirror, NFT545, KP685

ESI-3 TEM bright-field and low energy loss (30 to 50 eV) images for PSHEMA particles without (a-d) and with ruthenium complex (e-h).



The images at 40 eV (c and g) show that the shell of PSHEMA particles with Ru complexes present a slight higher contrast in relation to the core in comparison to PSHEMA particles without Ru complexes. This affirmation was confirmed by dividing the signal difference between the shell and the core by the background signal. All images were converted to gray scale and then to a colored (white to red) to facilitate the visualization.

ESI-4 Application of Ru-PSHEMA particles for conjugation with biomolecules using biotin-streptavidin interaction.

BSA coated PSHEMA particles were conjugated to streptavidin by adding 0.2 mg of protein to 400 μ L of an aqueous particle dispersion at 3 mg/mL. The suspension was stirred for 30 minutes at RT. Subsequently, 1.5 mg of EDC was added and mixed by vortexing and then adjusted to pH 6.5. The dispersion was kept on a shaker for 3 h at RT. To separate the protein-labeled particles from unbound proteins and EDC molecules, the suspension was centrifuged at 5000 rpm for 5 min at RT and washed twice with phosphate buffer 0.01 mol/L, pH 7.6, for 10 min at 4°C. Streptavidin particles were used to analyze biotin immobilized onto a glass slide using fluorescence microscopy. Amine coated slides were functionalized with albumin by adding a solution containing 5% of BSA and 100 mg of EDC in 4 mL of phosphate buffer 0.01 mol/L, pH 6, to the glass slide. The system was incubated in a humidity chamber for 1 h. Then, the glass slide was three times washed with

phosphate buffer 0.01 mol/L, pH 7.4, and dried at RT. Biotin-NHS was diluted in dimethylformamide for 1 mmol/L and dilutions from 10^{-4} to 10^{-10} mol/L were prepared using phosphate buffer 0.01 mol/L, pH 7.4. 2 μ L spots from each biotin solution were deposited on the albumin coated glass slide and kept in a humidity chamber for 1h at RT. A solution of streptavidin monoclonal antibody 0.01 mg/mL containing 0.2 mg of EDC was deposited on the albumin coated glass slide and was used as positive control. After 1 h, the glass slide was three times washed with phosphate buffer 0.01 mol/L, pH 7.4, and dried at RT. A dispersion of streptavidin coated particles 1% (w/v) in phosphate buffer 0.01 mol/L, pH 7.4, was deposited onto the glass slide, which has then kept in the humidity chamber for 20 minutes. After washing with water, the glass slide was dried and kept in the dark until analysis.

Biotin-streptavidin interaction was chosen as model system due to its extensive use to bind molecules such as antibodies and nucleic acids to the detection system, like fluorescent particles. Therefore, streptavidin was covalently bound to the PSHEMA particles. Bovine serum albumin was firstly immobilized on the particle surface as spacer for the conjugations to avoid conformation changes on the protein and to provide better steric accessibility to the forthcoming interaction. An amine coated glass slide was functionalized with biotin spots from 1 mmol/L to 0.1 nmol/L and a representative scheme of the functionalized glass slide is shown in Figure 1.

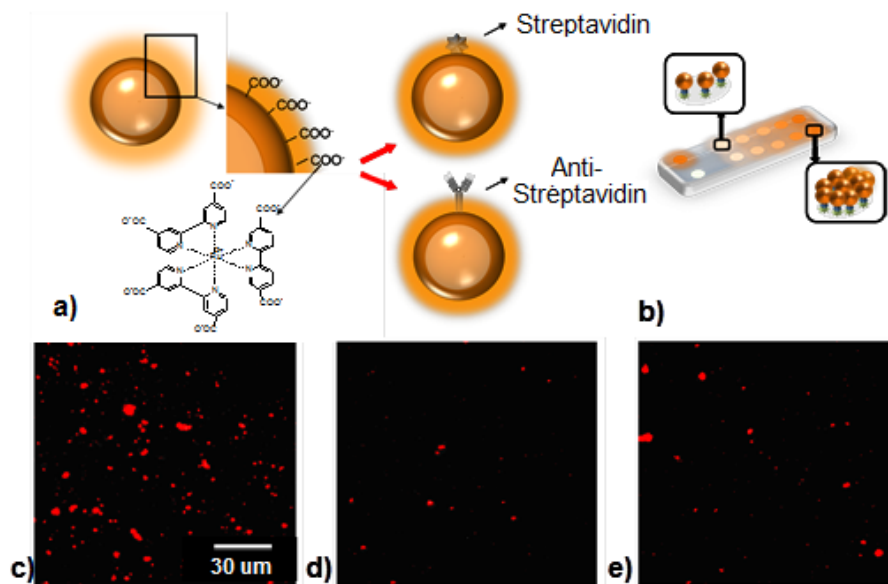


Figure 1. Scheme of particle structure (a) showing carboxylate groups used for bioconjugation with proteins and antibodies. Bioassay (b) based on streptavidin coated Ru-PSHEMA particles and biotin functionalized albumin glass slide. Digital fluorescence images of three spots: (c) 1 mmol/L biotin, (d) 0.01 μ mol/L biotin and (e) positive control consisting of anti-streptavidin antibody immobilized on the glass slide, 10 μ g/mL. The images were taken through a 40 x microscope objective.

Fluorescent particles attached to biotin-modified glass slides are clearly confirmed by the density of fluorescent dots in Figure 1c-e. The density of fluorescent particles per spot increased with the increase of biotin concentration immobilized on the glass slide. After 10 nmol L^{-1} , the particle density is similar to the observed in the negative control, caused by non-specific adsorption of particles on the glass slide. Positive control formed by anti-streptavidin antibody clearly shows high number of attached particles in contrast to the negligible number observed in negative control. These findings demonstrate that the test succeeds and that PSHEMA particles are successfully applied to bioconjugation. An image series is presented in the Figure 2.

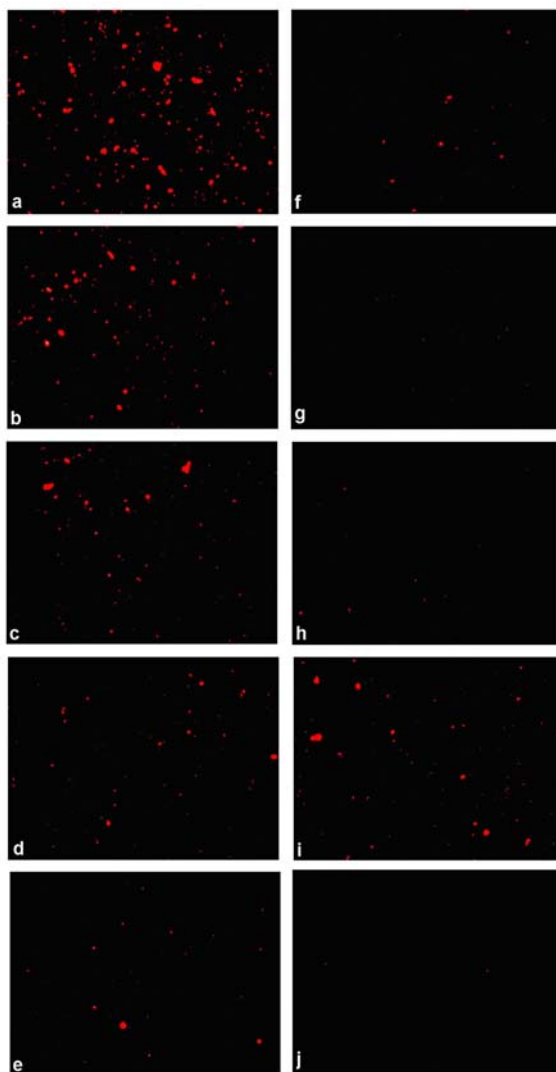
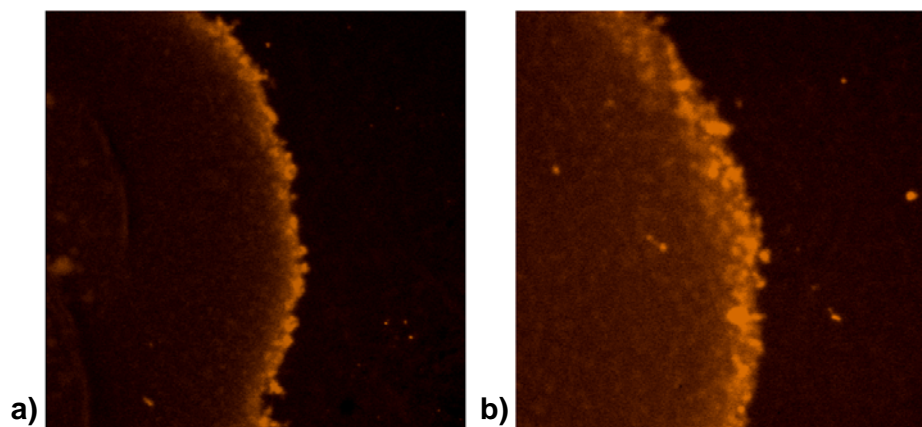
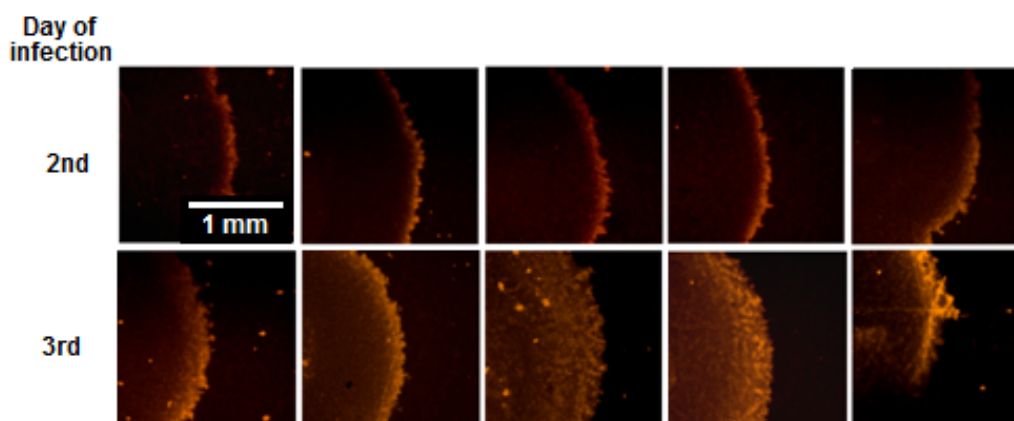


Figure 2. Digital fluorescence image of the bioassay on glass slide based on biotin-streptavidin interaction. The concentrations of biotin are (a) 1 mmol/L, (b) 0.1 mmol/L, (c) 0.01 mmol/L, (d) 1 $\mu\text{mol/L}$, (e) 0.1 $\mu\text{mol/L}$, (f) 0.01 $\mu\text{mol/L}$, (g) 1 nmol/L, 0.1 nmol/L, (h) 0.01 nmol/L (e) positive control consisting of anti-streptavidin antibody immobilized on the glass slide, 10 $\mu\text{g/mL}$ and (j) negative control formed by amine coated glass slide. The images were taken through a 40 x microscope objective.

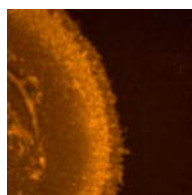
ESI-5 Digital fluorescence images of spots of serum samples after interacting with PSHEMA-Ru particles coated with anti-NS1 protein antibodies through (a) absorption and (b) covalent coupling. (Magnification: 100x)



ESI-6 Digital fluorescence images of spots of ten serum samples after interacting with PSHEMA-Ru particles covalently coated with anti-NS1 protein antibodies. (Magnification: 100x)

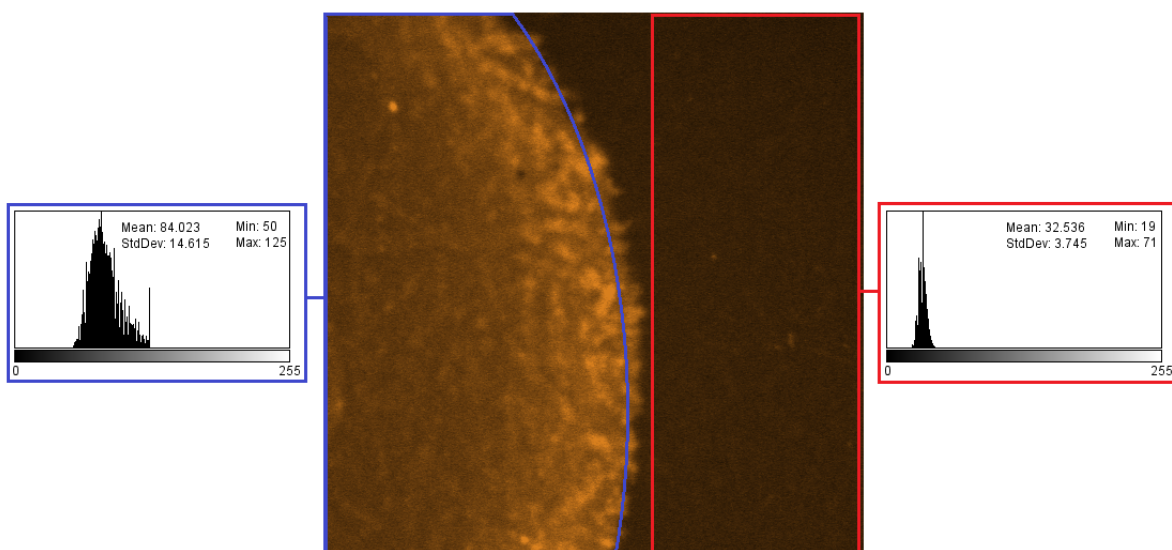


The image below is a serum spot detected with fluorescent nanoparticles used in the Chapter 3. Those particles show extensive agglomeration and tend to concentrate at the edge of the serum spot. Comparing the images of the serum spots with the luminescent particles, it is possible to observe the better performance of PSHEMA-Ru particles in comparison to fluorescent polystyrene particles.



ESI-7 Calculation of the spot intensities for plotting the analytical curve.

Five images were acquired from different areas of each serum spot of the analytical curve: four at the edge and one at the center. The image below shows an example of the analyzed area from the spot edge and the histograms obtained for each part (spot and background). An average of the mean background signal value was subtracted of the spot signal average and used to plot the curve according to the NS1 concentration. All images were obtained controlling the source intensity to operate at the same conditions and the same areas were analyzed for all spots.



CHAPTER 5

Enhanced lateral flow immunoassay based on gold and fluorescent particle clusters for Dengue detection: comparison with gold and carbon black label

Enhanced lateral flow immunoassay based on gold and fluorescent particle clusters for Dengue detection: comparison with gold and carbon black labels

Elisângela M. Linares^a, Claudio S. Pannuti^b and Stefan Thalhammer^{a,}*

^aHelmholtz Zentrum München - German Research Center for Environmental Health, Ingolstädter Landstrasse 1, 85764 Neuherberg, Germany; elisangela.linares@helmholtz-muenchen.de, stefan.thalhammer@helmholtz-muenchen.de;

^bLaboratory of Virology, Instituto de Medicina Tropical de São Paulo e Faculdade de Medicina, Universidade de São Paulo. Eneas de Carvalho Aguiar 470, 05403-000, São Paulo, Brazil; cpannuti@usp.br

CORRESPONDING AUTHOR FOOTNOTE

Stefan Thalhammer, Helmholtz Zentrum München, P.O. Box 6154 – 13084-971 – München – Germany. Phone: +49 089/3187-2893. Fax: +49 089/3187-3323. stefan.thalhammer@helmholtz-muenchen.de

Abstract

Dengue fever is a tropical viral disease that annually affects millions of people in developing countries and has a lack of sensitive tools for point-of-care diagnosis. Lateral flow immunoassays (LFIAs) are especially interesting for impoverished environments due to the ease of handling, low sample volume, low cost and rapid result. However, the challenge of these assays is the low sensitivity, which prevents the application for disease diagnostic in the early stages. In order to overcome the sensitivity limitation, we describe a novel detection system for LFIA that provides an enhanced visual signal based on clusters of gold and fluorescent nanoparticles. The detection system consists of gold nanoparticles concentrated in a cluster with antibodies to recognize each analyte, instead of only a single colored particle per analyte molecule. Additionally, when the colored spot is slightly positive, providing an uncertain result, a UV lamp can be used to excite the fluorescent particles containing fluorophores that emit in the visible spectrum. Similar to the gold particles, the cluster concentrates fluorescent nanoparticles, which increase the fluorescence emission signal. This set up allows improving the detection limit in comparison to current tests. LFIA based on nanoparticle cluster was prepared for Dengue fever detection, using a protein of the virus, NS1, as target biomolecule for early stage illness detection. These assays showed a detection limit, 2.5 ng/mL, for Dengue virus NS1 protein superior to standard gold nanoparticles, 500 ng/mL, and carbon black, 10 ng/mL. The clusters showed a detection limit 4 times superior to the best colored label for LFIA, carbon black, providing more confident results for early disease detection.

Keywords

Lateral flow immunoassay, immunospot assay, carbon black, gold nanoparticles, fluorescence, Dengue fever

Introduction

Dengue fever (DF) has emerged as a rapidly spreading vector-borne disease affecting mainly poor populations and also the leading cause of hospital admissions in several countries (WHO, 2010). DF results from viral infection transmitted by *Aedes aegypti*, a species of mosquito with a global distribution. The incidence of DF has dramatically grown over the world in the last decades. Over 2.5 billion people are now endangered from DF. The World Health Organization (WHO, 2012) estimates 100 million cases of dengue fever, 500 thousand cases of dengue hemorrhagic fever (DHF). For DHF, early medical care can save lives, decreasing mortality rates from more than 5% to less than 1% (Allwinn, 2011). Due to the low visibility in the rest of the world and limited access to interventions and support services, DF is considered as a neglected disease and causes thousands of victims every year (Wagstaff, 2002).

To attend this population in terms of affordable medical assistance, there is an increasing necessity for point-of-care (POC) assays that provide fast, specific, sensitive and low cost diagnostics. Lateral flow immunoassays (LFIAs) are currently appropriate technologies that fulfill most of these requirements. LFIA provides low-cost and fast analysis without trained personnel for handling or expensive apparatus for reading (Posthuma-Trumpie et al., 2009). Due to these characteristics, LFIA is a good alternative for off laboratory or resource-poor settings. The test allows analysis in the field, providing real-time results and avoiding expensive sample transportation and long waiting times for results (Bai et al., 2012). Besides human pathogens detection, LFIA can be used to detect different analytes and have been applied in various fields, such as food analysis (Lai et al., 2009; Kolosova et al., 2008), environmental monitoring (Fisher et al., 2009) and forensic diagnostics (Pathak et al., 2001).

The conventional LFIA employs colloidal gold (Ghandi et al., 2009; Zhang et al., 2011), dyes (Ho et al., 2008) or latex beads (Takanashi et al., 2008) as reporters to generate visual signals. An investigation indicated that 75% of LFIA have gold nanoparticles as labels for the detection of pathogen agents and chemical contaminants, followed by carbon black 4.2%, luminescent particles 4.2% and others (Ngom et al., 2010). Colloidal gold-based test strips, in particular, have been produced commercially in large amounts for a variety of applications (Bai et al., 2012). However, the applicability of LFIA is limited when low concentration of analyte should be detected, such as in early diagnosis of diseases like Dengue fever. Sensitivity limitations persist on commercial systems and reduce their applications, as exemplified for 8 commercial kits for DF based on IgG/IgM detection (Blacksell et al., 2006). From all kits, only one showed the necessary specificity (97.6%) and sensitivity (65.3%) to be considered of clinical use (>50%). It means that only one test

had the proportion of actual positives correctly identified (sensitivity) higher than 50% and the proportion of negatives correctly identified (specificity) higher than 50%. The need for tests with improved detection limit is not only highlighted for DF, but also for commercially available point-of-care tests (Fu et al., 2011), such as for Chlamydia (van Dommelen et al., 2010; Skidmore, 2010) and influenza (Vasoo et al., 2009; Drexler et al., 2009).

We recently showed a comparison of the four most used colored labels in LFIA and the results revealed that carbon black provides the best detection limit in comparison to gold nanoparticles, gold enhanced with silver and blue polystyrene particles (Linares et al., 2012a). Sensitivity in the picomolar range was achieved using carbon black, even by visual inspection (Gordon and Michel, 2008). Carbon black has been applied to detect different analytes (Posthuma-Trumpie et al., 2012), such as progesterone (Posthuma-Trumpie et al., 2008), methiocarb in water (Blažková et al., 2009), microorganism (Blažková et al., 2011), DNA (Kalogianni et al., 2011). Due to the fact that carbon black is cheap and provides good contrast and high sensitivity, it has some disadvantages for LFIA applications (Posthuma-Trumpie et al., 2012). It mainly concerns the presence of larger and irregularly shaped carbon particles that requires the use of nitrocellulose with larger pore openings and it causes relatively low captured ligand concentration/density, resulting in "relative diffuse" signal. In addition, some types of carbon with low oxidation require the addition of surfactants to obtain stable suspensions in aqueous media and such surfactants may interfere with test performance.

Fluorescent immunoassays are a promising alternative to conventional colorimetric detection methods due to their increased sensitivity (Linares et al., 2007, 2012b). Recently a work developed by Khreich and co-authors (Khreich et al., 2008) evaluated different labels (colloidal gold, fluorescent microsphere, dextrane rhodamine, dye microsphere and liposomes) for *Staphylococcus aureus* enterotoxin B (SEB) detection. Colorimetric labels allowed the detection of SEB close to 0.5 ng/mL. Colloidal gold was twice as sensitive as the dye microspheres. On the other hand, fluorescent microspheres showed better sensitivity than colorimetric labels, resulting in a strong increase in sensitivity with limit of detection close to 0.02 ng/mL.

Although fluorescent labels generally provide lower detection limit, it requires the use of fluorescence reader, which is contrary to the concept of a simple assay for impoverished environments. Therefore, there have been several attempts trying to enhance the sensitivity of fast immunoassays based on visible signal. Horton and colleagues (Horton et al., 1991) reported a 100-fold reduction of the detection limit via the immersion of a lateral flow strip into a silver enhancement solution. Reports include improvements in the detection limit of approximately 10-

fold, using an enzymatic amplification system (Parolo et al., 2012). However, in these studies, the user was still required to perform numerous time-consuming steps, limiting the format appropriateness for use as a POC.

Here, we describe a novel high sensitive detection system for LFIA based on clusters constituted by two structures: gold and fluorescent particles. The novel detection system provides an enhanced visual signal. Gold nanoparticles are concentrated in a cluster with at least one detection molecule to recognize each analyte molecule, instead of only one single gold nanoparticle to provide a visual signal for each analyte molecule. The assay performance is also enhanced by the combination of colored particles with fluorescent beads. When the colored spot is slightly positive, providing an uncertain result, a ultra-violet (UV) lamp or light emitted diode (LED) can be used to excite the fluorescent particles and the fluophores will emit in the visible range. Comparable to the gold particles, the cluster concentrates fluorescent nanoparticles, which previously concentrate fluophores, increasing the fluorescence emission signal. This set up allows improving the detection limit in comparison to current tests, which are usually based on single nanoparticles as detection label.

The use of clusters formed by two particles was already described in the literature. Bai and co-authors (Bai et al., 2012) bound CdTe quantum dots (QD) onto larger silica nanoparticles, which increased greatly the fluorescence intensity due to the QD accumulation. However, the silica particles were only used as a QD carrier to concentrate the labels and the detection was exclusively based on fluorescence. In another study, an immunodipstick assay was developed by Tang and co-authors (Tang et al., 2009) for the fast screening of aflatoxin B2 (AFT B2) in food. The detector reagent consisted of magnetic nanogold microspheres (MnGMS) with nano- Fe_2O_3 particles as core and gold nanoparticles as shell, and bio-functionalized with monoclonal anti-AFT B2 antibodies. Result showed that the cutoff detection value was 3 times lower than gold nanoparticles at 0.9 ng/mL AFT B2. However, the Fe_2O_3 nanoparticles act as a substrate for the assembly of gold nanoparticles and did not played a direct role in the signal intensification.

Herein, we describe the development of a lateral flow immunoassay, which combines both gold and fluorescent nanoparticles in a cluster as detection labels for Dengue fever diagnostics. The target molecule is the non-structural (NS1) protein of the virus, which is released in the blood stream on the first days of the infection after the outbreak of the symptoms. In order to compare the performance of our combined colorimetric/fluorescent assays, we produced LFIA for DF detection based on gold nanoparticles and carbon black, as the most sensitive colorimetric label for LFIA.

Materials and Methods

Chemicals and Materials

Gold nanoparticles (mean diameter: 40 nm), bovine serum albumin (BSA) powder, biotin, streptavidin, boric acid, anti-streptavidin IgG antibody, *N*-(3-Dimethylaminopropyl)-*N'*-ethylcarbodiimide hydrochloride (EDC), dialysis membranes (MWCO 100kDa and 130kDa), sucrose, potassium phosphate mono- and dibasic were purchased from Sigma-Aldrich (Milwaukee, USA). Streptavidin-labeled gold nanoparticles (mean diameter: 40 nm) was purchased from British Biocell (Cardiff, United Kingdom). FluoSpheres (PS) carboxylate-modified microspheres (excitation: 580 nm/ emission: 605 nm, see SI-1) 0.04 μ m, and nitrocellulose AC99 membrane were obtained from Invitrogen (Carlsbad, United States) and Whatman (Maidstone, United Kingdom), respectively. Sample and conjugate pad were obtained from Pall (Dreieich, Germany). Absorbent pad and backing card were provided from Millipore (Billerica, USA) and Lohmann (San Jose, USA). Dengue virus NS1 glycoprotein mouse monoclonal antibody (supernatant) and Melon gel IgG purification kit were obtained from Abcam (Cambridge, United Kingdom) and Thermo Scientific (Rockford, United States), respectively. Dengue NS1 Ag ELISA was purchased from Standard Diagnostics (Youngin, Korea). The solutions were prepared with water purified in a Milli-Q Millipore system and the actual pH of the buffer solutions was determined with a Cyberscan pH meter model 500 (Queensway, Singapore).

Serum samples

A total of 48 serum samples were obtained by the São Paulo Institute of Tropical Medicine, University of São Paulo. The tests were approved by the ethics committee from the university. The samples were analyzed for NS1 using the commercial kit PlateliaTMNS1 (Biorad Laboratories, Marnes-La-Coquette, France). The Dengue diagnostic procedure is described in the supplementary information.

Preparation of gold- and polystyrene-nanoparticle protein conjugates

Gold nanoparticle dispersions at 15% were adjusted to pH 8 with NaOH 0.01M and 30 μ L of an albumin solution at a concentration of 1 mg/mL was added to 0.3 mL of the gold dispersion. The

mixture was stirred for 30 min, and then, to remove the excess of proteins, it was centrifuged at 5000 rpm for 15 min at 4 °C. The clear supernatant was carefully removed, and the precipitated gold conjugates were resuspended in 400 µL of 0.01M phosphate buffer, pH 7.4, and stored at 4 °C. Gold nanoparticles conjugated with NS1 antibody was produced by following the same procedure. Albumin coated polystyrene nanoparticles were prepared as described by Linares and coauthors (Linares et al., 2012b).

Preparation of gold-polystyrene nanoparticle clusters

Colloidal gold and fluorescent particles, previously coated with albumin, were covalently bound by forming a peptide bond between albumin molecules using water-soluble carbodiimide to activate the surface carboxyl groups. Clusters were produced containing a gold:polystyrene nanoparticle ratio of 80:20, 60:40, 40:60, 20:80 (wt. %). For instance, to produce clusters with 80:20 (wt. %) of gold:PS, 300 µL of gold nanoparticles at 15% of solids was mixed with 562 µL of PS nanoparticles at 2% and incubated during 30 minutes in a shaker at RT. Both particles were dispersed in phosphate buffer 0.01M, pH 6. Subsequently, 2 mg of EDC was added to the suspension and incubated for 3 hours at RT. After, the suspension was centrifuged twice at 3000 rpm for 2 minutes and washed with 0.01M phosphate buffer, pH 7.4. The suspension was kept 48h hours in a black box and 600 µL were removed from the upper part of the dispersion (avoiding precipitates). The removed clusters were deposited on 1 mL of 1 mol/L sucrose solution in a centrifuge tube and centrifuged at 13000 rpm at 4°C for 45 min. An aliquot of 100 µL was removed from the top and the rest was divided in two aliquots. The aliquot on the upper part was used for the assay after washing steps with phosphate buffer 0.01M, pH 7.4.

Cluster functionalization with biomolecules

Clusters were conjugated to streptavidin and monoclonal NS1 Dengue antibody. An aliquot of 200 µL of cluster dispersion 80:20 gold:PS was added to 500 µL of a 0.5 mg/mL solution of protein dissolved in 0.01 phosphate buffer, pH 6. The suspension was incubated for 30 minutes at RT. Subsequently, 1 mg of EDC was added and mixed by vortexing and the pH was adjusted to 6.5 with diluted NaOH. The dispersion was incubated on a shaker for 3 hours at RT. To separate the protein-labeled clusters from unbound proteins, the suspension was centrifuged three times at 3000 rpm for 30 minutes at RT. The final suspension was kept in a phosphate buffer containing 1% BSA. A

scheme of the cluster preparation is shown in the Supplementary Information (SI-2).

Preparation of carbon black bioconjugates

Carbon black–streptavidin and carbon black–NS1 monoclonal antibodies covalently bound particle-conjugates were prepared according to Rayev and co-authors (Rayev et al., 2008) with modifications described by Linares and co-authors (Linares et al., 2012).

Strip tests and immunospot assay

Before setting up the strip test for clusters, all used membranes received different treatments: the sample pad was dipped into 0.01M phosphate buffer, pH 7.4, containing with 5% BSA and 0.05% Tween20 and dried for 2 hour at 60°C; the conjugate pad was previously immersed in 1mmol/L borate buffer, pH 9, with 10% of sucrose, and then clusters at 5% (w/v) was deposited and dried at RT; anti-NS1 protein antibody and biotinylated-albumin at a concentration of 1 mg/mL in 0.01 M phosphate buffer, pH 7.4, were spotted onto nitrocellulose to form the detection and control lines by using Dimatix printer from Fujifilm (Santa Clara, USA). BSA was biotinylated according to Guesdon and co-authors (1979). The detection pad was dried at RT; and the absorbent pad was used as received. Subsequently, all membranes were laminated on the backing card with an overlap of 2 mm between them. The membranes were cut at 4 mm wide. Serum samples were analyzed by adding 100 μ L on the sample pad. When the flow stopped, 100 μ L of 0.01 M phosphate buffer at pH 7.4 was added. The same buffer was used as blank. Analysis was performed after 25 min.

For the carbon black LFIA, the nitrocellulose was prepared as described for the LFIA. In this case, only the nitrocellulose and absorbent were laminated on the backing card. An aliquot of 50 μ L of serum sample was added to a microplate well and one extremity of the LFIA was immersed in it. After 10 minutes, the assay was positioned in another well containing 10 μ L of 2% streptavidin coated carbon black and 30 μ L of 2% anti-NS1 protein antibody coated carbon black. The test was removed again after 10 minutes and immersed in a well containing washing buffer for at least 5 minutes. The washing buffer contains 0.1 mol/L of borate buffer at pH 8.5, 1% (w/v) BSA, 1% (v/v) Tween20, 10% (w/v) sucrose and 0.9% (w/v) sodium chloride.

Atomic force microscopy (AFM) analysis

Particle dispersion was 10 min sonicated and rinsed on a glass slides resulting in a 0.01% dispersion of solid components. Particles were analyzed using an AFM (JPK Nanowizard 1, Berlin, Germany) in intermittent contact mode with 100 nm xy-scan range and 15 nm z-scan range and Si tips NSC 15 with 40 N/m spring constant from Mikromasch (Las Rozas de Madrid, Spain). Images were processed using JPK SPM Software (version 3.1 10/07) and Gwyddion 2.19.

Transmission electron microscopy

Images were also acquired using a Carl Zeiss Libra 120 kV transmission electron microscope (TEM) equipped with omega filter. Energy-filtered transmission electron microscopy (EFTEM) was used to obtain bright-field images with low chromatic aberration when the energy slit was selected to zero. Elemental map was acquired imaging inelastically scattered electrons by electron spectroscopy imaging (ESI). Energy selecting slits of 5eV were set at energy losses of carbon (303 eV). The images were recorded using a CCD camera and iTEM Universal TEM Imaging Platform. Samples were prepared by drying aqueous suspension droplets of gold and polystyrene nanoparticles, besides of clusters on carbon-coated parlodium films supported in 400-mesh copper grids (SPI supplies, West Chester, USA).

Results and Discussion

In order to produce a simple, fast, reliable and sensitive assay for Dengue fever detection, we developed a LFIA based on nanoparticle cluster as detection label. The clusters are formed by combining gold and fluorescent nanoparticles in a single structure. Gold and fluorescent nanoparticles were characterized using atomic force and transmission electron microscopy.

AFM non-contact image of the gold nanoparticles is depicted in Figure 1a and shows well dispersed particles with average diameter of 39 ± 5 nm. On the other hand, fluorescent nanoparticles (Figure 1b) demonstrate a slight aggregation likely occurred during the drying process, besides single particles. Dynamic light scattering measurements did not indicate aggregation with particles in solution (results are not shown). The particles have a mean diameter of 38 ± 8 nm. When AFM images are obtained for the clusters, bigger agglomerates are obtained in comparison to the fluorescent nanoparticles indicating successful coupling of nanoparticles.

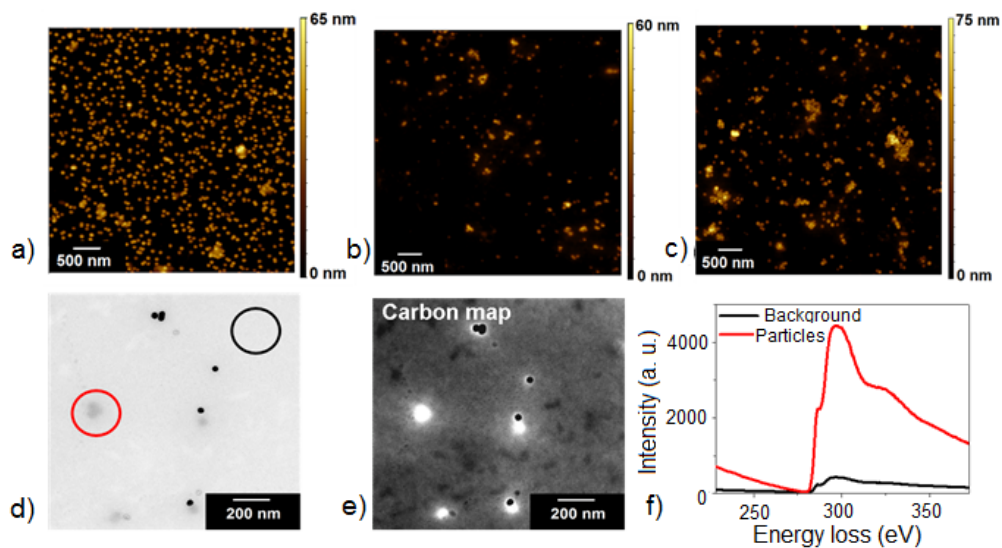


Figure 1. Microscopic characterization of nanoparticles and clusters. Atomic force microscopy images of (a) gold nanoparticles, (b) polystyrene nanoparticles and (c) cluster of gold and polystyrene nanoparticles. Transmission electron microscopy images of clusters (d) bright field, (e) 25 eV image and (f) carbon spectra of the background and the polystyrene particles.

TEM was used to provide more chemical information about the clusters. Bright field image and carbon map from the same area are depicted in the Figure 1d and 1e, respectively. Black particles in the bright field image are consisted by gold due to its higher atomic number in comparison to polystyrene nanoparticles. It is possible to observe small agglomerates consisted by gold-gold, gold-polystyrene and polystyrene-polystyrene. Carbon map indicates all materials containing carbon atoms in their composition with an intense bright signal. Hence, it demonstrates that there is organic material around the gold nanoparticles likely formed for biomolecules from the bioconjugation, as well as observed for the polystyrene nanoparticles evidenced by undefined borders around the particles. The agglomerates consisted by gold and polystyrene show their organic shell of biomolecules in contact, suggesting interactions between particles with different nature. The carbon map is confirmed by the electron energy loss spectroscopy (EELS), which shows the high intensity of carbon signal for the polystyrene nanoparticles in comparison to the parlodium background.

In order to achieve reproducible results, the cluster preparation needs to be controlled in terms of cluster composition. This task is not easy, but it is possible to have fractions that produce useful results. For that reason, they were centrifuged and two fractions were removed and analyzed. For these analyses, low energy loss TEM was used due to better resolution and less sample damage than in the high energy loss.

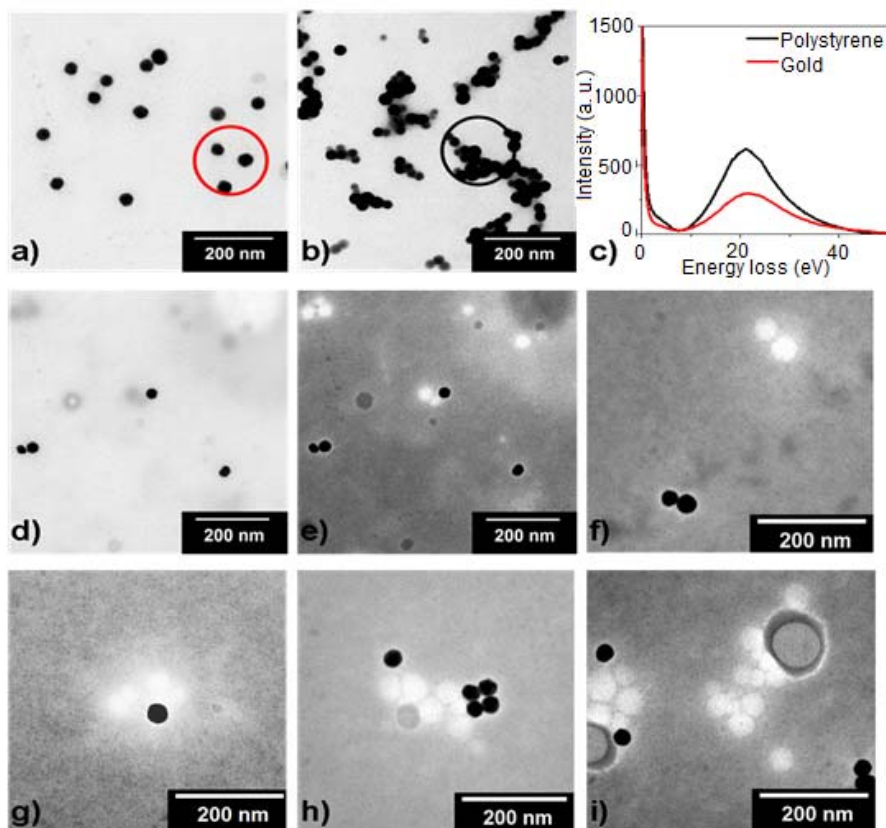


Figure 2. Transmission electron microscopy of clusters after separation. Bright field images of (a) gold nanoparticles, (b) polystyrene nanoparticles and (c) low energy loss spectra of gold and polystyrene nanoparticles. Bright field (d) and 25 eV energy loss (e) from the same area showing better resolution for polystyrene nanoparticles observation. Cluster images (e-g) at 25 eV of the fraction used in lateral flow tests and images (h and i) of the removed fraction of clusters.

Spectra from EELS were obtained for gold (Figure 2a) and polystyrene (Figure 2b) nanoparticles from the areas indicated in the images and are depicted in the Figure 2c. Polystyrene spectrum has higher intensity at the low energy loss than gold, and hence it will appear brighter in the energy image. The bright field (Figure 2d) and its respective image at 25 eV (Figure 2e) show clearer that polystyrene particles are poorly observed at bright field but better observed in the low energy loss image. The acquisition of maps at the low energy loss, also known as molecular maps (Linares et al., 2009, 2010) allows obtaining images with better resolution than bright field and fewer damages to the sample in comparison to high energy loss range. The first fraction (from up to down in the centrifuge tube) concentrates smaller clusters as observed in the Figures 2e-g, where it is possible to observe cluster up to 5 particles with mixed composition. The images from the second fraction indicate the presence of bigger clusters with variable composition and format. Tests with

each fraction showed that the first fraction produces better signal and reproducibility.

In order to use the immunoassay based on carbon black, the nanoparticles were analyzed by AFM and the image is shown in the Figure 3.

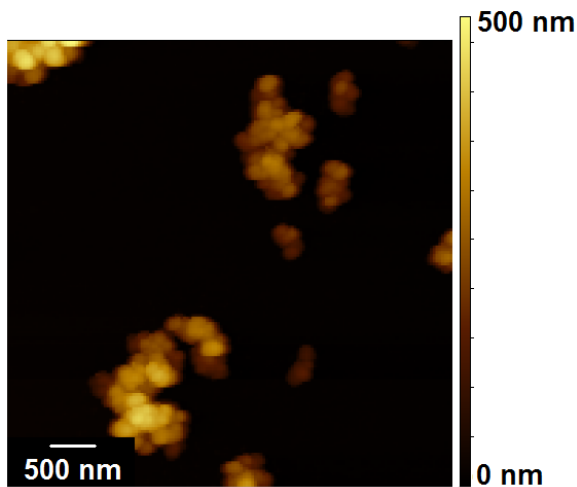


Figure 3. Microscopic characterization of carbon black. Atomic force microscopy non-contact image of carbon black.

It indicates that the carbon black nanoparticles tend to agglomerate in clusters from 400 to 2 μm . The particles have a mean diameter of 150 ± 48 nm. The microscopic characterization of the gold-nanoparticle and carbon black cluster are essential to understand and develop the immunoassays. A scheme of both assays is represented in the Figure 4.

The immunoassay with detection system based on carbon black is shown in the Figure 4a. The assay has a format of a LFIA, but one extremity is immersed in the serum sample. The test is formed by two parts: nitrocellulose membrane, where the test (monoclonal anti-NS1 antibody) and control (anti-streptavidin antibody) lines are deposited; and the absorbent pad, where the excess of liquid is absorbed and guarantee the flow of liquid through the membrane. Firstly the stick is immersed in the serum sample, and then the NS1 protein can flow through the sample and reaches the test line where it is trapped by the anti-NS1 capture antibody. The membrane does not only act as the support for the biomolecules, but also as a filter for the sample. Secondly the test is immersed in the carbon black dispersion and the anti-NS1 detection antibody previously immobilized on carbon black nanoparticles interact with the NS1 protein and forms the black line on the test, indicating the positive result for Dengue fever (Figure 4b).

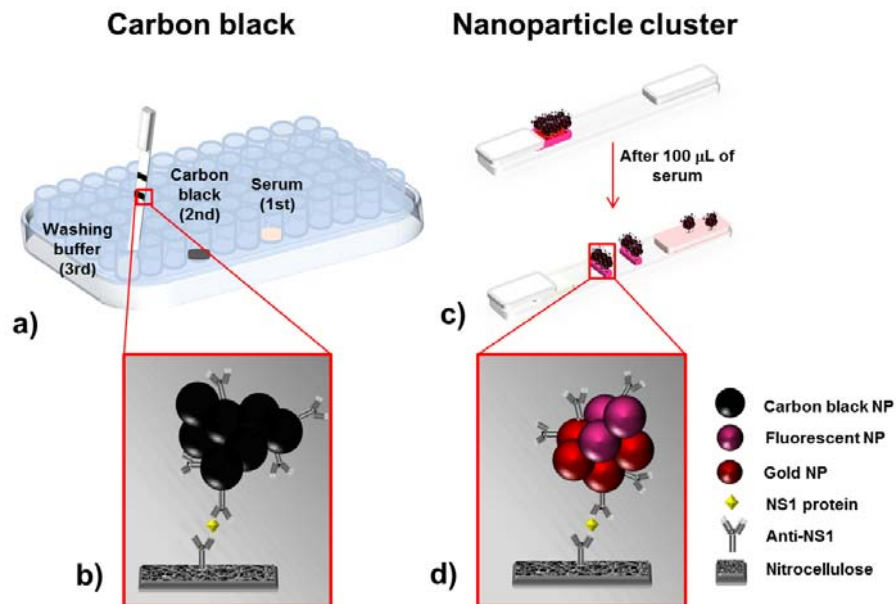


Figure 4. Scheme of the developed lateral flow immunoassays. LFIA based on carbon black (a) in a microplate after dipping one extremity in the serum, carbon black dispersion and washing buffer solution. Zoom of the test line (b) showing the carbon black agglomerate bound to the NS1 protein previously immobilized on the nitrocellulose membrane. Lateral flow immunoassay (c) based on gold-polystyrene nanoparticles clusters and zoom of the test line (d) showing the cluster bound to the NS1 protein previously immobilized on the nitrocellulose membrane.

In addition, streptavidin-carbon black conjugates added to the nanoparticles dispersion bind to the anti-streptavidin antibody and create the black control line, indicating a properly working test and positive control. The last step involves the immersion of the assay in a washing buffer, which is responsible for helping the flow of the carbon black nanoparticles, besides removing unspecific nanoparticles and cleaning the nitrocellulose membrane. It assures a better signal to noise ratio and lower detection limit. The LFIA with immersion in the sample format was preferred in relation to a conventional lateral flow test due to the microscopic characteristic of the carbon black agglomerates. As shown in the Figure 3, carbon black forms agglomerates up to 2 μm of mean diameter and this agglomeration is even intensified in the porous nitrocellulose membrane. Hence, this test avoids drying the conjugates on the membrane and provides better performance.

Lateral flow immunoassay format was chosen as result of the gold-fluorescent cluster structure. This test consists of four parts: the first membrane is the sample pad where the sample is applied and filtered; then the liquid flows to the second membrane and the protein NS1 binds to the anti-NS1 protein detection antibody previously immobilized on the cluster surface; the cluster-protein complexes flow through the nitrocellulose membrane and bind to the anti-NS1 capture antibody, forming the red-fluorescent line indicative of a serum sample positive for Dengue fever (Figure 4d);

the last pad is an absorbent membrane. The control line is also constituted of streptavidin coated cluster bound to biotin-albumin on the nitrocellulose membrane.

In order to evaluate the performance and detection limit, the assays based on clusters, gold and carbon black were tested with different concentrations of NS1 protein and the pictures are shown in the Figure 5.

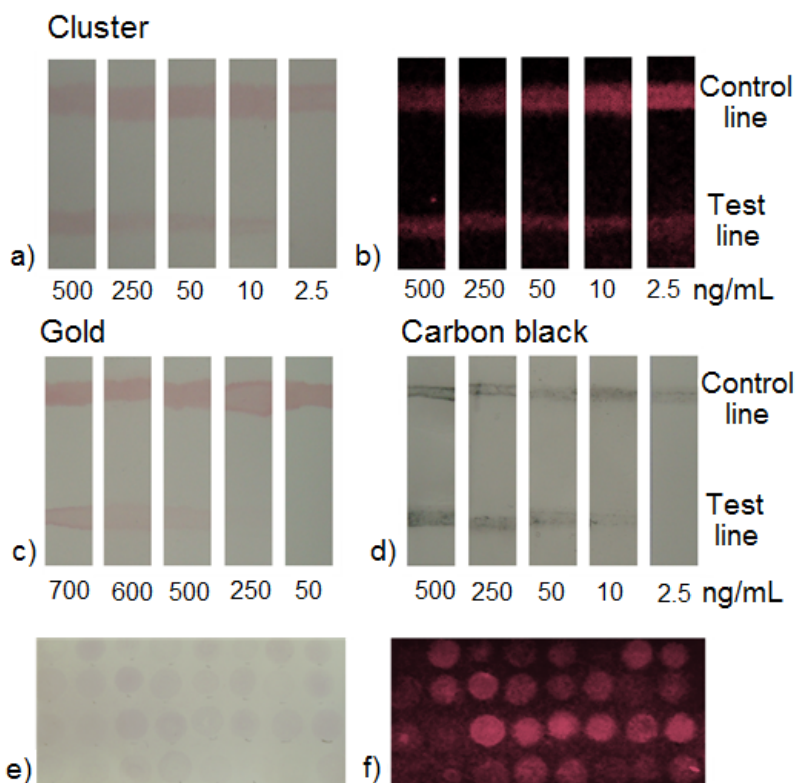


Figure 5. Lateral flow immunoassay and immunospot assay for Dengue virus NS1 protein detection. Pictures of the LFIA based on clusters (a) under UV light (b), gold nanoparticles (c) and carbon black (d). Immunospot assay based on clusters (e) under UV light (f).

LFIA based on clusters (Figure 5a) shows a visible signal up to 10 ng/mL, but when the strip tests are under UV light, the detection limit achieves lower values, up to 2.5 ng/mL. In order to compare the clustering effect on the detection limit, LFIA based on gold nanoparticles were built and depicted in the Figure 5c. It shows a visible test line until 500 ng/mL, once the signal at 250 ng/mL is barely observable. On the other hand, carbon black assay (Figure 5d) demonstrates a detection limit, 10 ng/mL, superior to gold nanoparticles, but comparable with the visible signal of the clusters. Accordingly, gold-fluorescent nanoparticles cluster provides comparable sensitivity to one of the best colored labels, carbon black, and even shows additional sensitivity provided by the

fluorescent nanoparticles. Thus, if the colored sign is slightly positive, indicating uncertain result, a lamp/LED can be used to excite the fluorescent particles and the fluorophores will emit in the visible spectrum. Additional results for an immunospot assay based on clusters are shown in the Figure 5e and 5f. A panel with 48 samples of Dengue infected patients were deposited on nitrocellulose and detected with gold-fluorescent nanoparticles cluster. The pictures indicate that the fluorescent nanoparticles provide an additional signal that contributes to a more reliable assay. Based on the exposed results, nanoparticle clusters represent a powerful option to overcome sensitivity limitations of LFIA.

Conclusion

The detection system based on gold-fluorescent nanoparticles cluster for LFIA provides an enhanced visual signal, because gold nanoparticles are concentrated in a cluster with NS1 protein antibodies to recognize the protein, instead of only a single colored particle per analyte. Furthermore, the signal is enhanced by combining colored particles with fluorescent beads. When the colored spot is slightly positive, providing an uncertain result, an UV lamp or LED can be used to excite the fluorescent particles and the fluorophores will emit in the visible spectrum. Similar to the colored particles, the cluster concentrates fluorescent beads, increasing the fluorescence emission signal. This set up allows improving the detection limit in comparison to current labels, which are usually based on single colored nanoparticles or carbon black.

Acknowledgement

The authors would like to thank the Sao Paulo Institute of Tropical Medicine for kindly providing the serum panel, especially Lucy Santos Vilas Boas and Clara Felix for the sample organization. We also thank Prof. Axel K. Walch for microscopy apparatus. EML acknowledges the fellowship from the International Doctorate Program NanoBioTechnology (IDK-NBT) funded by the Elite Network of Bavaria (ENB). This work was supported by the cluster of excellence Nano Initiative Munich (NIM), the Center of Nanoscience (CeNS), DAAD and CAPES.

References

- Allwinn, R., 2011. *Med. Microbiol. Immunol.*, 200, 155–159.
- Blažková, M., Mičková-Holubová, B., Rauch, P., Fukal, L. 2009. *Biosens. Bioelectron.* 25, 753–758.
- Fisher, M., Atiya-Nasagi, Y., Simon, I., Gordin, M., Mechaly, A., Yitzhaki, S. 2009. *Lett. Appl. Microbiol.* 48, 413–418.
- Bai, Y., Tian, C., Wei, X., Wang, Y., Wang, D., Shi, X. 2012. *RSC Advances* 2, 1778–1781.
- Blažková, M., Javůrková, B., Fukal, L., Rauch, P. 2011. *Biosens. Bioelectron.* 26, 2828–2834.
- Drexler, J. F., Helmer, A., Kirberg, H., Reber, U., Panning, M., Müller, M., Höfling, K., Matz, B., Drosten, C., Eis-Hübinger, A. M. 2009. *Emerging Infect. Dis.* 15, 1662–1664.
- Fu, E., Liang, T., Houghtaling, J., Ramachandran, S., Ramsey, S. A., Lutz, B., Yager, P. 2011. *Anal. Chem.* 83, 7941–7946.
- Gandhi, S., Caplash, N., Sharma, P., Suri, C. R. 2009. *Biosens. Bioelectron.* 25, 502–505.
- Gordon, J., Michel, G. 2008. *Clin. Chem.* 54, 1250–1251.
- Guesdon, J.L., Ternynck, T., Avrameas, S., 1979. *J. Histochem. Cytochem.* 27, 1131–1139.
- Ho, J. A. A., Zeng, S. C., Tseng, W. H., Lin, Y. J., Chen, C. H. 2008. *Anal. Bioanal. Chem.* 391, 479–485.
- Horton, J. K., Swinburne, S., O’Sullivan, M. J. J. 1991. *Immunol. Methods* 140, 131–134.
- Kalogianni, D. P., Boutsika, L. M., Kouremenou, P. G., Christopoulos, T. K., Ioannou, P. C. 2011. *Anal. Bioanal. Chem.* 400, 1145–1152.
- Kolossova, A. Y., Sibanda, L., Frederic, D., Janet, L., Etienne, D., Peteghem, C. V., De Saeger, S. 2008. *Anal. Chim. Acta* 616, 235–244.
- Khreich, N., Lamourette, P., Boutal, H., Deveilliers, K., Creminon, C., Vollad, H. 2008. *Anal. Biochem.* 377, 182–188.
- Lai, W., Fung, D. Y. C., Xu, Y., Liu, R., Xiong, Y. 2009. *Food Control* 20, 791–795.
- Linares, E.M., Trombeta, L.P., Moreira, A.B., Sotomayor, P., Kubota, L.T., 2007. *Anal. Lett.* 40, 573–583.
- Linares, E.M., Leite, C.A.P., Valadares, L.F., Silva, C.A., Rezende, C.A., Galembeck, F. 2009. *Anal. Chem.* 81, 2317–2324.
- Linares, E.M., Rippel, M.M., Galembeck, F., 2010. *ACS Appl. Mater. Interfaces* 2, 3648–3653.
- ^aLinares, E.M., Kubota, L.T., Michaelis, J., Thalhammer, S., 2012. *J. Immunol. Methods* 375, 264–270.
- ^bLinares, E. M., Pannuti, C., S., Kubota, L. T., Thalhammer, S. 2012. *Biosens. Bioelectron.*, *in press*.
- Ngom, B., Guo, Y., Wang, X., Bi, D. 2010. *Anal. Bioanal. Chem.* 397, 1113–1135.
- Parolo, C., Escosura-Muñiz, A., Merkoçi, A. 2012. *Biosens. Bioelectron.*, *in press*.
- Pathak, S., Choi, S., Arnheim, N., Thompson, M. 2001. *J. Am. Chem. Soc.* 123, 4103–4104.
- Posthuma-Trumpie, G.A., Korf, J., Amerongen, A., 2009. *Anal. Bioanal. Chem.* 393, 569–582.
- Posthuma-Trumpie, G. A., Wichers, J. H., Koets, M., Berendsen, L. B. J. M., van Amerongen, A. 2012. *Anal. Bioanal. Chem.* 402, 593–600.

- Rayev, M., Shmagel, K., 2008. *J. Immunol. Methods* 336, 9–15.
- Takanashi, S., Okame, M., Shiota, T., Takagi, M., Yagyū, F., Tung, P. G., Nishimura, S., Katsumata, N., Igarashi, T., Okitsu, S., Ushijima, H. 2008. *J. Virol. Methods* 148, 1–8.
- Tang, D., Saucedo, J. C., Lin, Z., Ott, S., Basova, E., Goryacheva, I., Biselli, S., Lin, J., Niessner, R., Knopp, D. 2009. *Biosens. Bioelectron.* 25, 514–518.
- van Dommelen, L., van Tiel, F. H., Ouburg, S., Brouwers, E. E. H. G., Terporten, P. H. W., Savelkoul, P. H. M., Morr , S. A., Bruggeman, C. A., Hoebe, C. J. P. A. 2010. *Sex. Transm. Infect.* 86, 355–359.
- Vasoo, S., Stevens, J., Singh, K. 2009. *Clin. Infect. Dis.* 49, 1090–1093.
- Skidmore, S. 2010. *Sex. Transm. Infect.* 86, 330.
- Zhang, D., Li, P., Zhang, Q., Zhang, W. 2011. *Biosens. Bioelectron.* 26, 2877–2882.
- Wagstaff, A. 2002. *Bulletin of the World Health Organization* 80, 97–105.

Web references:

- http://whqlibdoc.who.int/publications/2010/9789241564090_eng.pdf (last access date: 7/2012). *World Health Organization*, 2010.
- <http://www.who.int/mediacentre/factsheets/fs117/en/> (last access date: 7/2012). *World Health Organization*, 2012. Fact Sheet 117.

Supplementary Information

Enhanced lateral flow immunoassay based on gold and fluorescent particle clusters for Dengue detection: comparison with gold and carbon black labels

Elisângela M. Linares^a, Claudio S. Pannuti^b and Stefan Thalhammer^{a,}*

^aHelmholtz Zentrum München - German Research Center for Environmental Health, Ingolstädter Landstrasse 1, 85764 Neuherberg, Germany; elisangela.linares@helmholtz-muenchen.de, stefan.thalhammer@helmholtz-muenchen.de;

^bLaboratory of Virology, Instituto de Medicina Tropical de São Paulo e Faculdade de Medicina, Universidade de São Paulo. Eneas de Carvalho Aguiar 470, 05403-000, São Paulo, Brazil; cpannuti@usp.br

CORRESPONDING AUTHOR FOOTNOTE

Stefan Thalhammer, Helmholtz Zentrum München, P.O. Box 6154 – 13084-971 – München – Germany. Phone: +49 089/3187-2893. Fax: +49 089/3187-3323. stefan.thalhammer@helmholtz-muenchen.de

List of contents

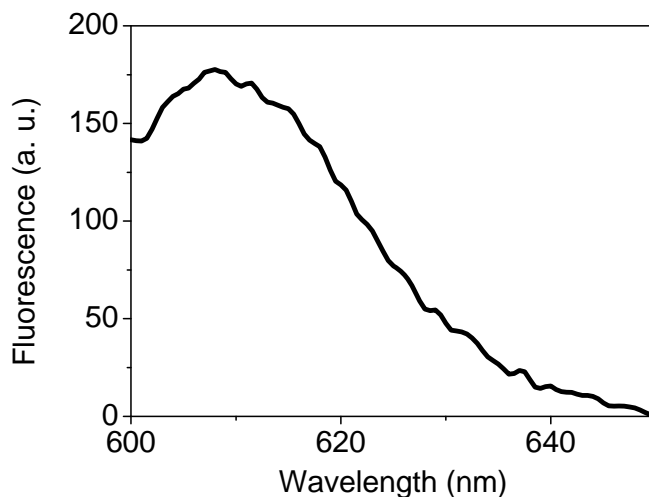
SI1 – Fluorescence spectrum of the polystyrene particles

SI2 – Scheme of preparation and bioconjugation of gold/fluorescent nanoparticle clusters: (a) reaction between the carboxylated nanoparticles and albumin and (b) interaction among the albumin coated particles to form the cluster.

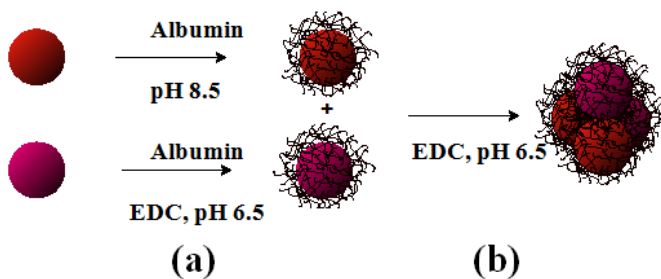
SI3 – Dimensions of a conventional lateral flow immunoassay and for a lateral flow immunoassay with immersion in the sample.

SI4 – Scheme of the immunospot for NS1 protein detection based on gold-polystyrene nanoparticle cluster.

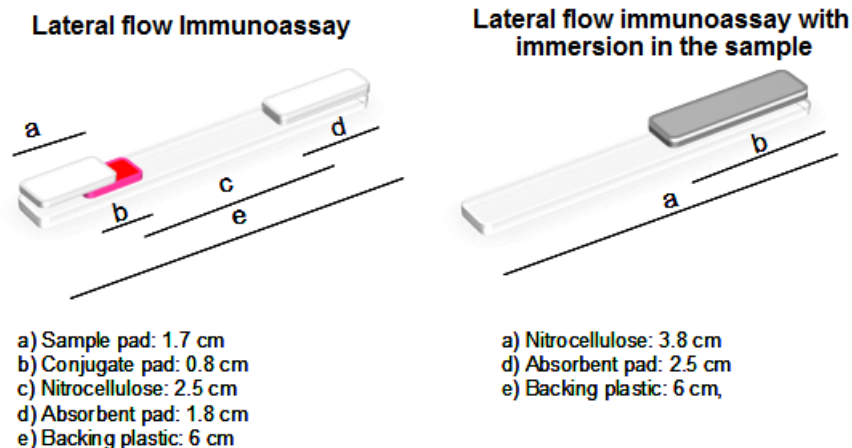
SI1 – Fluorescence spectrum of the polystyrene particles



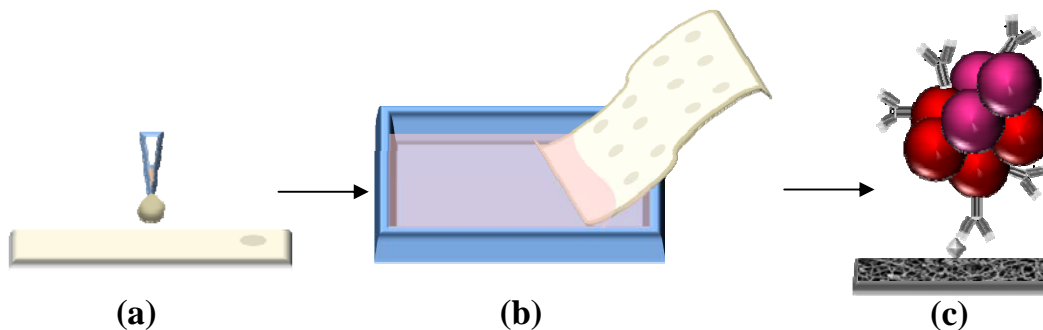
SI2 – Scheme of preparation and bioconjugation of gold/fluorescent nanoparticle clusters: (a) reaction between the carboxylated nanoparticles and albumin and (b) interaction among the albumin coated particles to form the cluster.



SI3 – Dimensions of a conventional lateral flow immunoassay and for a lateral flow immunoassay with immersion in the sample.



SI4 – Scheme of the immunospot for NS1 protein detection based on gold-polystyrene nanoparticle cluster.



For multiple tests, 4 μL of serum (a) was deposited on the nitrocellulose membrane (7cm x 10cm) with 15 mm spacing between each spot to avoid contamination and checking the alignment between them to fit on the wells of an ELISA microplate. This sample volume was the minimum volume necessary to observe a clear result. After 10 minutes, a blocking solution containing BSA 3% in phosphate buffer 0.01 mol/L, pH 7.4 was added to cover the entire membrane for 15 minutes at RT. Subsequently, the blocking solution was removed and 3 mL fluorescent conjugates 1% in phosphate buffer 0.01 mol/L, pH 7.4 was added and incubated for 30 minutes (b). Scheme of interaction is shown in (c).

Conclusion and outlook

In order to enhance the detection limit and applicability of immunoassays for uses in impoverished environments, different nanostructures were evaluated and tested as labels for Dengue fever infection detection. An increase in sensitivity can only be achieved by changing the detection label, if the best available antibody and the best combination of materials are already being used. The detection limits and signal intensity were compared among the four most used labels: gold, silver enhanced gold, blue latex bead and carbon black nanoparticles. The results indicate carbon black as a suitable colorimetric label for lateral flow immunoassays with a detection limit fifty times lower than obtained with standard gold nanoparticles. This higher sensitivity motivated its use to improve strip test detection.

An immunoassay for multiple analyses in epidemic periods was developed as an alternative for the time-consuming ELISA procedure. The assay combines principles of ELISPOT and FLISA and uses nitrocellulose as support membrane and commercial fluorescent nanoparticles as labels. This immunospotting assay shows detection limits hundred times lower than standard gold nanoparticles for Dengue fever detection, besides rapidity and lower cost in comparison to ELISA.

The current problem of polymer particle agglomeration in LFIA and ISA limits the label performance, and consequently affects the sensitivity, reproducibility and reliability. The one-step synthesis of luminescent $[\text{Ru}(4,4'\text{-dicarboxylate-}2,2'\text{-bpy})_3]$ labeled poly[styrene-co-(2-hydroxyethyl methacrylate)] core-shell particles was a further step to develop low agglomeration structures that can be applied as labels in immunoassays. These particles provide more homogeneous visual signal in comparison to commercial polymer particles based on polystyrene.

Finally, a label that combines the ease of optical visualization of gold nanoparticles with the high sensitivity of fluorescent nanoparticles was developed. The cluster formed by these nanostructures provides an enhanced visual signal, because gold nanoparticles are concentrated in a single structure and an additional enhancement is offered by fluorescent beads. When optical detection finds a sensitivity limitation, providing an uncertain result, an UV lamp or LED can be used to excite the fluorescent particles and to show a signal in the visible spectrum. This set up allows improving the detection limits by two hundred times in comparison to current assays based on gold nanoparticles.

The combination of different detection systems and principles of different assays can produce fast and high sensitive tests, which are suitable for impoverished environments and epidemic areas. In terms of applicability for early disease detection, these improvements provide immunoassays

with sensitivity enough to diagnose a patient with Dengue fever on the first day of infection, which is crucial in severe cases. I therefore conclude that sensitivity limitations can be overcome by using different approaches suggested in this thesis.

A careful screening of detection labels should be performed as a necessary step during an immunoassay development in order to enhance the detection limit in a final test system. These results can facilitate the development of immunoassays in terms of the suitable label choice in order to achieve a necessary sensitivity.

Drawback of the investigated labels

Despite improvements of immunoassay sensitivity described in this thesis, there are a number of issues that require more experiments and further development.

Carbon black particles are very promising as cheap and sensitive labels (Chapter 2 and 5); however the particles agglomerate in the conjugate membrane during the drying process and remain agglomerated during sample flow. It avoids the use of conventional lateral flow immunoassay set up and requires additional steps during operation in the field. Different carbon black particle sources and chemical treatment (surfactants, polymers etc) were used to overcome the problem, but the overall chemical adjust was disturbed and additional problems were created. For example, surfactants solved partially the agglomeration problem, but they were responsible for spreading the test and control lines. As a result, the antibodies in the lines were not covalently bound to the membrane, and therefore were detached from the nitrocellulose during the sample flow. Further experiments could be performed to overcome the agglomeration problem, including more detailed screening or controlled production of carbon black particles and use of different sets of conjugate and reaction membranes. A commercial system can be even developed using more than one step, but the design and the operation should remain simple, user-friendly and cheaper, as suggested by the WHO.

High sensitivity, rapidity of analysis and detection equipment versatility were obtained with fluorescent particles as labels for the immunospot assay (Chapter 3). Although it showed many advantages in comparison to conventional ELISA or FLISA, the use of equipment is not favorable when the assay must be performed in laboratories with low resources. Therefore, assays based on a UV-lamp or a LED are cheap and appropriate alternative. In this work, an UVB lamp was used to excite the fluorophores with high intensity emission based on the usual available equipment in impoverished clinical laboratories. The lamp emission does not peak on the fluorophore excitation

maximum, only exciting it in the tail excitation band. Further experiments with particles containing fluorophores with larger Stokes shift could allow getting closer to the fluorophore excitation maximum and consequently reducing the detection limit (200 ng/mL of NS1 protein based on the UVB) and enhancing the sensitivity (59%) based on the UVB (*See below Future general improvements for LFIA and ISA*).

PSHEMA particles (Chapter 4) demonstrated good performance for paper based immunoassays. The particles have very important characteristics as a diagnostic tool label: they show low agglomeration and ease of bioconjugation, they are monodisperse and surfactant free. However, the detection limit obtained with the particles is inferior to the commercial luminescent particles. Further experiments should be performed in order to produce higher luminescent particles by increasing the HEMA/styrene ratio in the reaction allowing more Ru complex incorporation, or use of soaked hydrophobic dye as emitter or incorporation of fluorophores with higher quantum yield.

Gold-fluorescent nanoparticle clusters (Chapter 5) showed lower detection limit in comparison to all other tested labels. The use of two particle kinds combines the practical colorimetric detection with high sensitivity from fluorescence. Further experiments can be focused on more precise composition control and stability over time.

Future general improvements for LFIA and ISA

In addition to the progress achieved with the presented results in this work, current available technologies used in other fields can be used to improve paper based immunoassays and lead them to a more reliable tool for point-of-care testing.

Following the arrangement of these assays, several limitations have been described about contaminants that cross-react with the detection molecules and show false-positive results. To avoid this interference, the sample should receive a pre-treatment to remove these compounds and this step must be incorporated in the assay for keeping simplicity. Therefore, technologies available for polymer reinforcement with coupling reaction of glass fibers into polymer matrix can be very useful for use as sample pad in LFIA/ISA. The sample pad is responsible for filtering undesired material from the sample. Currently this step is restricted to solid filtering, but it can be extended to a chemical trap by changing the chemical functionalities of the membrane. Specific proteins can be covalently bound to the membrane, removing undesired compounds.

The next challenge is associated with the labels used in the detection systems. The label choice is crucial to the assay sensitivity, as extensively discussed in this thesis, and requires a specific

knowledge of the sample and the necessary detection limit. Fluorescent labels incorporated in particles are very promising for high sensitive tests, but the fluorophores must be carefully chosen to provide high emission and to avoid interference with the sample and membrane fluorescence (background). For unskilled operators, misinterpretation may happen if the person is not able to separate the sample signal from the background signal, which has different emission wavelength (color). Chemiluminescence is very promising in terms of sensitivity and no background interference. Another interesting option is the technology of near infrared upconversion fluorescence resonance energy transfer. This process allows exciting a compound at the infrared range and reading out at the visible range, eliminating background interference.

Although numerous methods are very sensitive, the use of enzymes to catalyze reaction with colored products is still the most used sensitive detection method for immunoassays (e.g. ELISA). On the other hand, its use in point-of-care immunoassays is limited due to the harsh environmental conditions where the tests must be operated. For example, Dengue endemic regions are normally located in tropical regions that have high temperature, exceeding 30°C. The storage and operational conditions can affect the enzyme structure and activity. Therefore, the stabilization of enzymes can extend their application to field uses. A recent collaboration with Prof. Thomas Bein's group (Department of Chemistry, Ludwig Maximilians Universität) aims to use whole enzymes or enzyme active sites incorporated in mesoporous silica particle as label for LFIA. Up to date results promise to overcome enzyme stability problems and even enhance the sensitivity of immunoassays. The "synthetic enzymes" have the potential to combine the high sensitivity of ELISA with LFIA advantages for reliable field analysis.

Molecule stability is not only a challenge for enzymes but it is also an issue for antibodies. Depending on the environment conditions, antibodies show inappropriate performance, disabling the test. Hence, plastic antibodies can be a solution for LFIA that must be operated in harsh conditions. The technology uses the principles of molecular imprinting polymer, where polymerization of monomers is performed in the analyte presence. Complementary functional monomers polymerize around the analyte and create a template of the molecule in the polymer matrix, after its extraction. This mimics an antibody structure, but involved in a very robust polymer matrix. The polymers can be produced as colloidal structures with dye incorporation and used as labels for LFIA. Plastic antibodies increase the stability and even reduce the assay cost.

In cases where the price is the bottle neck for LFIA application, the costs from the most expensive part, the antibodies, should be reduced. Besides plastic antibodies, immunoglobulins produced by plants can be very promising. The technology is still in the beginning, but it shows

high potential for cheap antibody production.

Future prospects for Dengue fever diagnostics

Early Dengue fever detection is now possible given the results presented in this work. Although NS1 protein detection provides early disease diagnosis, it is only sensitive in the early phase of infection and therefore it is not suitable for sole use in dengue-endemic settings where late clinical presentations may occur. Hence, a complete immunoassay for Dengue fever diagnosis should combine NS1 protein and IgM antibody detection. Patients with secondary or later dengue infections are considered to have an increased risk of the more severe forms of the disease. The accurate detection of primary and secondary infection at presentation to a clinical facility may become a promising patient management tool. It is possible to differentiate primary and secondary dengue virus infections using the following criteria: (1) acute primary dengue virus infection defined as an IgM-positive and IgG-negative (IgM+/IgG-) result and (2) acute secondary dengue virus infection defined as IgM-positive and IgG-positive (IgM+/IgG+) or IgM-negative and IgG-positive (IgM-/IgG+) results. More precise results can be obtained by semi-quantitative IgM/IgG ratio detection. A simple colored scale bar could provide the necessary quantification. Based on that, a sensitive NS1 protein detection system combined with semi quantitative detection of IgM/IgG ratio is a powerful tool for point-of-care testing for Dengue fever diagnosis.

To take evidence based decisions about the usefulness of this test in clinical settings, it is recommended to assess its performance in consecutive patients with potential dengue infection under routine conditions at health centers with different levels of complexity. Further studies are required to assess the potential impact of implementing early laboratory diagnosis of dengue in terms of prognosis and cost-effectiveness. In order to further strengthen the current diagnostic accuracy estimates, prospective recruitment studies are required in different dengue-endemic locations, where there are variations in dengue infection status, days of illness, and prior to presentation. Further studies are also required to examine some of the more practical aspects of dengue immunoassay performance that includes the influence of operator training, interoperator variation, and ease of use of the assays.

List of abbreviations

A: absorbance

A': cross sectional area perpendicular to flow

Ab: antibody

AFM: atomic force microscopy

Ag: antigen

ASSURED: Affordable, Sensitive, Specific, User-friendly, Rapid and Robust, Equipment-free, Delivered to those who need it.

b: path length

Bpy: bipyridine

c: concentration

DF: dengue fever

DHF: dengue hemorrhagic fever

DL: detection limit

DV: dengue virus

E: electronic energy state

EDC: 1-ethyl-3-(3-dimethylaminopropyl)carbodiimide

EFTEM: energy filtered electron microscopy

ELISA: enzyme linked immunosorbent assay

ELISPOT: enzyme linked immunospotting

ESI: electron spectroscopy imaging

Fab: antigen-binding fragment

Fc: crystallizable fragment

FITC: fluorescein isothiocyanate

FLISA: fluorophore linked immunosorbent assay

GS: ground state

Ig: immunoglobulin

IgA: immunoglobulin type A

IgD: immunoglobulin type D

IgE: immunoglobulin type E

IgG: immunoglobulin type G

IgM: immunoglobulin type M

ISA: immunospot assay

List of abbreviations

ISC: intersystem crossing

K: permeability

K' : constant that depends on the efficiency quantum of the fluophore

k: rate constant

L: liquid height

LED: light emitting diode

LF: ligand field

LFIA: lateral flow immunoassay

LSPR: localized surface Plasmon resonance

mAb: monoclonal antibody

NHS: N-hydroxysuccinimide

NS1 protein: non-structural protein 1

NP: nanoparticles

P: light beam

PEG: polyethylene glycol

PSHEMA: poly(styrene-co-2-hydroxyethylmethacrylate)

PSHEMA-Ru: poly(styrene-co-2-hydroxyethylmethacrylate) containing ruthenium complex PVA: polyvinylalcohol

PVP: polyvinylpyrrolidone

Q: volumetric flow rate

R: Ab-Ag complex

r: effective pore radius

RT-PCR: real-time polymerase chain reaction

T: transmittance

TEM: transmission electron microscopy

TRIS: tris(hydroxymethyl)aminomethane

UV: ultraviolet

WHO: World Health Organization

ΔP : pressure gradient

ϵ : molar absorptivity

γ : surface tension

η : solution viscosity

θ : contact angle

Curriculum Vitae

Personal details

Name: Elisângela Moura Linares

Date and place of birth: 1.21.1985 in Campinas, São Paulo, Brazil

Nationality: Brazilian

Email: elis_linares@yahoo.com.br

Education

- 2009-2012 PhD candidate in Chemistry, Ludwig-Maximilians University, Munich, Germany
Department of Physical-Chemistry, Prof. Jens Michaelis
Helmholtz Zentrum Munich, PD. Dr. Stefan Thalhammer
Thesis: “Nanostructured labels for enhanced paper based assays”
(Defense: January 2013)
- 2007-2009 Master in Chemistry, University of Campinas, Brazil
Department of Physical-Chemistry, Prof. Fernando Galembeck
Dissertation: “Microstructural characterization of latex blend films”
- 2007-2008 Bachelor in Technological Chemistry, University of Campinas, Brazil
- 2003-2006 Bachelor in Chemistry, University of Campinas, Campinas, Brazil

Fellowships

- 2010-2012 German Academic Exchange Service (DAAD)
- 2009-2012 Elite Network of Bavaria, IDK-NanoBioTechnology (IDK-NBT)
- 2007-2009 São Paulo Research Foundation (FAPESP) – Master student
- 2004-2006 São Paulo Research Foundation (FAPESP) – Bachelor student

Courses and Internships

- 7-8.2008 Summer school, Nanosystem Initiative Munich (NIM), Prof. Hermann Gaub, Ludwig Maximilian Universität, Munich, Germany
- 2007 Industry internship Rhodia Poyamide and Specialties, Paulínia, Brazil
- 2003-2006 Two undergraduate research projects: “Development of a spot test for salicylate determination” and “Characterization of nanocomposites of rubber and clay using atomic force microscopies”
- 2001-2002 Technical course in Biochemistry, Campinas, Brazil

Publications

- (1) LINARES, E. M.; Pannuti, C.S.; Kubota, L.T.; Thalhammer, S. "Immunospot assay based on fluorescent nanoparticles for Dengue fever detection", *Biosensors and Bioelectronics* **2012**, in press.
- (2) LINARES, E. M.; Kubota, L. T.; Michaelis, J., Thalhammer, S. "Enhancement of the detection limit for lateral flow immunoassays: evaluation and comparison of bioconjugates", *Journal of Immunological Methods* **2012**, 375, 264.
- (3) Rippel, M. M.; LINARES, E. M.; Bragança, F. C.; Valadares, L. F.; Galembeck, F. "Electrostatic adhesion: an effective mechanism for rubber adhesion and blending", *Journal of Adhesion Science and Technology* **2012**, 26, 767.
- (4) LINARES, E. M.; Jannuzzi, S. A. V.; Galembeck, F. "Electrostatic contributions in the increased compatibility of polymer blends", *Langmuir* **2011**, 27, 15199.
- (5) LINARES, E. M.; Rippel, M. M.; Galembeck, F. "Clay platelet partition within polymer latex blend films: an EFTEM study", *Applied Materials and Interfaces* **2010**, 2, 3648.
- (6) LINARES, E. M.; Valadares, L. F.; Silva, C. A.; Rezende, C. A.; Galembeck, F. "Molecular mapping by low-loss-energy EFTEM imaging", *Analytical Chemistry* **2009**, 81, 2317.
- (7) Valadares, L. F.; LINARES, E. M.; Braganca, F. C.; Galembeck, F. "Electrostatic adhesion of nanosized particles: the cohesive role of water", *Journal of Physical Chemistry C* **2008**, 112, 8534.
- (8) LINARES, E. M.; Trombeta, L. P.; Moreira, A. B.; Sotomayor, P.; Kubota, L. T. "A fluorescence spot test for salicylate determination", *Analytical Letters* **2007**, 40, 573.

Submitted:

- (9) LINARES, E. M.; Formiga, A.; Galembeck, F.; Kubota, L. T.; Thalhammer, S.: Core-shell polymer nanoparticles containing Ruthenium complex: bioconjugates and bio- applications.
- (10) Miranda, B. S.; LINARES, E. M.; Thalhammer, S.; Kubota, L. T. Development of a disposable and highly sensitive paper-based immunosensor for early diagnosis of soybean rust.

In preparation:

- (11) LINARES, E. M.; Pannuti, C.S.; Thalhammer, S. Enhanced lateral flow immunoassay based on gold and fluorescent particle cluster for Dengue fever detection, *article* (ready).
- (12) Correa, C. C.; LINARES, E. M.; Thalhammer, S.; Kubota, L. T. Development of a rapid test for troponin T detection based on enzyme coated gold nanoparticles, *article*.
- (13) LINARES, E. M.; Thalhammer, S Low energy loss transmission electron microscopy for bioconjugate characterization, *letter*.

Patent (submitted)

Rapid test detection system based on nanoparticle clusters.

Appendix

A1: Invention disclosure, Helmholtz Zentrum München.

Helmholtz Zentrum München · Postfach 11 29 · 85758 Neuherberg

Dr. Wolfgang Nagel

Innovationsmanagement

Telefon +49(0) 89 3187-1210
Telefax +49(0)89 3187-4000
wolfgang.nagel@helmholtz-muenchen.de

21.09.12
INNO/WN

Erfindungsmeldung „Rapid test detection system based on particle clusters“

Sehr geehrte Damen und Herren,

hiermit wird bestätigt, dass die oben genannte Erfindungsmeldung in der Abteilung Innovationsmanagement beim Helmholtz Zentrum München eingegangen ist und das Aktenzeichen PLA12A19 erhalten hat (Eingangsstempel: 13.9.2012). Als Erfinder sind PD Dr. Stefan Thalhammer und Frau Elisangela Linares genannt. Die vorliegende Erfindungsmeldung basiert dabei auf den Arbeiten zur Dissertation von Frau Linares. Derzeit wird geprüft, ob die uns vorliegende Erfindung zum Schutzrecht angemeldet wird. Bis zur Einreichung beim Patentamt darf jedoch der Inhalt der vorliegenden Dissertation auf keinen Fall in die Öffentlichkeit gelangen.

Hiermit möchte ich Sie bitten, die Dissertations-Unterlagen als „vertraulich“ zu behandeln und vorerst unter strengem Verschluss zu halten, um eine potentielle Patentierung nicht zu gefährden.

Für Fragen stehe ich gerne zur Verfügung.

Mit den besten Grüßen

i.A.

Dr. Wolfgang Nagel
Innovationsmanagement

Helmholtz Zentrum München
Deutsches Forschungszentrum für
Gesundheit und Umwelt (GmbH)
Ingolstädter Landstraße 1
85764 Neuherberg
Telefon +49 (0) 89 3187 (0)
Telefax +49 (0) 89 318733 22

info@helmholtz-muenchen.de
www.helmholtz-muenchen.de

Aufsichtsratsvorsitzende:
MinDir'in Bärbel Brumme-Bothe

Geschäftsführer:
Prof. Dr. Günther Wess
Dr. Nikolaus Blum

Registergericht:
Amtsgericht München HRB 6466
USt-IdNr. DE 129521671

Bankverbindung:
Münchner Bank eG
Konto-Nr. 2 158 620
BLZ 701900 00
IBAN DE04 7019 0000 0002 1586 20
BIC GENODEF1M01